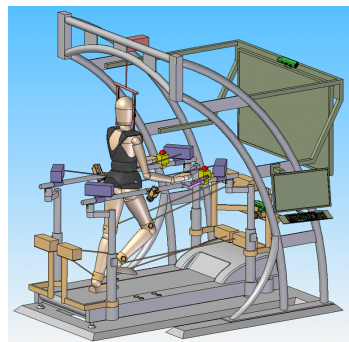




Institut für  
Werkzeugmaschinen und Fabrikbetrieb  
Technische Universität Berlin

# Bachelor Thesis

## Determination of a Suitable CDPR-based Forward Kinematics for a Hip Actuation System in Rehabilitation of Stroke Patients



**Friedrich-Maximilian Weberling**

Matrikel-Nr.: 363820

Date: 26th March, 2018

Supervisor: Dipl.-Ing. Jean-Paul Goppold, Fraunhofer IPK

Examiner: Prof. Dr.-Ing. Jörg Krüger, TU Berlin/Fraunhofer IPK



**Fraunhofer**  
IPK  
INSTITUT  
PRODUKTIONSANLAGEN UND  
KONSTRUKTIONSTECHNIK



**Technische Universität Berlin**  
Institut für Werkzeugmaschinen  
und Fabrikbetrieb

**Rehabilitation Robotics Group**



Hiermit erkläre ich, dass ich die vorliegende Arbeit selbstständig und eigenhändig sowie ohne unerlaubte fremde Hilfe und ausschließlich unter Verwendung der aufgeführten Quellen und Hilfsmittel angefertigt habe.

Die selbstständige und eigenständige Anfertigung versichert an Eides statt:

Berlin, den 26.03.2018

---

Unterschrift



Berlin, den 20.12.2017

Fraunhofer IPK  
Sekretariat PTZ 4  
Pascalstraße 8-9  
10587 Berlin  
Tel+49 (0) 30 / 39006-109

### **Bachelorarbeit auf dem Gebiet Industrielle Robotik**

Name: Friedrich-Maximilian Weberling

Matrikelnummer: 363820

Fakultät und Studiengang: Fachbereich V - Maschinenbau

Voraussichtliche Bearbeitungsdauer: 01.01.2018 - 31.03.2018

#### **Thema: Determination of a suitable CDPR-based Forward-Kinematics for a Hip-Actuation System in Rehabilitation of Stroke-Patients**

**Motivation:** Für die Gangrehabilitation bereits grundsätzlich gehfähiger neurologischer Patienten wird in der klinischen Praxis routinemäßig die sog. Laufbandtherapie angewandt. Hierbei übt der Patient das Gehen auf der Ebene auf einem Laufband mit dem Ziel der Verbesserung der eigenständigen Gehfähigkeit und Gangsicherheit. Moderne Ansätze streben eine robotergestützte Therapierung an, die eine Entlastung der Therapeuten sowie verbessertes Training für den Patienten ermöglichen. Fokus bestehender Systeme liegt dabei klassischerweise auf der Unterstützung der Beinführung. Neuere Untersuchungen zeigen jedoch, dass das Erlernen korrekter Hüftbewegungen für das Wiedererlernen eines korrekten Gangbildes nicht minder entscheidend ist. Bestehende Hüftführungssysteme unterbinden Hüftbewegung teils gänzlich oder unterdrücken Teile notwendiger Bewegungsfreiheiten und verzerrn das Gangbild teils gravierend. Das in der Abschlussarbeit zu behandelnde neu entwickelte Hüftführungssystem auf Basis von Seilaktuierung unterliegt derartigen Beschränkungen nicht.

**Aufgabenstellung:** Für die Implementierung von kraftgeregelten Unterstützungsszenarien während der Therapie ist die genaue Kenntnis des Endeffektors (hier der Patientenhüfte) unerlässlich. Aufgrund des Aufbaus der Kinematik ist eine analytisch bestimmte Herleitung der Position nur auf iterativem Weg möglich. Im Rahmen der Abschlussarbeit sollen hierfür gängige Iterationsverfahren auf deren Eignung untersucht werden. Die Echtzeitfähigkeit von iterativen Algorithmen hängt maßgeblich von der Komplexität des angewendeten kinematischen Modells ab. Daher soll als zweites Ziel der Abschlussarbeit eine Untersuchung zum Einfluss von Modellierungsgrößen auf die Positionsgenauigkeit erfolgen. Die Auswahl einer finalen Kombination von iterativem Verfahren und Modellierungsansatz erfolgt abschließend in Absprache mit dem Betreuer.



Fraunhofer

IPK

Folgende Aufgabenpakete sind im Rahmen der Bachelorarbeit zu bearbeiten:

- I. Recherche zum Stand der Technik für Hüftaktuierungen und Einarbeitung in die Grundproblematik der Rehabilitationsrobotik
- II. Allgemeine Recherche möglicher Berechnungsverfahren für die Positionsbestimmung und Implementierung zweier iterativer Verfahren (Powell's-Dog-Leg & Levenberg-Marquardt)
- III. Allgemeine Recherche möglicher Modellierungen von Seilkinematiken und Implementierung des Standardmodells sowie des um den Einfluss der Trommelgeometrie erweiterten Modells
- IV. Alle Modellbetrachtungen sollen grundsätzlich auf die Transversalebene reduziert erfolgen
- V. Für die Abschätzung von Fehlereinflüssen durch rein transversale Betrachtung soll zusätzlich die Implementierung des Standardmodells mit sechs Freiheitsgraden erfolgen
- VI. Diskussion der gefundenen Lösung hinsichtlich Echtzeitfähigkeit (Anforderungen diesbezüglich werden vom Betreuer festgelegt)
- VII. Sämtliche Programmierungen sollen mit Matlab erstellt werden
- VIII. Dokumentation der Ergebnisse

Für das Erreichen der Bestnote ist die Durchführung von Arbeitspaket V nicht erforderlich, sie gibt aber die Möglichkeit Bonuspunkte zu erzielen.

Die Arbeit erfolgt in ständigem Kontakt mit dem Fachbetreuer Dipl.-Ing. Jean-Paul Goppold und wird am Fraunhofer Institut für Produktionsanlagen und Konstruktionstechnik (IPK), Berlin, durchgeführt.

Der Empfang der Aufgabenstellung und das Einverständnis mit der Überlassung zweier Exemplare der Ausarbeitung an das Institut werden hiermit bestätigt.

Friedrich-Maximilian Weberling

Friedrich-Maximilian Weberling

Jean-Paul Goppold

# Short Summary

This thesis examines the CDPR-based forward kinematics of a hip actuation system in gait rehabilitation of stroke patients. The hip actuation system, proposed in [5], has to be applied to the assist-as-needed control concept, in which the hip actuation system follows the patient's motions and only acts when the patient leaves a certain shell around the trajectory's path. Therefore it is crucial to gain a profound knowledge of the pose of the human hip. Determining the pose through the CDPR-based forward kinematics is challenging. The CDPR-based forward kinematics is kinematically overdetermined because the planar hip actuation system actuates three degrees of freedom via four cables. Therefore numerical approaches are necessary.

The CDPR-based forward kinematics in this thesis is solved by the iterative optimization algorithms, Levenberg-Marquardt and Powell's Dog Leg, with algebraic initial estimate methods. It is especially important for the applicability to the assist-as-needed control concept that these algorithms fulfil real-time constraints. In addition the hip actuation system needs to be accurate. Therefore influences on the system's accuracy are discussed with a special focus on the impact of spatial hip movements on the planar hip actuation system as well as the influence of the radius of the winches drum's which is neglected by the Standard Kinematic Model.

All tests in this thesis are conducted on a computer. The forward kinematic algorithms based on the Standard Kinematic Model fulfil the real-time requirements according to industrial applications which is defined as information up to a rate of 1kHz. The forward kinematics algorithms based on the Standard Kinematic Model could also be implemented on a programmable logic controller (PLC) which guarantees real-time feasibility. It is also determined that the impact of spatial hip movements on the accuracy of the planar hip actuation system is negligibly small. To deal with the drum's radius an Extended Kinematic Model is introduced. The tested forward kinematics algorithms based on the Extended Kinematic Model are not real-time feasible according to industrial applications but it is discussed that for rehabilitation purposes information up to a rate of 100Hz should be acceptable. Applying this lower rate would also allow forward kinematics algorithms based on the EKM to be real-time feasible. However, contrary to algorithms based on the Standard Kinematic Model, the algorithms based on the Extended Kinematic Model cannot be implemented on a programmable logic controller. Testing the forward kinematics algorithms based on the Standard Kinematic Model with cable lengths determined through the Extended Kinematic Model also yields accurate results for the pose of the hip. Therefore the

## *Short Summary*

---

standard forward kinematics algorithms should be prospectively applicable to the hip actuation system.

Nevertheless since the testing in this thesis is only conducted on a computer, the final answer to the question, if the algorithms solve the CDPR-based forward kinematics real-time feasible and are applicable to rehabilitation purposes, has still to be determined by testing the algorithms applied to the hip actuation system and to rehabilitation purposes.

# Kurze Zusammenfassung

Diese Arbeit untersucht die Vorwärtskinematik eines auf einem parallelen Seilroboter (engl. *cable-driven parallel robot (CDPR)*) basierenden Hüfttaktierungssystems für die Gangrehabilitation von Schlaganfallpatienten. Das Hüfttaktierungssystem soll auf ein *Assist-As-Needed* Regelungskonzept angewendet werden, in dem das Hüfttaktierungssystem den Bewegungen des Menschen folgt und nur aktiv wird, wenn der Patient eine gewisse Hülle um den Pfad der Trajektorie herum verlässt. Dafür ist es entscheidend, fundierte Informationen über die Pose der menschlichen Hüfte zu verfügen. Die Ermittlung der Pose durch die Vorwärtskinematik des parallelen Seilroboters ist anspruchsvoll. Die Vorwärtskinematik des parallelen Seilroboters ist kinematisch überbestimmt, weil das planare Hüfttaktierungssystem drei Freiheitsgrade über vier Seile aktuiert. Daher sind numerische Ansätze erforderlich.

Die Vorwärtskinematik des parallelen Seilroboters wird in dieser Arbeit durch die iterativen Optimierungsalgorithmen, Levenberg-Marquardt and Powell's Dog Leg, mit algebraischen Methoden zur Schätzung eines Anfangswertes gelöst. Es ist besonders wichtig für die Anwendbarkeit auf das *Assist-As-Needed* Regelungskonzept, dass diese Algorithmen Echtzeitanforderungen, aber auch Genauigkeitsanforderungen erfüllen müssen. Deswegen werden Einflüsse auf die Genauigkeit diskutiert mit einem besonderen Fokus auf die Auswirkungen räumlicher Hüftbewegungen auf das planare Hüfttaktierungssystem sowie die Auswirkungen des Radius der Seiltrommeln, der im *Standard Kinematic Model* vernachlässigt wird.

Alle Experimente in dieser Arbeit werden auf einem Computer durchgeführt. Die Vorwärtskinematikalgorithmen, die auf dem *Standard Kinematic Model* beruhen, erfüllen die Echtzeitanforderungen für industrielle Anforderungen, die als 1 kHz Taktung der Information definiert ist. Die auf dem *Standard Kinematic Model* basierenden Vorwärtskinematikalgorithmen können auch auf einer Speicherprogrammierbaren Steuerung, die Echtzeit garantiert, implementiert werden. Es wird auch festgestellt, dass die Auswirkungen räumlicher Hüftbewegungen auf die Genauigkeit des planaren Hüfttaktierungssystems vernachlässigbar klein sind. Um den Einfluss des Radius der Seiltrommel zu analysieren, wird ein *Extended Kinematic Model* eingeführt. Die getesteten Vorwärtskinematikalgorithmen basierend auf dem *Extended Kinematic Model* erfüllen keine Echtzeitanforderungen in Bezug auf industrielle Anwendungen aber es wird diskutiert, dass eine Taktung mit 100 Hz für Rehabilitationsanwendungen ausreichen sollte. Wendet man diese langsamere Taktung an, würden die Vorwärtskinematikalgorithmen basierend auf dem *Extended Kinematic Model* auch echtzeitfähig

## Kurze Zusammenfassung

---

sein. Allerdings können die Vorwärtskinematikalgorithmen basierend auf dem *Extended Kinematic Model* im Gegensatz zu den Algorithmen, die auf dem *Standard Kinematic Model* beruhen, nicht auf einer Speicherprogrammierbaren Steuerung implementiert werden. Tests der auf dem *Standard Kinematic Model* basierenden Vorwärtskinematikalgorithmen mit Seillängen, die durch das *Extended Kinematic Model* berechnet werden liefern auch genaue Resultate für die Pose der Hüfte. Deswegen sollten die Vorwärtskinematikalgorithmen, die auf dem *Standard Kinematic Model* beruhen, vorraussichtlich anwendbar auf das Hüfttaktierungssystem sein.

Dennoch kann eine finale Antwort auf die Fragestellung, ob die Algorithmen die auf einem parallelen Seilroboter basierende Vorwärtskinematik des Hüfttaktierungssystems echtzeitfähig und anwendbar auf Rehabilitationszwecke lösen, erst bestimmt werden, wenn die Algorithmen am Hüfttaktierungssystem und in einem Rehabilitationstraining getestet werden.

# Table of Contents

<b>1</b>	<b>Introduction</b>	<b>1</b>
<b>2</b>	<b>State of the Art</b>	<b>3</b>
2.1	Hip Actuation Systems . . . . .	3
2.2	Cable-Driven Parallel Robots . . . . .	5
2.2.1	Standard Kinematic Model . . . . .	6
2.2.2	Degree of Redundancy . . . . .	9
2.2.3	Forward Kinematics . . . . .	10
2.3	Related Work . . . . .	11
2.3.1	Solving the Forward Kinematics under Real-Time Constraints	11
2.3.2	Influences on the System's Accuracy . . . . .	17
<b>3</b>	<b>Proposed Solution</b>	<b>19</b>
3.1	Initial Estimate Methods . . . . .	19
3.1.1	Center Method . . . . .	19
3.1.2	Box Method Applied to the Planar Case . . . . .	20
3.1.3	Circle Method . . . . .	22
3.2	Iterative Optimization Algorithms . . . . .	25
3.2.1	Levenberg-Marquardt Algorithm . . . . .	26
3.2.2	Powell's Dog Leg Algorithm . . . . .	28
3.3	Standard Forward Kinematics Algorithms . . . . .	31
3.4	Consideration of Influences affecting the System's Accuracy . . . . .	32
3.4.1	Cable Elasticity . . . . .	34
3.4.2	Deflection due to Gravitational Effects . . . . .	35
3.5	Extended Kinematic Model . . . . .	39
3.6	Extended Forward Kinematics Algorithms . . . . .	42
<b>4</b>	<b>Experimental Results</b>	<b>45</b>
4.1	Robot Prototype for Simulations . . . . .	45
4.2	Setup of the Simulations . . . . .	46
4.3	Testing the Standard Forward Kinematics . . . . .	47
4.4	Testing the Extended Forward Kinematics . . . . .	48
4.5	Testing the Standard Forward Kinematics based on the Extended Kinematic Model . . . . .	50
4.6	Testing the Impact of General Pelvic Movements . . . . .	51

*Table of Contents*

---

<b>5 Analysis</b>	<b>53</b>
5.1 Evaluation of the Standard Forward Kinematics Algorithms with Pahl/Beitz . . . . .	53
5.2 Evaluation of the Extended Forward Kinematics Algorithms with Pahl/Beitz . . . . .	58
5.3 Standard Forward Kinematic Algorithms based on Extended Kinematic Model . . . . .	60
5.4 Impact of General Pelvic Movements . . . . .	62
5.5 A Suitable Real-Time Feasible Algorithm . . . . .	64
<b>6 Conclusion &amp; Outlook</b>	<b>67</b>
<b>7 Appendix</b>	<b>69</b>
7.1 Comparison of the Box- and the Circle-Method . . . . .	69
7.2 Comparison of the Standard Kinematic Model and the Extended Kinematic Model . . . . .	70
7.3 Contour Plots of the Standard Forward Kinematics Algorithm . . . . .	71
7.4 Contour Plots of the Extended Forward Kinematics Algorithm . . . . .	76
7.5 Contour Plots of the Standard Forward Kinematics Algorithm based on EKM . . . . .	81
7.6 Contour Plots of General Pelvic Movements . . . . .	86
<b>Bibliography</b>	<b>91</b>

# List of Figures

1.1	Hip Actuation System and Gait Rehabilitation Robot . . . . .	1
2.1	Pelvic Motions . . . . .	3
2.2	Planar CDPR Configuration . . . . .	5
2.3	Kinematic Model (spatial) . . . . .	6
2.4	Static and Kinetic Model (spatial) . . . . .	8
2.5	Box Method . . . . .	16
3.1	Circle Method . . . . .	22
3.2	Circle Intersection Model . . . . .	23
3.3	Cable Sagging . . . . .	36
3.4	Determining $u_{krit}$ . . . . .	38
3.5	Extended Kinematic Model (planar) . . . . .	39
3.6	Correcting Factor . . . . .	41
5.1	Contour Plots SKM DL Circle Method in Transverse Plane . . . . .	57
5.2	Contour Plots EKM DL Circle Method in Transverse Plane . . . . .	60
5.3	Contour Plots SKM DL Circle Method based on EKM in Transverse Plane . . . . .	61
5.4	Contourplots SKM DL Circle Method Pelvic Movements Transverse Plane . . . . .	63
7.1	Comparison of SKM and EKM Relating to the Radius $r_d$ . . . . .	70
7.2	Contour Plots SKM LM Center Method in Transverse Plane . . . . .	71
7.3	Contour Plots SKM LM Box Method in Transverse Plane . . . . .	72
7.4	Contour Plots SKM LM Circle Method in Transverse Plane . . . . .	73
7.5	Contour Plots SKM DL Center Method in Transverse Plane . . . . .	74
7.6	Contour Plots SKM DL Box Method in Transverse Plane . . . . .	75
7.7	Contour Plots EKM LM Center Method in Transverse Plane . . . . .	76
7.8	Contour Plots EKM LM Box Method in Transverse Plane . . . . .	77
7.9	Contour Plots EKM LM Circle Method in Transverse Plane . . . . .	78
7.10	Contour Plots EKM DL Center Method in Transverse Plane . . . . .	79
7.11	Contour Plots EKM DL Box Method in Transverse Plane . . . . .	80
7.12	Contour Plots SKM LM Center Method based on EKM in Transverse Plane . . . . .	81

## *List of Figures*

---

7.13 Contour Plots SKM LM Box Method based on EKM in Transverse Plane . . . . .	82
7.14 Contour Plots SKM LM Circle Method based on EKM in Transverse Plane . . . . .	83
7.15 Contour Plots SKM DL Center Method based on EKM in Transverse Plane . . . . .	84
7.16 Contour Plots SKM DL Box Method based on EKM in Transverse Plane . . . . .	85
7.17 Contour Plots SKM DL Circle Method Pelvic Drop in Transverse Plane . . . . .	86
7.18 Contour Plots SKM DL Circle Method Anterior Tilt in Transverse Plane . . . . .	87
7.19 Contour Plots SKM DL Circle Method z-Translation in Transverse Plane . . . . .	88
7.20 Contour Plots SKM DL Circle Method Usual Pelvic Movements in Transverse Plane . . . . .	89

# List of Tables

2.1	Influences on the System's Accuracy . . . . .	17
3.1	Levenberg-Marquardt Algorithm . . . . .	27
3.2	Dog Leg Step . . . . .	28
3.3	Determination of $\beta$ . . . . .	28
3.4	Powell's Dog Leg Algorithm . . . . .	30
3.5	Experimental Results Cable Elasticity . . . . .	35
4.1	Robot Prototype . . . . .	45
4.2	Parametrisation and Inputs Standard Forward Kinematics Algorithms . . . . .	47
4.3	Experimental Results Standard Forward Kinematics Algorithms . . . . .	48
4.4	Parametrisation and Inputs Extended Forward Kinematics Algorithms . . . . .	49
4.5	Experimental Results Extended Forward Kinematics Algorithms . . . . .	50
4.6	Experimental Results SKM DL Circle Method based on EKM . . . . .	50
4.7	Impact of General Pelvic Movements . . . . .	52
5.1	Weighting of Evaluation Criteria . . . . .	54
5.2	Rating Scale VDI 2225 . . . . .	54
5.3	Grading of the Standard Forward Kinematics Algorithms . . . . .	56
5.4	Determining the Most Suitable Algorithm . . . . .	56
5.5	Grading of the Extended Forward Kinematics Algorithms . . . . .	59
5.6	Determining the Most Suitable Algorithm . . . . .	59
7.1	Experimental Results Comparison Box and Circle Method . . . . .	69

*List of Tables*

---

# List of Abbreviations

$\alpha$	Size of step with steepest descent direction
$h_{SD}$	
$\beta$	Factor ensuring the step size $\Delta$
$\beta_i$	Calibration angle
$\chi_i$	Rotation direction of actuator $A_i$
$\Delta\phi_z$	Average error in orientation (associated property of orientation accuracy)
$\Delta\bar{k}$	Average number of executed iterations (associated property of iteration's efficiency)
$\Delta\bar{r}$	Average error in position (associated property of position accuracy)
$\Delta\bar{t}$	Average time (associated property of duration)
$\Delta\phi_z$	Error in orientation between $\phi_z^{calc}$ and $\phi_z^*$
$\Delta k$	Number of executed iterations
$\Delta l$	Error in cable length between SKM and $l_{sag}$
$\Delta r$	Error in position between $r^{calc}$ and $r^*$
$\Delta t$	Time, needed by a forward kinematics algorithm
$\Delta$	Radius of trust region
$\delta_i$	Angle $\angle B_i A_i D_i$ for cable $i \in \{i; \dots; m\}$
$\varepsilon_1$	First stopping criterion of Levenberg-Marquardt and Powell's Dog Leg algorithm
$\varepsilon_2$	Second stopping criterion of Levenberg-Marquardt and Powell's Dog Leg algorithm
$\varepsilon_3$	Third stopping criterion of Powell's Dog Leg algorithm
$\gamma_d$	Cable's weight per metre
$\mu$	Damping parameter of Levenberg-Marquardt algorithm
$\mu_0$	Initial damping parameter of Levenberg-Marquardt algorithm
$v$	Factor of damping parameter $\mu$
$\phi_x$	Pelvic drop
$\phi_y$	Anterior tilt
$\phi_z$	Transverse rotation

## List of Abbreviations

---

$\phi_z^*$	Actual orientation of pelvis (planar)
$\phi_z^{calc}$	Orientation of pelvis (planar) determined through forward kinematics algorithm
$\tau_P$	Torque vector summarizing all torques acting on platform
$A^T$	Structure matrix transforming cable forces to end-effector wrenches, only used in subsection (2.2.1) and (2.2.2)
$A_0$	Abbreviation for $J^T(x_0)J(x_0)$
$A_D$	Diagonal matrix of $A$
$a_i = [a_{ix}, a_{iy}, a_{iz}]^T$	Position of $A_i$
$A$	Abbreviation for $J^T J$
$a$	Step with size $\alpha$ and direction of the steepest descent $h_{SD}$
$b_i = [b_{ix}, b_{iy}, b_{iz}]^T$	Position of $B_i$
$b$	Synonym for Gauss-Newton step $h_{GN}$
$f_c = [f_{c,i}; \dots; f_{c,m}]^T$	Cable force vector containing all $f_{c,i}$
$f_{c,i} = [f_{c,ix}, f_{c,iy}, f_{c,iz}]^T$	Cable force vector of cable $i$
$f_{EKM} = [f_{EKM,i}; \dots; f_{EKM,m}]^T$	Cable length error vector of EKM
$f_P$	Force vector summarizing all forces acting on platform
$f_{SKM} = [f_{SKM,i}; \dots; f_{SKM,m}]^T$	Cable length error vector of SKM
$f$	Error vector to define objective function $F$
$f = [f_1; \dots; f_m]^T$	Gradient for Levenberg-Marquardt and Powell's Dog Leg algorithm
$g$	Step of Powell's Dog Leg algorithm
$h_{DL}$	Step of the Gauss-Newton algorithm
$h_{GN}$	Step of the Levenberg-Marquardt algorithm
$h_{LM}$	Steepest descent direction
$I$	$n \times n$ identity matrix
$J$	$J=J(x)$
$J(x)$	$m \times n$ Jacobian matrix
$l_{act} = [l_{act,i}; \dots; l_{act,m}]^T$	Actual cable length vector
$l_{SKM,i,\beta} = [l_{SKM,i,\beta,x}, l_{SKM,i,\beta,y}]^T$	Cable vector of SKM w.r.t $K_{\beta,i}$
$l_{SKM,i}^0 = [l_{SKM,ix}^0, l_{SKM,iy}^0]^T$	Cable vector of SKM in calibration pose for cable $i \in \{1; \dots; m\}$
$l_{SKM,i} = [l_{SKM,ix}, l_{SKM,iy}, l_{SKM,iz}]^T$	Cable vector of the SKM for cable $i$
$q_{EKM} = [l_{EKM,i}; \dots; l_{EKM,m}]^T$	Inverse kinematic solution of the EKM
$q_{SKM} = [l_{SKM,i}; \dots; l_{SKM,m}]^T$	Inverse kinematic solution of the SKM
$r^* = [r_x^*, r_y^*]^T$	Actual position of pelvis

$\mathbf{r}^{1,2} = [r_x^{1,2}, r_y^{1,2}]^T$	Upper bound of intersection region in Circle Method
$\mathbf{r}^{1,3} = [r_x^{1,3}, r_y^{1,3}]^T$	Right bound of intersection region in Circle Method
$\mathbf{r}^{2,4} = [r_x^{2,4}, r_y^{2,4}]^T$	Left bound of intersection region in Circle Method
$\mathbf{r}^{3,4} = [r_x^{3,4}, r_y^{3,4}]^T$	Lower bound of intersection region in Circle Method
$\mathbf{r}^{calc} = [r_x^{calc}, r_y^{calc}]^T$	Pelvic position determined through forward kinematics algorithm
$\mathbf{r}^{high}$	Higher bound of intersection region
$\mathbf{r}^{low}$	Lower bound of intersection region
$\mathbf{r}_0^{box}$	Estimate to position $\mathbf{r}$ determined by Box Method
$\mathbf{r}_0^{circle}$	Estimate of Circle Method to position $\mathbf{r}$
$R_{2 \times 2}$	$2 \times 2$ rotational matrix
$\mathbf{r}_i^{high} = [r_{i,x}^{high}, r_{i,y}^{high}, r_{i,z}^{high}]^T$	Higher bound of box around $A_i$
$\mathbf{r}_i^{low} = [r_{i,x}^{low}, r_{i,y}^{low}, r_{i,z}^{low}]^T$	Lower bound of box around $A_i$
$\mathbf{r}_x^{high} = [r_{i,x}^{low}, \dots, r_{m,x}^{high}]^T$	Vector containing all $x$ -components of $\mathbf{r}_i^{high}$ of cable $i \in \{i; \dots; m\}$
$\mathbf{r}_x^{low} = [r_{i,x}^{low}, \dots, r_{m,x}^{low}]^T$	Vector containing all $x$ -components of $\mathbf{r}_i^{low}$ of cable $i \in \{i; \dots; m\}$
$\mathbf{r}_y^{high} = [r_{i,y}^{high}, \dots, r_{m,y}^{low}]^T$	Vector containing all $y$ -components of $\mathbf{r}_i^{high}$ of cable $i \in \{i; \dots; m\}$
$\mathbf{r}_y^{low} = [r_{i,y}^{low}, \dots, r_{m,y}^{low}]^T$	Vector containing all $y$ -components of $\mathbf{r}_i^{low}$ of cable $i \in \{i; \dots; m\}$
$\mathbf{R}$	$3 \times 3$ Rotation matrix using Kardan angles $\{\phi_x, \phi_y, \phi_z\}$
$\mathbf{r} = [r_x, r_y, r_z]^T$	Position of $K_P$ , also position of pelvis
$\mathbf{u}_i$	Cable unit vector of cable $i$
$\mathbf{w}$	Wrench acting on the platform
$\mathbf{x}^*$	Platform (pelvis) pose determined by the forward kinematics
$\mathbf{x}_0$	Initial estimate to platform (pelvis) pose $\mathbf{x}^*$
$\mathbf{x}_0^{box} = [\mathbf{r}_0^{box}, \mathbf{0}]^T$	Initial estimate to pose $\mathbf{x}^*$ determined by Box Method
$\mathbf{x}_0^{center}$	Initial estimate of Center Method
$\mathbf{x}_0^{circle} = [\mathbf{r}_0^{circle}, 0]^T$	Initial estimate of Circle Method to pose $\mathbf{x}^*$
$\mathbf{x}_{new}$	Sum of pose $\mathbf{x}$ and either the step $\mathbf{h}_{LM}$ or step $\mathbf{h}_{DL}$
$\mathbf{x} = [\mathbf{r}, \phi_x, \phi_y, \phi_z]^T$	Pose of platform (pelvis)
$\psi$	Argument of trigonometric function

## List of Abbreviations

---

$\rho$	Gain ratio of Levenberg-Marquardt and Powell's Dog Leg algorithm
$\tau$	User defined factor of the initial damping parameter $\mu_0$
$\theta_i$	Angle between $x$ -axis of $K_{\beta,i}$ and $l_{SKM,i}$
$a$	Index $a \in \{1, 2, 3, 4, 5, 6\}$ indicating the forward kinematics algorithm with 1 = SKM LM Center Method, 2 = SKM LM Box Method, 3 = SKM LM Circle Method, 4 = SKM DL Center Method, 5 = SKM DL Box Method, 6 = SKM DL Circle Method according to the standard forward kinematics algorithms and 1 = EKM LM Center Method, 2 = EKM LM Box Method, 3 = EKM LM Circle Method, 4 = EKM DL Center Method, 5 = EKM DL Box Method, 6 = EKM DL Circle Method according to the extended forward kinematics algorithms
$A_i$	Actuator belonging to cable $i$
$a_{ii}^0$	Components of the diagonal matrix of $\mathbf{A}_0$
$B_i$	Cable attachment belonging to cable $i$
$c$	Abbreviation for $\mathbf{a}^T(\mathbf{b} - \mathbf{a})$
$C_k$	Center point of circle with radius $r_k$
$C_l$	Center point of circle with radius $r_l$
$c_\psi$	$\cos(\psi)$
$C_i^0$	Fixed calibration point of cable $i \in \{i; \dots; m\}$
$C_i^{new}$	Wrong calibration point in new pose
$C_{k,l}^{low}$	Lower circle intersection point
$C_{k,l}^{up}$	Upper circle intersection point
$CP$	Center point of platform (pelvis)
$D_i$	Cable exit point for cable $i \in \{1; \dots; m\}$
$d_{k,l}$	Distance between point $C_k$ and $C_l$
$e_{pa}$	Generalized term for associated property with the associated property $p \in \{1, 2, 3, 4\}$ and the algorithm $a \in \{1, 2, 3, 4, 5, 6\}$
$e_{pa}$	Graded associated property with the associated property $p \in \{1, 2, 3, 4\}$ and the algorithm $a \in \{1, 2, 3, 4, 5, 6\}$
$F$	Objective function
$F_G$	Weight force

$f_{c,i}$	Euclidean norm of cable force vector $\mathbf{f}_{c,i}$
$g$	Standard acceleration due to gravity
$Gwga$	Absolute evaluation of an entire algorithm
$a \in \{1, 2, 3, 4, 5, 6\}$	
$H$	Horizontal pull of cable
$h_{k,1}$	Horizontal distance between point $C_k$ and point $C_{k,l}^{up}$ w.r.t coordinate frame in figure (3.2)
$i$	Index, indicating the cable $i \in \{1; \dots; m\}$
$k$	Number of executed iterations
$k, l$	Indices indicating the associated boundary ( $\{1, 2\}, \{1, 3\}, \{2, 4\}, \{3, 4\}$ )
$K_0$	Coordinate frame of the fixed base
$K_P$	Coordinate frame of the CDPR's platform (pelvis)
$K_{\beta,i}$	Coordinate frame rotated by $\beta_i$ w.r.t $K_0$
$k_{max}$	Maximum number of iterations
$l$	Cable length neglecting cable sagging
$L(\mathbf{0}) - L(\mathbf{h}_{DL})$	Linear model of $\mathbf{f}$
$l_{\delta,i}$	Wrapped cable length of cable $i \in \{1; \dots; m\}$
$l_{act,i}$	Actual cable length of cable $i$ measured by the encoder
$l_{corr,i}$	Correcting factor of cable length $l_{EKM,i}$ for cable $i \in \{1; \dots; m\}$
$l_{f,i}$	Free cable length of cable $i \in \{1; \dots; m\}$
$l_{min}$	Minimal cable length controllable by motor resolution
$l_{sag}$	Length of sagging cable
$l_{SKM,i}$	Cable length of cable $i$ determined by SKM
$l_{SKM,i}^0$	Cable length in calibration pose for cable $i \in \{1; \dots; m\}$
$M$	Midpoint of distance between $C_{k,l}^{up}$ and $C_{k,l}^{low}$
$m$	Mass
$m$	Maximum number of cable
$n$	Number of degrees of freedom
$p$	Index $p \in \{1, 2, 3, 4\}$ indicating the associated property with ( $\Delta\bar{r} = 1$ , $\Delta\bar{\phi}_z = 2$ , $\Delta\bar{k} = 3$ , $\Delta\bar{t} = 4$ )
$q_0$	Distributed load
$r_d$	Radius of drum
$r_k$	Radius of circle with center point $C_k$
$r_l$	Radius of circle with center point $C_l$

## List of Abbreviations

---

$S$	Pretension
$s_\psi$	$\sin(\psi)$
$SKM$	Index indicating the Standard Kinematic Model
$u$	$\frac{g_0 l}{2H}$
$u_{krit}$	Parameter to determine the horizontal pull
$v_{k,l}$	Vertical distance between point $M$ and point $C_{k,l}^{up}$ as well as distance between point $M$ and point $C_{k,l}^{low}$ w.r.t coordinate frame in figure (3.2)
$v_{k,l}^+$	Vertical distance between point $M$ and point $C_{k,l}^{up}$ w.r.t coordinate frame in figure (3.2)
$v_{k,l}^-$	Vertical distance between point $M$ and point $C_{k,l}^{low}$ w.r.t coordinate frame in figure (3.2)
$w(x)$	Cable deflection
$w_{max}$	Maximum sag
$w_{pa}$	Weighting of the evaluation criteria with the associated property $p \in \{1, 2, 3, 4\}$ and the algorithm $a \in \{1, 2, 3, 4, 5, 6\}$
$Wg_a$	Relative evaluation of an entire algorithm $a \in \{1, 2, 3, 4, 5, 6\}$
$wg_{pa}$	Weighted value of the graded associated property with the associated property $p \in \{1, 2, 3, 4\}$ and the algorithm $a \in \{1, 2, 3, 4, 5, 6\}$
ADL	Activities-of-daily-living
CDPR	Cable-driven parallel robot
CRPM	Completely Restrained Positioning Mechanism
DL	Powell's Dog Leg algorithm
EKM	Extended Kinematic Model
GT-I	Gait Trainer
IRPM	Incompletely Restrained Positioning Mechanism
LM	Levenberg-Marquardt algorithm
PAM	Pelvic Assist Manipulator
PLC	Programmable logic controller
RRPM	Redundantly Restrained Positioning Mechanism
SKM	Standard Kinematic Model

# 1 Introduction

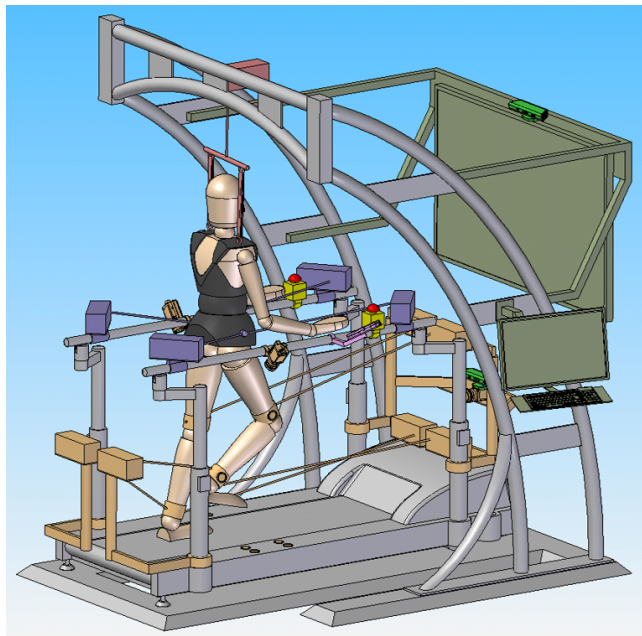


**Figure 1.1:** Hip Actuation System and Gait Rehabilitation Robot

Stroke belongs to the major causes of morbidity and mortality in adults and is the most significant cause for disabilities in the Western hemisphere as emphasized by [1]. According to the Stiftung Deutsche Schlaganfall-Hilfe [27], 270,000 German citizens suffer a stroke each year and the frequency of strokes increases with an advancing age. That is especially disturbing, considering statistics in [18] that predict 22.8 million people of the German population are 65 years old or elder in 2050 which corresponds to a 38% increase compared to 2007. This means, the number of disabled people could drastically rise because strokes often provoke physical impairments such as hemiplegia, the most severe form of hemiparesis. Hemiplegia limits the gait performance due to the complete paralysis of half the body. To recover gait, stroke patients require a rehabilitation but a standard rehabilitation seems to be insufficient if 50% cannot perform activities-of-daily-living (ADL) without support as emphasized in [1]. Therefore research seeks to improve gait rehabilitation techniques.

A prospective improvement integrates robotic devices in gait recovery training to intensify the therapy due to the robot's advantages such as precise controllability,

## *1 Introduction*

---

repeatability and accuracy as well as to the potential of extending the therapy. The first designed rehabilitation robots for gait recovery are based on electromechanical exoskeletons, e.g. the Lokomat, on end-effectors, e.g. the Haptic Walker or on treadmills with some sort of body weight support as pointed out in [5]. These robotic systems primarily focus on the movements of the legs and neglect hip movements even though hip movements fulfil important functions for energy preserving abilities and for an energy efficient gait pattern as pointed out in [17].

This thesis examines the hip actuation system proposed in [5] and depicted in figure (1.1) consisting of a cable-driven parallel robot (CDPR) actuating the human hip via four electrically driven cables in the transverse plane. The system is demanded to be applicable to the assist-as-needed control concept, a new assistance paradigm encouraging the active motion of the patient and assigning the robot a merely supporting function as outlined in [1]. As a consequence of the assist-as-needed strategy, the hip actuation system has to follow the patient's hip, as long as the hip moves along a defined trajectory and within a certain shell around the trajectory's path. This is known as zero-impedance control mode. Only if the hip leaves the shell the robot has to act to bring the human back onto the trajectory's track and within the shell around it. This is achieved through a force control mode. To apply these control modes a profound knowledge about the pose of the hip is necessary. The determination of the pose through the CDPR-based forward kinematics of the hip actuation system is challenging because the system actuates three degrees of freedom with four cables in the transverse plane and is therefore kinematically overdetermined. Thus, in this thesis a suitable solution to the forward kinematics is sought, which has to be accurate and real-time feasible for gait rehabilitation applications.

## 2 State of the Art

This chapter examines the state of the art of hip actuation systems and their often neglected importance for gait rehabilitation. The existing systems are shortly introduced with a special focus on the to be studied CDPR-based hip actuation system and the advantages of a CDPR application. Then the CDPR's kinematic model is presented concentrating on the inverse and forward kinematics to give the theoretical background for this thesis.

### 2.1 Hip Actuation Systems

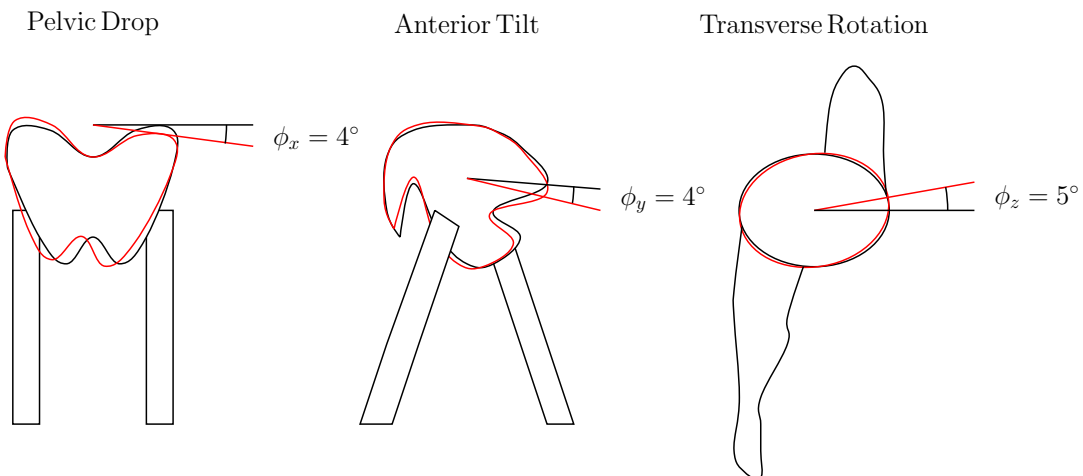


**Figure 2.1:** Pelvic Motions

The term *hip actuation system* is inspired by the German technical term. In English it is more convenient to refer to *hip actuation systems* as *pelvic actuation systems*. Therefore this thesis only uses the term *pelvic actuation system* from now on.

Although the pelvic movements are crucial for a proper gait pattern most rehabilitation robots neglect them as described by [5]. These pelvic movements, described in [17], cover six degrees of freedom and are rather small. Considering the translation, the pelvis moves asynchronously in all three directions during each stride. Considering the rotation, the pelvis performs the pelvic drop  $\phi_x$ , the anterior tilt  $\phi_y$ , and the transverse rotation  $\phi_z$  as depicted in figure (2.1). During a normal stride the covered

angle of the pelvic drop  $\phi_x$  and the anterior tilt  $\phi_y$  can both reach an average of  $4^\circ$  whereas the backwards and forwards transverse rotation reaches an angle of  $10^\circ$  ( $5^\circ$  forward and  $5^\circ$  backward). This might lead to the assumption that it seems tolerable to ignore these movements but they are important for energy preserving abilities and for an energy efficient gait pattern as referred to [17]. It was even recognized that rehabilitation robots which restrict pelvic movements cannot restore a normal gait pattern as pointed out in [29]. Therefore actuation systems allowing pelvic movements were developed.

A detailed description of the state of the art of pelvic actuation systems is majorly presented in [5] and will be shortly reviewed. So far four different end-effector setups were designed.

A rather simple one belongs to the Gait Trainer GT-I only allowing lateral movements. A phase-synchronous left-right movement of the pelvis is generated through an end-effector system which is directly linked to the drive. This movement cannot adapt and follows a fixed pattern. Hence, the system is able to cover one degree of freedom but is insufficient for a general actuation of the complex pelvic motion.

Contrary to the GT-I, the "Pelvic Assist Manipulator", abbreviated as PAM, has a pelvic system capable of actuating five degrees of freedom. The motions are realized through two pneumatic drives that are linked to the pelvis via ball joints. Another actuation module covering multiple degrees of freedom is proposed in [31] but also executes body weight support functions.

An CDPR-based approach is the STRING-MAN. Actually the STRING-MAN was created as body weight support system applying cables for a parallel manipulator but if several cables were added a pelvic actuation could also be achieved. However, such an approach seems to be complicated as referred to [5].

The to be studied actuation system is based on a planar CDPR and introduced in [5]. Depicted in figure (2.2), the CDPR consists of four cables covering two translational and one rotational degree of freedom. The four cables, coiled and uncoiled by the actuators  $A_i$ , are attached to a platform. Applied to rehabilitation robotics and the pelvic actuation system, the platform is the human pelvis. When talking about CDPRs in general, this thesis therefore always considers the technical term platform as a synonym for the human pelvis. The to be studied pelvic actuation system uses configuration 2 because it is more compact than configuaration 1 and reaches a greater workspace. Therefore it is more suitable to gait training as discussed in [5]. An introduction in CDPRs and their possible advantages for rehabilitation applications are given in the next section with a detailed focus on their kinematic model, especially their inverse and forward kinematics.

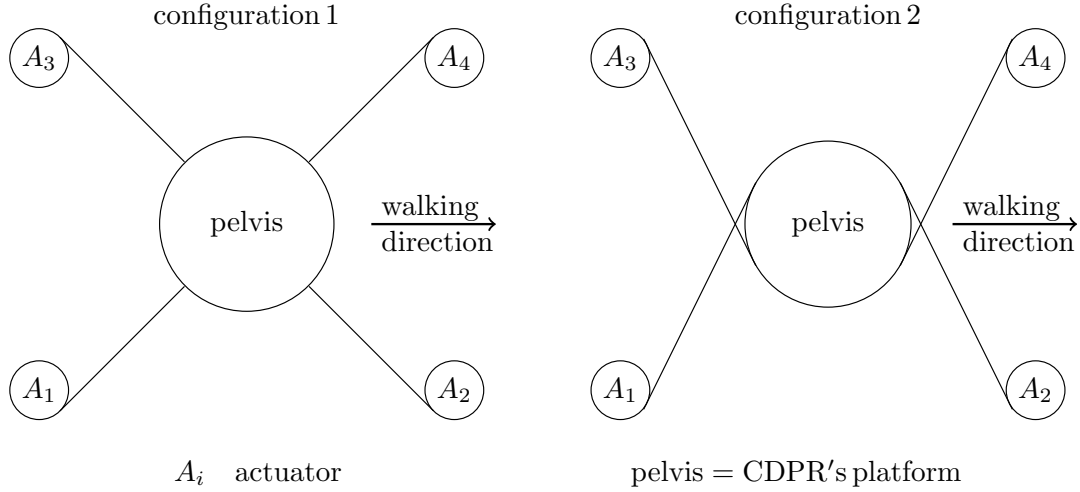


**Figure 2.2:** Planar CDPR Configuration

## 2.2 Cable-Driven Parallel Robots

Cable-driven parallel robots (CDPRs), a special type of parallel manipulators, were firstly proposed with six degrees of freedom in the United States in 1989 and during the last three decades a lot was contributed to their research as referred to in [30]. The fundamental setup of a CDPR consists of a mobile platform, which is connected to a fixed base via cables. Each cable is linked to an electric driven winch which is attached to the base as already mentioned in the previous section.

Many abilities of CDPRs seem to be advantageous for rehabilitation application as referred to [5]. The comparatively low mass of the CDPR's components causes small inertial forces which enable the CDPR to achieve high velocities and accelerations. A CDPR can also cover both extremely large and small workspaces, is quite energy efficient due to the fact that the actuators are fixed to a base and the load can be subdivided between the actuators. This also allows the CDPR to achieve a high load capacity. As a consequence the energy efficiency is a reason for low operational costs. In addition the acquisition is rather cheap considering the CDPR's components. Favourable for rehabilitation robotics a CDPR is intrinsically safe since the actuators can be installed outside of the workspace and the CDPR's compact design makes the robot more acceptable for the patient. Considering the control, a CDPR has a high bandwidth predestining it for haptic interactions. The CDPR's setup is also reconfigurable which enables to apply the robot for different rehabilitation therapies.

Nevertheless CDPRs also have negative aspects, as explained in [30]. Cables are not as rigid as links and can only be pulled but not compressed. Therefore all cable forces of a CDPR must be positive. Also the cables forces must range between a min-

imum cable force to avoid cable sagging and a maximum cable force to avoid cable breaking, pointed out in [22]. As a result, the workspace of CDPRs is restricted which is analysed in [30]. Finding the optimal cable force distribution also causes difficulties requiring certain algorithms, proposed in [23]. As mentioned in the introduction, one of the most challenging negative aspects concerns the forward kinematics, because a CDPR with more cables than actuated degrees of freedom is a kinematically over-determined system.

The pelvic actuation system, studied in this thesis, requires exactly a suitable solution to that CDPR-based forward kinematics since the assist-as-needed strategy can only function if the pose of the human pelvis is known. To gain the theoretical background for the forward kinematics, the robot model of a CDPR is reviewed in the following subsection (2.2.1).

### 2.2.1 Standard Kinematic Model

The robot model applied in this thesis is based on [10] and adopts its definitions. It is also known as the Standard Kinematic Model (SKM) and is abbreviated with the index *SKM* in the following formulas. The model is derived for six degrees of freedom although the pelvic actuation system is only actuating three degrees of freedom. However, a robot model with six degrees of freedom is advantageous for further investigations concerning the impact of general pelvic movements. For a direct derivation in three degrees of freedom it is referred to [6].

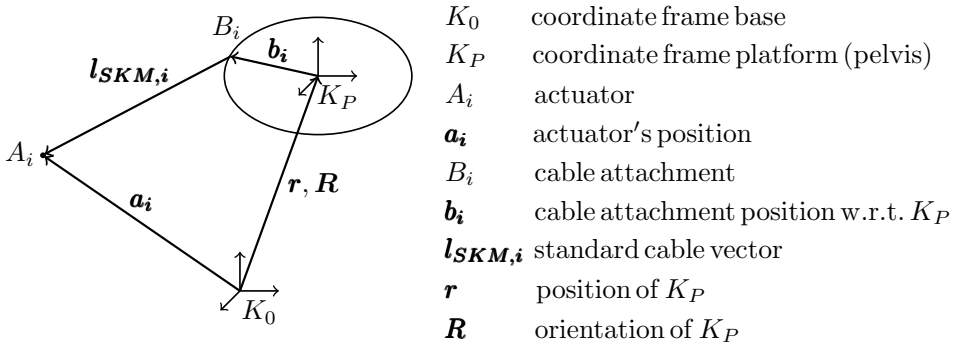


**Figure 2.3:** Kinematic Model (spatial)

The CDPR consists of  $m$  cables for  $n$  degrees of freedom. The inverse kinematics of the SKM aims to determine the length  $l_{SKM,i}$  of the cable  $i$  where the index  $i \in \{1; \dots; m\}$  indicates each cable. Considering figure (2.3), the coordinate frame of the fixed base is  $K_0$ . Vector  $r = [r_x, r_y, r_z]^T$  describes the position of the CDPR's platform coordinate frame  $K_P$  which is located at the platform's centre of gravity. Using Kardan angles  $\{\phi_x, \phi_y, \phi_z\}$ ,  $c_\psi$  as abbreviation for  $\cos$  and  $s_\psi$  as abbreviation for  $\sin$  with the index

$\psi$  being the argument of the trigonometric function, the platform's orientation with reference to  $K_0$  is given by the rotation matrix

$$\mathbf{R} = \begin{bmatrix} c_{\phi_x}c_{\phi_z} & -c_{\phi_y}s_{\phi_z} & s_{\phi_y} \\ c_{\phi_x}s_{\phi_z} + s_{\phi_x}s_{\phi_y}c_{\phi_z} & c_{\phi_x}c_{\phi_z} - s_{\phi_x}s_{\phi_y}s_{\phi_z} & -s_{\phi_x}c_{\phi_y} \\ s_{\phi_x}s_{\phi_z} - c_{\phi_x}s_{\phi_y}c_{\phi_z} & s_{\phi_x}c_{\phi_z} + c_{\phi_x}s_{\phi_y}s_{\phi_z} & c_{\phi_x}c_{\phi_y} \end{bmatrix}. \quad (2.1)$$

The Kardan angles applied in equation (2.1) correspond to the pelvic drop  $\phi_x$ , the anterior tilt  $\phi_y$  and the transverse rotation  $\phi_z$  and form together with the position  $\mathbf{r} = [r_x, r_y, r_z]^T$  the platform's pose  $\mathbf{x} = [r_x, r_y, r_z, \phi_x, \phi_y, \phi_z]^T$ . Applied to rehabilitation robotics,  $\mathbf{x}$  is therefore equivalent to the pose of the human pelvis. The cable's attachment point on the platform represented by  $B_i$  is described through the vector  $\mathbf{b}_i$  with reference to  $K_P$ . Each actuator is assumed as point-shaped and indicated through the point  $A_i$ . Its position with reference to  $K_0$  is given by the vector  $\mathbf{a}_i$ . The cable vector  $\mathbf{l}_{SKM,i}$  points from  $B_i$  to  $A_i$  and can be simply calculated applying the depicted vector loop in figure (2.3) yielding

$$\mathbf{l}_{SKM,i} = \mathbf{a}_i - \mathbf{r} - \mathbf{R}\mathbf{b}_i. \quad (2.2)$$

Taking the euclidean norm of equation (2.2), the standard cable length  $l_{SKM,i}$  is received by

$$l_{SKM,i} = \|\mathbf{l}_{SKM,i}\|_2. \quad (2.3)$$

The CDPR's inverse kinematic solution  $\mathbf{q}_{SKM}$  contains the cable length of each cable  $i \in \{1; \dots; m\}$ . Using equation (2.3) the inverse kinematic solution of the SKM results in

$$\mathbf{q}_{SKM} = \begin{bmatrix} l_{SKM,1} \\ \vdots \\ l_{SKM,m} \end{bmatrix}. \quad (2.4)$$

Applied to the CDPR-based pelvic actuation system with  $m = 4$  cables for  $n = 3$  degrees of freedom, the inverse kinematic solution is given by

$$\mathbf{q}_{SKM} = \begin{bmatrix} l_{SKM,1} \\ l_{SKM,2} \\ l_{SKM,3} \\ l_{SKM,4} \end{bmatrix}. \quad (2.5)$$

Before the forward kinematics of the CDPR is derived, the static and kinetic model is presented as introduced in [30] on the one hand to complete the SKM on the other

hand to analyse the degree of redundancy of a CDPR and the resultant problem concerning the forward kinematics.

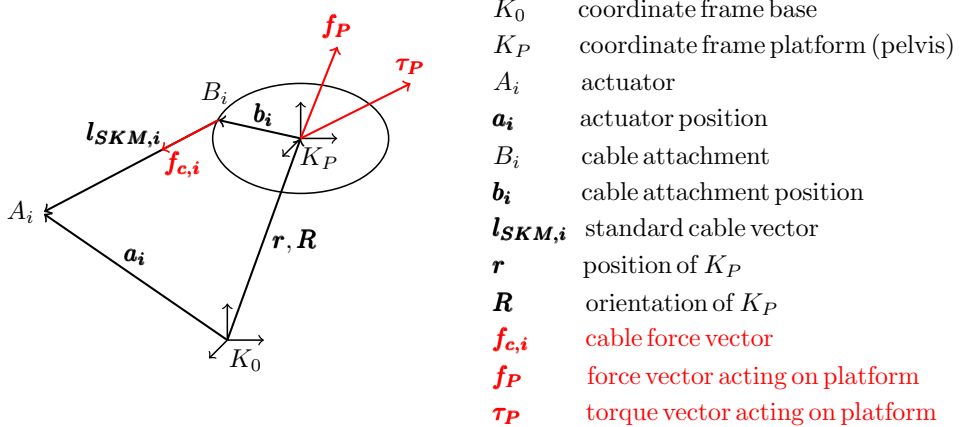


**Figure 2.4:** Static and Kinetic Model (spatial)

In order to derive the static and kinetic behaviour of a CDPR, the kinematic model in figure (2.3) is adopted, and the cable force vector  $f_{c,i}$ , acting along the cable vector  $l_{SKM,i}$ , as well as the force vector  $f_P$  and the torque vector  $\tau_P$  are added as depicted in figure (2.4). The force vector  $f_P$  and the torque vector  $\tau_P$  summarize all forces and torques acting on the platform respectively including gravity and inertia. Thus, the following derivation yields not only the static but also the kinetic model of the CDPR. The force equilibrium

$$\sum_{i=1}^m f_{c,i} + f_P = \mathbf{0} \quad (2.6)$$

and the torque equilibrium

$$\sum_{i=1}^m b_i \times f_{c,i} + \tau_P = \mathbf{0} \quad (2.7)$$

are formulated. Applying equations (2.2) and (2.3) the cable force vector  $f_{c,i}$  is rewritten as

$$f_{c,i} = f_{c,i} \frac{l_{SKM,i}}{\|l_{SKM,i}\|} = f_{c,i} u_i, \quad (2.8)$$

where  $u_i$  represents the cable unit vector and  $f_{c,i}$  the euclidean norm of the cable force vector. The force equilibrium in equation (2.6) and the torque equilibrium in equation (2.7) are combined and using equation (2.8) the general force equilibrium can be written in matrix notation as

$$\begin{bmatrix} \mathbf{u}_1 & \cdots & \mathbf{u}_m \\ \mathbf{b}_1 \times \mathbf{u}_1 & \cdots & \mathbf{b}_m \times \mathbf{u}_m \end{bmatrix} \begin{bmatrix} f_{c,1} \\ \vdots \\ f_{c,m} \end{bmatrix} + \begin{bmatrix} \mathbf{f}_p \\ \boldsymbol{\tau}_p \end{bmatrix} = \mathbf{0}. \quad (2.9)$$

This matrix equation is commonly abbreviated as

$$\mathbf{A}^T \mathbf{f}_c + \mathbf{w} = \mathbf{0} \quad (2.10)$$

where  $\mathbf{A}^T$  is called structure matrix,  $\mathbf{f}_c$  the cable force vector, also often described as force distribution, and  $\mathbf{w}$  the wrench acting on the CDPR's platform according to [10]. Equation (2.10) is the most general form to describe the kinetic and static model of the CDPR. Further equations describing the cable velocity and acceleration using the structure matrix  $\mathbf{A}^T$  are given in [10]. More interesting for this thesis are the consequences resulting of equation (2.10). Due to the fact that cables can only be tensed but not compressed, the cable force vector  $\mathbf{f}_c$  always needs to be positive. Therefore equation (2.10) has to yield positive solutions as pointed out in [30]. This ultimately leads to an analysis of the degree of redundancy of CDPR outlining certain problems for the forward kinematics.

## 2.2.2 Degree of Redundancy

CDPRs actuating an equal number of degrees of freedoms with the equal number of cables exist but their workspace is restricted because cables cannot be compressed, as mentioned above. For industrial applications CDPRs shall be able to operate in large workspaces. Therefore such CDPRs have often more  $m$  cables than  $n$  degrees of freedom. For these industrially applied CDPRs, following classification based on the dimension of the structure matrix  $\mathbf{A}^T$  in equation (2.9) is introduced in [30].

This classification states, CDPRs having a smaller or even number of cables than actuated degrees of freedom ( $m \leq n$ ) lack the ability to actuate the  $n$  degrees of freedom and are therefore classified as Incompletely Restrained Positioning Mechanisms (IRPMs). CDPRs that need to actuate  $n$  degrees of freedom, possess an additional cable fulfilling the case  $m = n + 1$  that classifies them as Completely Restrained Positioning Mechanisms (CRPMs). If a CDPR fulfills the case  $m > n + 1$  it is considered as Redundantly Restrained Positioning Mechanism (RRPM) as referred to [30].

The pelvic actuation system, studied in this thesis, has  $m = 4$  cables for  $n = 3$  degrees of freedom. It is therefore a CRPM according to the classification in [30]. The CDPR's forward kinematics seeks to calculate the pose  $\mathbf{x}$  of the platform given certain cable lengths. A CDPR classified as CRPM is therefore an over-constrained kinematic system making the determination of a suitable solution to the forward kinematics

complicated but the pelvic actuation system requires exactly such a suitable solution to provide a profound knowledge of the pelvic pose.

### 2.2.3 Forward Kinematics

Contrary to a CDPR's inverse kinematics, finding a suitable forward kinematics solution is a challenging task as highlighted above. This is particularly complicated if a real-time feasible solution, meaning that the algorithm must be strictly bounded and its computation time must not exceed the range of milliseconds on real-time hardware, is sought as clarified in [20]. The to be studied CDPR-based pelvic actuation system exactly needs this suitable real-time feasible forward kinematics to be applicable to the assist-as-needed strategy.

According to [3], parallel manipulators possess up to 40 possible solutions. A real-time feasible solution in closed-form to the forward kinematics of a CDPR with six degrees of freedom is possible but only under the special geometric requirements of the so called "3-2-1" configuration which is presented in [19]. However, a closed form solution for the to be studied CDPR-based pelvic actuation system with three degrees of freedom, as depicted in configuration 2 in figure (2.2), has not been found so far.

To receive an equation for the forward kinematics, as given in [10], it is demanded that the  $m$  actual cable lengths  $l_{act,i}$ , measured by the encoder through the actuator's rotation angle, and written as  $m$ -dimensional vector  $\mathbf{l}_{act} = [l_{act,1}; \dots; l_{act,m}]^T$  equal their inverse kinematic solution  $\mathbf{q}_{SKM}$  from equation (2.4) resulting into

$$\mathbf{l}_{act} = \mathbf{q}_{SKM}. \quad (2.11)$$

Equation (2.11) is valid if the platform's pose  $\mathbf{x}^*$  is known because that enables the inverse kinematic solution  $\mathbf{q}_{SKM}$  to yield the cable lengths equivalent to the ones in the actual cable length vector  $\mathbf{l}_{act}$ . In the case of the CDPR-based forward kinematics the platform's pose  $\mathbf{x}^*$  is unknown. Therefore it is difficult to determine an inverse kinematic solution  $\mathbf{q}_{SKM}$  equal to the actual cable length vector  $\mathbf{l}_{act}$ . It is only possible to give an estimate  $\mathbf{x}$  to the platform's pose  $\mathbf{x}^*$ . Thus, the corresponding inverse kinematic solution  $\mathbf{q}_{SKM}$  of the estimate  $\mathbf{x}$  differs from the actual cable length vector  $\mathbf{l}_{act}$  making equation (2.11) invalid. In fact, an error between the actual cable length vector  $\mathbf{l}_{act}$  and the inverse kinematics solution  $\mathbf{q}_{SKM}$  of the estimate  $\mathbf{x}$  exists. Therefore equation (2.11) must be rewritten as

$$\mathbf{f}_{SKM}(\mathbf{x}) = \mathbf{q}_{SKM} - \mathbf{l}_{act} \quad (2.12)$$

with  $\mathbf{f}_{SKM} : \mathbb{R}^n \rightarrow \mathbb{R}^m$  being the error between the cable length  $\mathbf{l}_{act}$  given by the encoder and the inverse kinematics solution  $\mathbf{q}_{SKM}$  of an estimated pose  $\mathbf{x}$ . It is often proposed, such as in [20], to state equation (2.12) as the mathematical optimization problem

$$\mathbf{x}^* = \operatorname{argmin}_{\mathbf{x}} \{F(\mathbf{x})\} \quad (2.13)$$

with  $\mathbf{x}^*$  being the desired pose that minimizes the objective function  $F : \mathbb{R}^m \rightarrow \mathbb{R}$

$$F(\mathbf{x}) = \frac{1}{2} (\mathbf{f} \mathbf{f}') \quad (2.14)$$

which is defined for the SKM with equation (2.12) by applying the error vector

$$\mathbf{f} = \mathbf{f}_{SKM}(\mathbf{x}). \quad (2.15)$$

Physically speaking, if the cables are interpreted as springs, the pose is sought with the lowest potential energy, which is the one with the smallest displacement. For the SKM the displacement is the cable length error  $\mathbf{f}_{SKM}(\mathbf{x})$ .

Different approaches to solve the forward kinematics in equation (2.13) exist and will be reviewed in the following section (2.3).

## 2.3 Related Work

Since CDPRs are a highly discussed research topic, lots of researches concentrated on solving the forward kinematics. Also many works considered the issue of real-time feasibility and possible modelling influences affecting the accuracy. Therefore this section aims to present the researches that contributed to finding the proposed solution in chapter (3).

### 2.3.1 Solving the Forward Kinematics under Real-Time Constraints

Real-time constraints limit the approaches to find a suitable solution to a CDPR's forward kinematics. In [24] real-time feasibility means that a computation has to be completed within a determined time frame otherwise errors occur. A real-time information must be strictly in a range of milliseconds which is usually defined at a rate up to 1 kHz for industrial applications. If this rate is also necessary for rehabilitation purposes will be discussed in section (5.5). Real-time constraints make the computation especially difficult if no dynamic memory allocation is designable because it causes that less computational power is available for kinematic modelling as explained in

[24]. Therefore too detailed kinematic models should be avoided to fulfil real-time constraints.

In [25] the general techniques to deal with the forward kinematics are pointed out. Each one has certain advantages and disadvantages. Hence, the different methods are often combined to exploit each one's advantages.

Interval arithmetic algorithms are based on extensive search algorithms that can find the desired solution and were tested in [15]. First, a box with its dimension corresponding to the dimension of the position  $\mathbf{r}$  is defined in which the solution must be. The box is then repeatedly subdivided in smaller boxes whilst in each repetition an evalution is executed determining if the solution lies inside or outside the box. If a solution lies outside the box, it does not need to be further investigated. Anyhwen a box is so small that it can be considered as a solution. In addition interval arithmetic delivers all possible solutions not just a specific one. Concerning the CDPR-based forward kinematics, interval arithmetic algorithms might be favourable because they can guarantee a solution and the algorithm's time frame can be strictly fixed but they lack the ability to perform in a real-time enviroment according to [25] and [20]. Thus, interval arithmetic algorithms alone cannot provide a solution to the CDPR-based forward kinematics of the pelvic actuation system and are not further investigated in this thesis.

Another approach are neural networks. They resemble their biological eponyms forming complex equations whose coefficients can be trained to certain geometries. Using the inverse kinematics of the CDPR, a set of poses can be created to teach each neuron. Hence, trained neural networks can achieve extremely high speeds linear correlated to their size. However, neural networks are not very flexible because they have to be retrained to every deviating geometry. A real-time feasible algorithm combining neural networks and interval arithmetic was successfully implemented, but is not taken into account in thesis, because in [25] it is analysed that such an algorithm cannot excel the performance of techniques applying iterative optimization.

Besides applying interval arithmetic algorithms and neural networks, the forward kinematics could even be solved by genetic algorithms as pointed out in [16] but the focus of this thesis is on iterative optimization techniques because they are proven to provide real-time feasible solutions in [20] and are therefore now discussed in detail.

### Iterative Optimization

The most prospective technique to challenge the CDPR-based forward kinematics of the pelvic actuation system is iterative optimization. Iterative optimization algorithms repeatedly calculate poses  $\mathbf{x}$ , starting from a given initial estimate pose  $\mathbf{x}_0$ . These repeatedly calculated poses  $\mathbf{x}$  shall converge to the desired pelvic pose  $\mathbf{x}^*$  that minimizes

the optimization problem of the forward kinematics in equation (2.13).

This thesis utilizes two iterative optimization algorithms: the Levenberg-Marquardt (LM) and the Powell's Dog Leg (DL) which are extensively explained in [12]. Both algorithms apply the error vector  $\mathbf{f}(\mathbf{x})$  in equation (2.15) and the implementation of the first partial derivatives' components of  $\mathbf{f}(\mathbf{x})$  displayed as  $m \times n$  Jacobian matrix

$$\mathbf{J}(\mathbf{x}) = \begin{bmatrix} \frac{\partial f_1(\mathbf{x})}{\partial x_1} & \dots & \frac{\partial f_1(\mathbf{x})}{\partial x_n} \\ \vdots & \ddots & \vdots \\ \frac{\partial f_m(\mathbf{x})}{\partial x_1} & \dots & \frac{\partial f_m(\mathbf{x})}{\partial x_n} \end{bmatrix}. \quad (2.16)$$

In order to increase clarity in the following equations, the notations  $\mathbf{J} = \mathbf{J}(\mathbf{x})$  and  $\mathbf{f} = \mathbf{f}(\mathbf{x})$  as well as the abbreviation  $\mathbf{A} = \mathbf{J}^T \mathbf{J}$  are introduced.

The Levenberg-Marquardt and the Powell's Dog Leg algorithm base on two methods, the Steepest Descent method, also known as Gradient method, and the Gauss-Newton method. The Steepest Descent applies with the error vector  $\mathbf{f}$  in equation (2.15) and the Jacobian matrix  $\mathbf{J}$  in equation (2.16) the gradient

$$\mathbf{g} = \mathbf{J}^T \mathbf{f} \quad (2.17)$$

to determine the locally steepest descent direction  $\mathbf{h}_{SD}$  towards the minimum of the objective function  $F$  through solving

$$\mathbf{h}_{SD} = -\mathbf{g}. \quad (2.18)$$

This method converges but its convergence is linear and rather slow. The Steepest Descent method has often a good performance at the start of iterative optimization algorithms where the current  $\mathbf{x}$  is far away from the desired minimizer  $\mathbf{x}^*$ .

Contrary to the Steepest Descent method, the Gauss-Newton method can yield quadratic convergence if the current estimate  $\mathbf{x}$  is close to the desired minimizer  $\mathbf{x}^*$ . The Gauss-Newton step  $\mathbf{h}_{GN}$  is determined through solving

$$\mathbf{A} \mathbf{h}_{GN} = -\mathbf{g}. \quad (2.19)$$

Both the Levenberg-Marquardt and the Powell's Dog Leg seek to combine the advantages of the Steepest Descent and the Gauss Newton Method. Therefore the Levenberg-Marquardt algorithm introduces the damping parameter  $\mu \geq 0$ . The step  $\mathbf{h}_{LM}$  of the Levenberg-Marquardt algorithm is determined by solving

$$(\mathbf{A} + \mu \mathbf{I}) \mathbf{h}_{LM} = -\mathbf{g} \quad (2.20)$$

where  $\mathbf{I}$  is the identity matrix. The damping parameter  $\mu$  has an impact on the direction of the step  $\mathbf{h}_{LM}$  and its size in three ways:

- (1)  $\forall \mu \geq 0 \quad (\mathbf{A} + \mu \mathbf{I}) > \mathbf{0}$
- (2)  $\forall \mu \gg 0 \quad \mathbf{h}_{LM} \approx -\frac{1}{\mu} \mathbf{g} = \frac{1}{\mu} \mathbf{h}_{SD}$
- (3)  $\forall \mu \rightarrow 0 \quad \mathbf{h}_{LM} \approx \mathbf{h}_{GN}$

The first way guarantees that  $\mathbf{h}_{LM}$  is at descent direction, the second way allows a short step rather in the steepest descent direction  $\mathbf{h}_{SD}$ , which is important if the current  $\mathbf{x}$  is far away from the minimizer  $\mathbf{x}^*$ , and the third way allows an undamped Gauss-Newton step  $\mathbf{h}_{GN}$  towards the solution which is advantageous if the current  $\mathbf{x}$  is near to  $\mathbf{x}^*$ .

The convergence of the Levenberg-Marquardt algorithm can be further improved by changing the determination of the step  $\mathbf{h}_{LM}$  introduced in equation (2.20) according to [13] into

$$(\mathbf{A} + \mu \mathbf{A}_D) \mathbf{h}_{LM} = -\mathbf{g} \quad (2.21)$$

with  $\mathbf{A}_D$  being the diagonal matrix of  $\mathbf{A}$ . The diagonal matrix  $\mathbf{A}_D$  weights the gradient contrary to the identity matrix  $\mathbf{I}$  in a way that the greater components of the gradient are more taken into account than the smaller components. Thus, the convergence of the algorithm can be accelerated if the direction of the gradient is small. This improvement of the Levenberg-Marquardt algorithm in equation (2.21) is applied in all following chapters.

The Powell's Dog Leg algorithm is fairly similar to the Levenberg-Marquardt method but is even able to control the step size directly through the radius  $\Delta$  of the so called trust region. The algorithm calculates the Gauss-Newton step  $\mathbf{h}_{GN}$  by solving equation (2.19) and a possible step direction obtained by the steepest descent direction  $\mathbf{h}_{SD}$  in equation (2.18). The step size  $\alpha$  of the step in steepest descent direction  $\mathbf{h}_{SD}$  is determined by

$$\alpha = \frac{\|\mathbf{g}\|_2^2}{\|\mathbf{J}\mathbf{g}\|_2^2}, \quad (2.22)$$

applying equations (2.16) and (2.17). The Powell's Dog Leg step  $\mathbf{h}_{DL}$  is now chosen between the two possible steps  $\mathbf{a} = \alpha \mathbf{h}_{SD}$  and  $\mathbf{b} = \mathbf{h}_{GN}$  or a combination of both using the trust region's radius  $\Delta$  and limiting the step's maximum size to even that

radius  $\Delta$ . Further explanations of this process are given in subsection (3.2.2) together with detailed explanations of the Levenberg-Marquardt in subsection (3.2.1) and the Powell's Dog Leg algorithm in subsection (3.2.2) concerning the updating of the steps, the stopping criteria and the entire algorithms' structure.

The Levenberg-Maquardt algorithm yields a decent real-time feasible solution to the CDPR-based forward kinematics as analysed in [20]. The Powell's Dog Leg algorithm has yet not been applied to CDPR-based forward kineamtics but in a different optimization problem the Powell's Dog Leg outperforms the Levenberg-Marquardt pointed out in [11]. Therefore both algorithms are taken into account for the determination of the suitable solution to the CDPR-based forward kinematics of the pelvic actuation system in chapter (3).

In [24] it is noted that iterative optimization provokes a high and varying computational load and cannot guarantee a solution contrary to interval arithmetic but the number of iterations can be limited. Besides if a solution is found, its validity cannot be defined if multiple solutions exist. However, iterative optimization is also flexible, very fast, and configurable. In addition it works under any type of noise condition. Especially interesting is that iterative optimization allows an estimate of the error, so that the accuracy of a solution can be adjusted. Also the parametrisation of the applied algorithm to enhance accuracy is underlined. Especially important for the performance of the chosen iterative optimization algorithm is the determination of a good initial estimate  $\mathbf{x}_0$  explained in [24]. Therefore initial estimate methods are now discussed.

### Initial Estimate Methods

Initial estimate methods influence the performance of iterative optimization algorithms extensively as pointed out in [24]. The duration of of an algorithm can be much longer if the initial estimate  $\mathbf{x}_0$  is far away from the desired minimizer  $\mathbf{x}^*$ . Thus, initial estimates close to  $\mathbf{x}^*$  are sought. A method to determine an initial estimate favourably close to the CDPR's pose  $\mathbf{x}^*$  is introduced in [20]. This initial estimate method is inspired by interval arithmetic but can be implemented using simple algebraic equations. The method is shortly presented because it is further applied to the CDPR-based forward kinematics of the pelvic actuation system in the following chapters.

To determine the initial estimate the vector loop of the SKM in figure (2.3) is considered. Subtracting  $\mathbf{r}$  from  $\mathbf{a}_i$  results into the vector  $\mathbf{a}_i - \mathbf{r}$  pointing from the platform's center point at which  $K_P$  is located to  $A_i$ . This vector  $\mathbf{a}_i - \mathbf{r}$  forms together with  $\mathbf{l}_{SKM,i}$  and  $\mathbf{b}_i$  a triangle removing the rotation matrix  $\mathbf{R}$ . Applying the triangle inequality yields

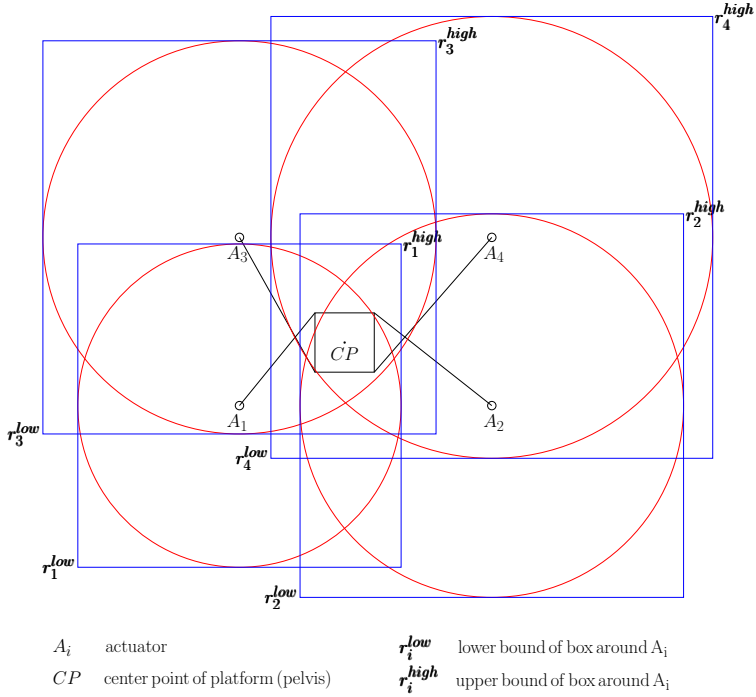


Figure 2.5: Box Method

$$\|\mathbf{a}_i - \mathbf{r}\|_2 \leq l_{SKM,i} + \|\mathbf{b}_i\|_2, \quad (2.23)$$

meaning that the platform's center point (*CP*) lies inside a sphere with the radius  $l_{SKM,i} + \|\mathbf{b}_i\|_2$  and whose center point is at  $A_i$ . Considering figure (2.5), shows the result if equation (2.23) is applied to a planar SKM-based CDPR with four cables. Due to the planar case the spheres are circles. These circles intersect with each other and *CP* lies inside the intersection area of all circles. Back to the general case, the spheres are enclosed into boxes using interval arithmetic. Thus, the boxes' bounds can be obtained by

$$\left. \begin{aligned} \mathbf{r}_i^{low} &= \mathbf{a}_i - (l_{SKM,i} + \|\mathbf{b}_i\|_2)[1, 1, 1]^T \\ \mathbf{r}_i^{high} &= \mathbf{a}_i + (l_{SKM,i} + \|\mathbf{b}_i\|_2)[1, 1, 1]^T \end{aligned} \right\} \quad (2.24)$$

As in figure (2.5) depicted, *CP* lies inside the boxes' intersection region. To gain an estimate for *CP*, this intersection box needs to be calculated through applying the bounds determined in equation (2.24). This initial estimate method, from now on called Box Method, is applied to the planar case of the CDPR-based forward kinematics of the pelvic actuation system in subsection (3.1.2).

According to [20], the Box Method delivers a close initial estimate  $\mathbf{x}_0$  to the platform's pose  $\mathbf{x}^*$ , but takes only the platform's position  $\mathbf{r}$  not the orientation into account. In [20] it is pointed out that an even better estimate to the position  $\mathbf{r}$  could be received through calculating the intersection region of the spheres but is disregarded as too complicated for CDPRs with six degrees of freedom. The intersection region is easier to calculate since the pelvic actuation system consists of a planar CDPR. This approach is further elaborated in subsection (3.1.3) for a new initial estimate method which is limited to the planar case.

Nevertheless even if a real-time feasible solution to the CDPR-based forward kinematics of the pelvic actuation system is determined through a suitable initial estimate method combined with an iterative optimization algorithm, the possibility exists that the system does not fulfil its function due to the various idealization of the SKM and other factors that could have an impact on the system's accuracy. These possible influences are summarized in the next subsection (2.3.2).

### 2.3.2 Influences on the System's Accuracy

Classification	Influence
Cable Properties	<ul style="list-style-type: none"> <li>- Cable Elasticity</li> <li>- Creep</li> <li>- Deflection due to Gravitational Effects</li> <li>- Cable Torsion</li> <li>- Geometrical Deformation leading to Cable Ovalization</li> <li>- Cable Wear</li> <li>- Hysteresis</li> <li>- Temperature</li> <li>- Cable Bending Stiffness</li> </ul>
Drive Train	<ul style="list-style-type: none"> <li>- Manufacturing Inaccuracies</li> <li>- Friction</li> <li>- Stiffness</li> <li>- Hysteresis in Cable Positioning</li> <li>- Coiling Errors</li> <li>- Effect of Non-linear Cable Length to Drive Ratio</li> <li>- Motor Resolution</li> <li>- Radius of Winches' Drum</li> </ul>
Platform and Frame	<ul style="list-style-type: none"> <li>- Setup of Frame</li> <li>- Softness of Platform (Pelvis)</li> <li>- Geometrical Issues (Singularities)</li> </ul>
Unknown Factor	<ul style="list-style-type: none"> <li>- General Pelvic Movements</li> </ul>

**Table 2.1:** Influences on the System's Accuracy

A lot of influences on the system's accuracy exist but most of them are negligibly small. Most of the to be discussed influences on CDPR-based systems are outlined and analysed in [24]. The influences are classified as factors due to cable properties, due to the drive train, due to the CDPR's platform frame and unknown factors. They are summarized in table (2.1). These influences on the pelvic actuation system's accuracy are also considered for the proposed solution to the CDPR-based forward kinematics in the following chapter.

# 3 Proposed Solution

As explained in subsection (2.3.1) the CDPR-based forward kinematics of the to be studied pelvic actuation system in equation (2.13) can be most prospectively solved using iterative optimization. Crucial to iterative optimization is a good initial estimate  $\mathbf{x}_0$ . Therefore section (3.1) proposes three different estimation methods applied to the CDPR-based forward kinematics of the pelvic actuation system. The iterative optimization algorithms, Levenberg-Marquardt and Powell's Dog Leg, are further elaborated in section (3.2). Following in section (3.3), the estimation methods are combined with the Levenberg-Marquardt and the Powell's Dog Leg algorithms to six different solutions of the forward kinematics that are based on the SKM in subsection (2.2.1). Influences on the system's accuracy, introduced in subsection (2.3.2), are discussed in section (3.4). As a result an Extended Kinematic Model is developed in section (3.5). This model is also applied to the forward kinematics in section (3.6).

## 3.1 Initial Estimate Methods

The importance of initial estimate methods is stressed in subsection (2.3.1). The initial estimate  $\mathbf{x}_0$  has a significant impact on the efficiency of the chosen iterative optimization method. Three estimation methods, the Center Method, the Box Method from subsection (2.3.1) applied to the planar case, and the newly developed Circle Method which is closely related to the Box Method challenge this problem.

### 3.1.1 Center Method

The forward kinematics aims to determine the pose  $\mathbf{x}^*$  of the CDPR's platform given the cable lengths  $l_{act,i}$  provided by the encoder. Considering the pelvic actuation system, the CDPR's forward kinematics determines the pelvic pose

$$\mathbf{x} = \begin{bmatrix} r_x \\ r_y \\ \phi_z \end{bmatrix} \quad (3.1)$$

only for a planar case. Therefore  $\mathbf{x}$  contains three components indicating the three actuated degrees of freedom with the two translational being the pelvic position  $\mathbf{r} = [r_x; r_y]^T$ . The considered rotational degree of freedom is the pelvis' transverse rotation  $\phi_z$ . All initial estimate methods covered in this thesis only seek to determine

### 3 Proposed Solution

---

an estimate to the pelvic position  $\mathbf{r}$  and neglect the transverse rotation  $\phi_z$ . The rotation complicates the forward kinematics extensively. Taking the rotation into account for initial estimate methods might cause algorithms that do not consist of simple algebraic equations. Therefore it is advantageous to ignore the rotation as referred to [24].

The four actuators of the CDPR-based pelvic actuation system form a rectangle as depicted in configuration 2 of figure (2.2). The coordinate frame  $K_0$  of the fixed base of the CDPR is located at the center of the rectangle formed by the CDPR's actuators  $A_i$ . The depicted walking direction is equivalent to the  $x$ -axis of  $K_0$  and the  $y$ -axis points towards the rectangle's side defined through  $A_3$  and  $A_4$ . According to [5] the human is in the center of this rectangle during gait rehabilitation training and due to the assist-as-needed strategy the force control always aims to move the human back onto a trajectory close to the center if he leaves a specified shell around it. Hence the pelvis can be expected to be in the center most of the times. The pelvic position should therefore be always close to  $\mathbf{r} = [0\text{m}; 0\text{m}]^T$ . This assumption is adopted by the Center Method. Since the transverse rotation  $\phi_z$  is neglected for initial estimate methods ( $\phi_z = 0^\circ$ ), the initial estimate of the Center Method yields

$$\mathbf{x}_0^{\text{center}} = \begin{bmatrix} 0\text{m} \\ 0\text{m} \\ 0^\circ \end{bmatrix}. \quad (3.2)$$

The Center Method is a very simple method to find an initial estimate but especially in the case when the pelvis moves out of the center it would be better to have a method that adapts the initial estimate to that change. Such methods are the Box Method and the Circle Method.

#### 3.1.2 Box Method Applied to the Planar Case

The general Box Method was already presented in subsection (2.3.1) as interval arithmetic inspired method but can be implemented using simple algebraic equation. Applied to the planar case and the CDPR-based pelvic actuation system, the Box Method seeks to determine a close estimate to the position  $\mathbf{r} = [r_x; r_y]^T$  of the pelvis. This planar case is already depicted in figure (2.5). Hence, the boxes are reduced to squares altering the boxes' bounds of equation (2.24) to

$$\left. \begin{array}{l} \mathbf{r}_i^{\text{low}} = \mathbf{a}_i - (l_{act,i} + \|\mathbf{b}_i\|_2)[1, 1]^T \\ \mathbf{r}_i^{\text{high}} = \mathbf{a}_i + (l_{act,i} + \|\mathbf{b}_i\|_2)[1, 1]^T \end{array} \right\} \quad (3.3)$$

with  $i \in \{1; 2; 3; 4\}$ . It is also noted that equation (3.3) uses the actual cable lengths  $l_{act,i}$  contrary to equation (2.24) because the CDPR-based forward kinematics of the pelvic actuation system determines the initial estimate  $\mathbf{x}_0$  via the cable lengths  $l_{act,i}$

that belong to the desired pose  $\mathbf{x}^*$ . Considering figure (2.5), an estimate to the position of  $CP$  is gained through determining the intersection box, in which  $CP$  is located. Therefore the components of  $\mathbf{r}_i^{low}$  and  $\mathbf{r}_i^{high}$  in equation (3.3) are studied separately in following vectors

$$\begin{aligned}\mathbf{r}_x^{low} &= \begin{bmatrix} r_{1,x}^{low} \\ \vdots \\ r_{4,x}^{low} \end{bmatrix} & \mathbf{r}_y^{low} &= \begin{bmatrix} r_{1,y}^{low} \\ \vdots \\ r_{4,y}^{low} \end{bmatrix} \\ \mathbf{r}_x^{high} &= \begin{bmatrix} r_{1,x}^{high} \\ \vdots \\ r_{4,x}^{high} \end{bmatrix} & \mathbf{r}_y^{high} &= \begin{bmatrix} r_{1,y}^{high} \\ \vdots \\ r_{4,y}^{high} \end{bmatrix}.\end{aligned}\quad (3.4)$$

The lower bound  $\mathbf{r}^{low}$  of the intersection box, in which  $CP$  lies, is received through determining the greatest components for  $\mathbf{r}_x^{low}$  and  $\mathbf{r}_y^{low}$  in equation (3.4) resulting into

$$\mathbf{r}^{low} = \begin{bmatrix} \max_i \mathbf{r}_x^{low} \\ \max_i \mathbf{r}_y^{low} \end{bmatrix}. \quad (3.5)$$

Contrary, the upper bound of the intersection box is received through determining the smallest components for  $\mathbf{r}_x^{high}$  and  $\mathbf{r}_y^{high}$  in equation (3.4) yielding

$$\mathbf{r}^{high} = \begin{bmatrix} \min_i \mathbf{r}_x^{high} \\ \min_i \mathbf{r}_y^{high} \end{bmatrix}. \quad (3.6)$$

Applying equations (3.5) and (3.6) the estimate to the pelvic position yields

$$\mathbf{r}_0^{box} = \frac{1}{2}(\mathbf{r}^{low} + \mathbf{r}^{high}). \quad (3.7)$$

Since the Box Method also neglects the transverse rotation  $\phi_z$  of the pelvis, the initial estimate of the Box Method applied to the CDPR-based forward kinematics of the pelvic actuation system is determined with equation (3.7) by

$$\mathbf{x}_0^{box} = \begin{bmatrix} \mathbf{r}_0^{box} \\ 0^\circ \end{bmatrix} \quad (3.8)$$

As mentioned in subsection (2.3.1) a possibly even more accurate estimate to the position  $\mathbf{r}$  is obtained by considering the intersection region of the circles instead of the boxes in figure (2.5). This intersection region is much smaller compared to the intersection region of the Box Method. This idea gives rise to the Circle Method in the following subsection (3.1.3).

### 3.1.3 Circle Method

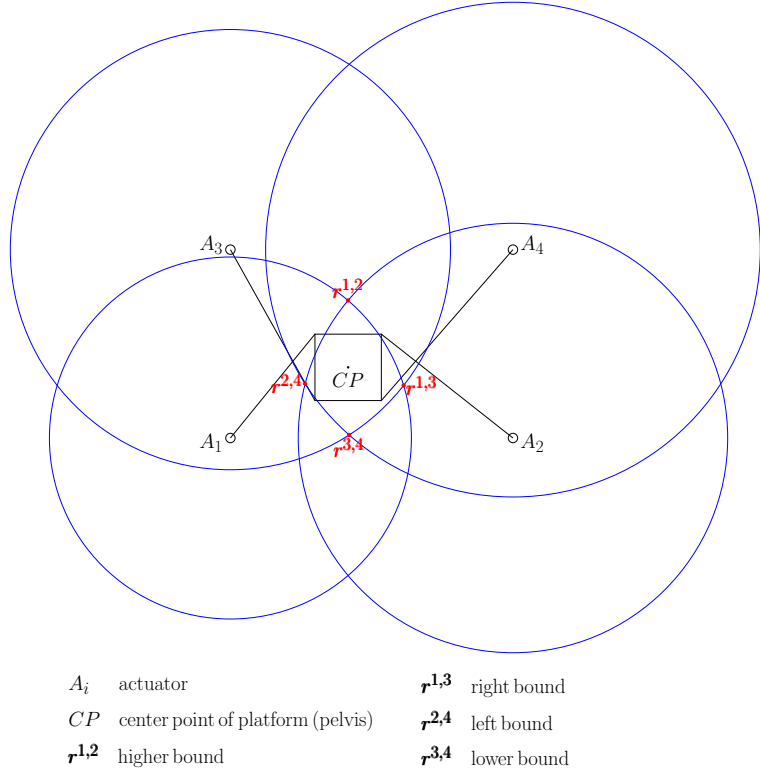
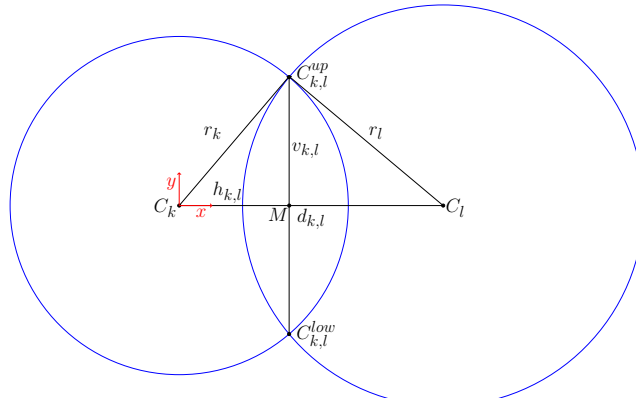


**Figure 3.1:** Circle Method

The Circle Method is applicable to planar CDPRs whose actuators form a rectangle configuration as depicted in figure (2.2). Therefore this method should be considered as a rather problem specific initial estimate method. The idea of the Circle Method is to derive an initial estimate for the position  $\mathbf{r}$  of  $CP$  through the bounds  $\mathbf{r}^{1,2}$ ,  $\mathbf{r}^{1,3}$ ,  $\mathbf{r}^{2,4}$ , and  $\mathbf{r}^{3,4}$  of the intersection region given by all circles as depicted in figure (3.1). Equally to the Box Method, the orientation of the platform is neglected so that  $\phi_z = 0^\circ$ . The radii of the circles around the actuators  $A_i$  are obtained by  $l_{act,i} + \|\mathbf{b}_i\|_2$ . To determine the bounds of the intersection region, the intersection of two circles, as depicted in figure (3.2), is shortly reviewed.

Considering figure (3.2), Two circles with the known radii  $r_k$  and  $r_l$  around their corresponding centres  $C_k$  and  $C_l$  intersect in  $C_{k,l}^{up}$  and  $C_{k,l}^{low}$  in a 2-dimensional Cartesian coordinate frame. The distance  $d_{k,l}$  between  $C_k$  and  $C_l$  is known. Determining the coordinates of  $C_{k,l}^{up}$  is equivalent to finding the horizontal distance  $h_{k,l}$  between the points  $C_k$  and  $C_{k,l}^{up}$  as well as the vertical distance  $v_{k,l}$  between the points  $C_k$  and  $C_{k,l}^{up}$ . The points  $C_k$ ,  $M$  and  $C_{k,l}^{up}$  form the rectangular triangle  $\triangle C_k M C_{k,l}^{up}$ . Applying Pythagoras theorem to  $\triangle C_k M C_{k,l}^{up}$  yields



$C_k$	centre point of circle with radius $r_k$	$C_{k,l}^{up}$	upper circle intersection point
$C_l$	centre point of circle with radius $r_l$	$C_{k,l}^{low}$	lower circle intersection point
$r_k$	radius of circle with centre point $C_k$	$M$	midpoint of distance between $C_{k,l}^{low}$ and $C_{k,l}^{up}$
$r_l$	radius of circle with centre point $C_l$	$h_{k,l}$	horizontal distance between $C_k$ and $C_{k,l}^{up}$
$d_{k,l}$	distance between $C_k$ and $C_l$	$v_{k,l}$	vertical distance between $C_k$ and $C_{k,l}^{up}$

**Figure 3.2:** Circle Intersection Model

$$h_{k,l}^2 = r_k^2 - v_{k,l}^2. \quad (3.9)$$

Similarly, the points  $M$ ,  $C_l$ ,  $C_{k,l}^{up}$  form the rectangular triangle  $\triangle MC_lC_{k,l}^{up}$  to which Pythagoras theorem is applied resulting in

$$v_{k,l}^2 = r_l^2 - (d_{k,l} - h_{k,l})^2. \quad (3.10)$$

Inserting equation (3.10) in equation (3.9) and converting obtains for  $C_{k,l}^{up}$  as well as for  $C_{k,l}^{low}$  the  $x$ -coordinate

$$h_{k,l} = \frac{r_k^2 - r_l^2 + d_{k,l}^2}{2d_{k,l}}. \quad (3.11)$$

Remaining is the determination of  $v_{k,l}$ . Converting equation (3.9) delivers both the  $y$ -coordinate for  $C_{k,l}^{up}$  and  $C_{k,l}^{low}$  through

$$v_{k,l} = \pm \sqrt{r_l - h_{k,l}} \quad (3.12)$$

with  $h_{k,l}$  given by equation (3.11). The positive value of equation (3.12) corresponds to  $C_{k,l}^{up}$  yielding

### 3 Proposed Solution

---

$$v_{k,l}^+ = \sqrt{r_l - h_{k,l}} \quad (3.13)$$

and the negative value of equation (3.12) corresponds to  $C_{k,l}^{low}$  yielding

$$v_{k,l}^- = -\sqrt{r_l - h_{k,l}}. \quad (3.14)$$

Having revisited the intersection of circles in general, the bounds  $\mathbf{r}^{1,2}$ ,  $\mathbf{r}^{1,3}$ ,  $\mathbf{r}^{2,4}$ , and  $\mathbf{r}^{3,4}$  can now be evaluated with equations (3.11) and (3.12). The indices  $k$  and  $l$  are adapted to the corresponding bound (e.g.  $k,l = 1, 2$  for  $\mathbf{r}^{1,2}$ ) Considering figure (3.1), the components of  $\mathbf{r}^{1,2}$  are obtained by

$$\mathbf{r}^{1,2} = \begin{bmatrix} h_{1,2} + a_{1x} \\ v_{1,2}^+ + a_{1y} \end{bmatrix} \quad (3.15)$$

applying equation (3.11) and equation (3.13) with the radii  $r_1 = l_{act,1} + \|\mathbf{b}_1\|_2$ ,  $r_2 = l_{act,2} + \|\mathbf{b}_2\|_2$ , and  $d_{1,2} = a_{2x} - a_{1x}$ . Similar the bound  $\mathbf{r}^{3,4}$  is determined through

$$\mathbf{r}^{3,4} = \begin{bmatrix} h_{3,4} + a_{3x} \\ v_{3,4}^- + a_{3y} \end{bmatrix} \quad (3.16)$$

using equation (3.11) and equation (3.11) and f equation (3.14) with the radii  $r_3 = l_{act,3} + \|\mathbf{b}_3\|_2$ ,  $r_4 = l_{act,4} + \|\mathbf{b}_4\|_2$ , and  $d_{3,4} = a_{4x} - a_{3x}$ . The evaluation of both bound  $\mathbf{r}^{2,4}$  and  $\mathbf{r}^{1,3}$  requires to utilize equation (3.11) for the bound's  $y$ -component as well as equations (3.13) and (3.14) for the bound's  $x$ -component since the circles intersection points lay on a horizontal line instead of a vertical as assumed in the derivation of equation (3.11) and (3.12). Therefore the bound  $\mathbf{r}^{2,4}$  is obtained by

$$\mathbf{r}^{2,4} = \begin{bmatrix} v_{2,4}^+ + a_{2x} \\ h_{2,4} + a_{2y} \end{bmatrix} \quad (3.17)$$

applying equation (3.11) for the  $y$ -component and equation (3.13) for the  $x$ -component with  $r_2 = l_{act,2} + \|\mathbf{b}_2\|_2$ ,  $r_4 = l_{act,4} + \|\mathbf{b}_4\|_2$ , and  $d_{2,4} = a_{4y} - a_{2y}$ . The determination of bound  $\mathbf{r}^{1,3}$  works accordingly yielding

$$\mathbf{r}^{1,3} = \begin{bmatrix} v_{1,3}^- + a_{1x} \\ h_{1,3} + a_{1y} \end{bmatrix} \quad (3.18)$$

through applying equation (3.11) for the  $y$ -component and equation (3.14) for the  $x$ -component with  $r_1 = l_{act,1} + \|\mathbf{b}_1\|_2$ ,  $r_3 = l_{act,3} + \|\mathbf{b}_3\|_2$ , and  $d_{1,3} = a_{3y} - a_{1y}$ .

Similar to the Box Method in equation (3.7) the estimate to the position of the platform's center point  $CP$  is determined by

$$\mathbf{r}_0^{circle} = \frac{1}{2} \begin{bmatrix} r_x^{1,3} + r_x^{2,4} \\ r_y^{1,2} + r_y^{3,4} \end{bmatrix} \quad (3.19)$$

with the  $x$ -components of equations (3.18) and (3.17) and the  $y$ -components of equations (3.15) and (3.16). It should be noted that the Circle Method as the Box Method involves only simple algebraic equation. The Circle Method's bounds  $\mathbf{r}^{1,2}$ ,  $\mathbf{r}^{1,3}$ ,  $\mathbf{r}^{2,4}$ , and  $\mathbf{r}^{3,4}$  enclose a smaller intersection region in which the center point  $CP$  is located and yields therefore a closer estimate to the platform's position  $\mathbf{r}$  than the Box Method. The validation of this hypothesis is explained in the appendix in section (7.1). However, the Circle Method does not give an estimate to the orientation of the CDPR's platform. Therefore the intersection region can look much different if the value of the rotation angle is  $\phi_z \neq 0^\circ$ . The applied bounds in equation (3.19) might even be not as accurate as others. To challenge this issue a more accurate estimate could be determined by calculating all intersection points and attempting to find the critical bounds dependent on the rotation. This approach leads to a much longer algorithm that possibly even involves loops in the implementation. Since the CDPR-based forward kinematics of the pelvic actuation system needs to fulfil real time constraints, the shown algorithm is chosen because of its simplicity and its briefness. Applying the Circle Method to the CDPR-based pelvic actuation system, the initial estimate of the Circle Method is obtained by

$$\mathbf{x}_0^{circle} = \begin{bmatrix} \mathbf{r}_0^{circle} \\ 0^\circ \end{bmatrix} \quad (3.20)$$

with the transverse rotation  $\phi_z = 0^\circ$  and  $\mathbf{r}_0^{circle}$  as the estimate of the pelvic position given by equation (3.19).

The Center Method, the Box Method, and the Circle Method provide the initial estimate  $\mathbf{x}_0$  for the iterative algorithms that aims to solve the CDPR-based forward kinematics in equation (2.13). Hence, the three estimation methods will be combined with the Levenberg-Marquardt algorithm and the Powell's Dog Leg algorithm respectively. The structure of the Levenberg-Marquardt and the Powell's Dog Leg algorithm is presented in the following section.

## 3.2 Iterative Optimization Algorithms

The two iterative optimization algorithms, Levenberg-Marquardt and Powell's Dog Leg, which shall solve the CDPR-based forward kinematics of the pelvic actuation

system, were introduced in subsection (2.3.1) together with the determination of their corresponding steps. This section explains the updating of the steps, the algorithms' structure and the stopping criteria according to [12].

### 3.2.1 Levenberg-Marquardt Algorithm

According to subsection (2.3.1) the Levenberg-Marquardt algorithm uses the damping parameter  $\mu$  to adapt the step  $\mathbf{h}_{LM}$  to the Gauss-Newton step  $\mathbf{h}_{GN}$  and to a step in the steepest descent direction  $\mathbf{h}_{SD}$ . The updating of  $\mu$  is controlled through the gain ratio

$$\rho = \frac{F(\mathbf{x}) - F(\mathbf{x} + \mathbf{h}_{LM})}{\frac{1}{2}\mathbf{h}_{LM}^T(\mu\mathbf{h}_{LM} - \mathbf{g})}. \quad (3.21)$$

During each iteration the gain ratio  $\rho$  compares  $\frac{1}{2}\mathbf{h}_{LM}^T(\mu\mathbf{h}_{LM} - \mathbf{g})$ , which is the linear model of  $\mathbf{f}$  in equation (2.12), to the objective function  $F$  in equation (2.14) resulting into two possible outcomes:

- (1)  $\forall \rho > 0 \quad \mu \downarrow$
- (2)  $\forall \rho \leq 0 \quad \mu \uparrow$

If outcome (1) occurs, the linear model of  $\mathbf{f}$  is a good estimation to the objective function  $F$ . Therefore the  $\mu$  is decreased to perform the next step rather as a Gauss-Newton step  $\mathbf{h}_{GN}$ . If outcome (2) occurs the linear model is a poor estimation to the objective function  $F$ . Therefore  $\mu$  is increased to perform a step closer to the steepest descent step direction  $\frac{1}{\mu}\mathbf{h}_{SD}$  and to decrease the step length. The algorithm's initial damping parameter  $\mu_0$  is received through

$$\mu_0 = \tau \max_j(a_{jj}^{(0)}), \quad (3.22)$$

with  $j \in \{1; \dots; n\}$  and  $a_{jj}^{(0)}$  being the components of the diagonal matrix of  $\mathbf{A}_0 = \mathbf{J}^T(\mathbf{x}_0)\mathbf{J}(\mathbf{x}_0)$ . The factor  $\tau$  is hereby chosen by the user and important for the algorithms parametrisation.

The Levenberg-Marquardt algorithm either iterates until the stopping criterion  $\|\mathbf{g}\|_\infty \leq \varepsilon_1$  is reached, or the change in  $\mathbf{x}$  is small which is reflected by  $\|\mathbf{x}_{new} - \mathbf{x}\|_2 \leq \varepsilon_2(\|\mathbf{x}\|_2 + \varepsilon_2)$ , or if the number of executed iterations  $k$  exceeds the maximum number of iterations  $k_{max}$  to avoid an infinite loop. The stopping criteria  $\varepsilon_1$ ,  $\varepsilon_2$ , and  $k_{max}$  are also user defined.

Having presented the updating of the damping parameter  $\mu$  and introduced the user defined parameters, the structure of the Levenberg-Marquardt is implemented for testing as summarized in table (3.1). The algorithm's structure is oriented to [12]. The

Levenberg Marquardt algorithm shall deliver the pelvic pose  $\mathbf{x}^*$  of the CDPR-based forward kinematics of the pelvic actuation system. Therefore the algorithm is combined with the initial estimate methods and applied to the forward kinematics. The structure of the Powell's Dog Leg algorithm is presented in the following subsection (3.2.2).

Sequence	Work Step
1	Definition of Inputs and Parameters: $k := 0; v := 2; \mathbf{x} := \mathbf{x}_0; \mathbf{A} := \mathbf{J}(\mathbf{x})^T \mathbf{J}(\mathbf{x}); \mathbf{g} := \mathbf{J}(\mathbf{x})^T \mathbf{f}(\mathbf{x});$ $\tau := \text{user defined}; \mu = \tau \max_i(a_{ii}); k_{\max} := \text{user defined}$
2	Definition of first stopping criterion <b>if</b> ( $\ \mathbf{g}\ _\infty \leq \varepsilon_1$ ) $\text{found} = \text{true}$ <b>else</b> $\text{found} = \text{false}$ <b>end</b>
3	Iterative Optimization <b>while</b> ( <b>not</b> $\text{found}$ <b>and</b> $k < k_{\max}$ ) $k := k + 1;$ Solve $(\mathbf{A} + \mu \mathbf{A}_D) \mathbf{h}_{LM} = -\mathbf{g}$ Definition of second stopping criterion <b>if</b> ( $\ \mathbf{h}_{LM}\ _2 \leq \varepsilon_2 (\ \mathbf{x}\ _2 + \varepsilon_2)$ ) $\text{found} = \text{true}$ <b>else</b> $\mathbf{x}_{new} := \mathbf{x} + \mathbf{h}_{LM}$ Determining Gain Ratio $\rho$ through equation (3.21) <b>if</b> ( $\rho > 0$ ) $\mathbf{x} := \mathbf{x}_{new}$ $\mathbf{A} := \mathbf{J}(\mathbf{x})^T \mathbf{J}(\mathbf{x}); \mathbf{g} := \mathbf{J}(\mathbf{x})^T \mathbf{f}(\mathbf{x})$ <b>if</b> ( $\ \mathbf{g}\ _\infty \leq \varepsilon_1$ ) $\text{found} = \text{true}$ <b>else</b> $\text{found} = \text{false}$ <b>end</b> $\mu := \mu \max(\frac{1}{3}, 1 - (2\rho - 1)^3); v := 2$ <b>else</b> $\mu := \mu v; v := 2v$ <b>end</b> <b>end</b> <b>end</b>

**Table 3.1:** Levenberg-Marquardt Algorithm

### 3.2.2 Powell's Dog Leg Algorithm

In subsection (2.3.1) it is introduced that the Powell's Dog Leg step  $\mathbf{h}_{DL}$  is chosen between the two possible steps  $\mathbf{a} = \alpha \mathbf{h}_{SD}$  in steepest descent direction and the Gauss-Newton step  $\mathbf{b} = \mathbf{h}_{GN}$  using the trust region's radius  $\Delta$  which also limits the step's maximum size to even that radius  $\Delta$ . This is conducted through the procedure shown in table (3.2).

Sequence	Work Step
1	Dog Leg step is Gauss-Newton step <b>if</b> ( $\ \mathbf{b}\ _2 \leq \Delta$ ) $\mathbf{h}_{DL} := \mathbf{b}$ $L(\mathbf{0}) - L(\mathbf{h}_{DL}) = F(\mathbf{x})$
2	Dog Leg step is in steepest descent direction with size $\Delta$ <b>elseif</b> ( $\ \mathbf{a}\ _2 \geq \Delta$ ) $\mathbf{h}_{DL} := \left( \frac{\Delta}{\ \mathbf{h}_{SD}\ _2} \right) \mathbf{h}_{SD}$ $L(\mathbf{0}) - L(\mathbf{h}_{DL}) = \frac{\Delta(2\ \mathbf{a}\ _2 - \Delta)}{2\alpha}$
3	Dog Leg step is combination of $\mathbf{a}$ and $\mathbf{b}$ with size $\Delta$ <b>else</b> $\mathbf{h}_{DL} := \mathbf{a} + \beta(\mathbf{b} - \mathbf{a})$ $L(\mathbf{0}) - L(\mathbf{h}_{DL}) = \frac{1}{2}\alpha(1 - \beta)^2\ \mathbf{g}\ _2^2 + \beta(2 - \beta)F(\mathbf{x})$ <b>end</b>

**Table 3.2:** Dog Leg Step

Using  $c = \mathbf{a}^T(\mathbf{b} - \mathbf{a})$ , the factor  $\beta$  in the third sequence of table (3.2) ensures the step size  $\Delta$  through the procedure in table (3.3).

Sequence	Work Step
1	<b>if</b> ( $c \leq 0$ ) $\beta = \frac{-c + \sqrt{c^2 + \ \mathbf{b} - \mathbf{a}\ _2^2(\Delta^2 - \ \mathbf{a}\ _2^2)}}{\ \mathbf{b} - \mathbf{a}\ _2^2}$
2	<b>else</b> $\beta = \frac{\Delta^2 - \ \mathbf{a}\ _2^2}{c + \sqrt{c^2 + \ \mathbf{b} - \mathbf{a}\ _2^2(\Delta^2 - \ \mathbf{a}\ _2^2)}}$

**Table 3.3:** Determination of  $\beta$

Besides choosing the step  $\mathbf{h}_{DL}$  the linear model  $L(\mathbf{0}) - L(\mathbf{h}_{DL})$  of  $\mathbf{f}$  to determine the gain ratio  $\rho$  is also chosen in the procedure in table (3.2). Similar to the Levenberg-Marquardt algorithm the gain ratio

$$\rho = \frac{F(\mathbf{x}) - F(\mathbf{x} + \mathbf{h}_{DL})}{L(\mathbf{0}) - L(\mathbf{h}_{DL})} \quad (3.23)$$

controls the updating of the radius  $\Delta$  for the next iteration. As the Levenberg-Marquardt the Powell's Dog Leg stops if the maximum number of iterations  $k_{max}$  is exceeded. Contrary to the Levenberg-Marquardt the Powell's Dog Leg has three stopping criteria  $\|\mathbf{g}\|_\infty \leq \varepsilon_1$ ,  $\Delta \leq \varepsilon_2(\|\mathbf{x}\|_2 + \varepsilon_2)$ , and  $\|\mathbf{f}(\mathbf{x})\|_\infty \leq \varepsilon_3$  because of the Powell's Dog Leg specific radius of the trust region  $\Delta$ . The entire structure of the Powell's Dog Leg algorithm is summarized in table (3.4).

### 3 Proposed Solution

---

Sequence	Work Step
1	Definition of Inputs and Parameters: $k := 0; \mathbf{x} := \mathbf{x}_0; \mathbf{g} := \mathbf{J}(\mathbf{x})^T \mathbf{f}(\mathbf{x}); k_{max} := \text{user defined}; \Delta := \text{user defined}$
2	Definition of stopping criteria <b>if</b> ( $\ \mathbf{g}\ _\infty \leq \varepsilon_1$ <b>or</b> $\ \mathbf{f}(\mathbf{x})\ _\infty \leq \varepsilon_3$ ) <i>found</i> = <b>true</b> <b>else</b> <i>found</i> = <b>false</b> <b>end</b>
3	Iterative Optimization <b>while</b> ( <b>not</b> <i>found</i> <b>and</b> $k < k_{max}$ ) $k := k + 1$ ; Compute $\alpha$ through equation (2.22); $\mathbf{h}_{SD} := -\mathbf{g}$ ; Determine $\mathbf{h}_{GN}$ by solving equation (2.19) Compute $\mathbf{h}_{DL}$ by table (3.2) Definition of stopping criterion <b>if</b> ( $\ \mathbf{h}_{DL}\ _2 \leq \varepsilon_2 (\ \mathbf{x}\ _2 + \varepsilon_2)$ ) <i>found</i> := <b>true</b> <b>else</b> $\mathbf{x}_{new} := \mathbf{x} + \mathbf{h}_{DL}$ Determination of gain ratio $\rho$ through equation (3.23) <b>if</b> ( $\rho > 0$ ) $\mathbf{x} := \mathbf{x}_{new}; \mathbf{g} := \mathbf{J}(\mathbf{x})^T \mathbf{f}(\mathbf{x})$ <b>if</b> ( $\ \mathbf{g}\ _\infty \leq \varepsilon_1$ <b>or</b> $\ \mathbf{f}(\mathbf{x})\ _\infty \leq \varepsilon_3$ ) <i>found</i> := <b>true</b> <b>else</b> <i>found</i> := <b>false</b> <b>end</b> <b>if</b> ( $\rho > 0.75$ ) $\Delta := \max(\Delta, 3\ \mathbf{h}_{DL}\ _2)$ <b>elseif</b> ( $\rho < 0.25$ ) $\Delta := \frac{\Delta}{2}$ <b>if</b> ( $\Delta \leq \varepsilon_2 (\ \mathbf{x}\ _2 + \varepsilon_2)$ ) <i>found</i> := <b>true</b> <b>else</b> <i>found</i> := <b>false</b> <b>end</b> <b>end</b> <b>end</b> <b>end</b> <b>end</b>

**Table 3.4:** Powell's Dog Leg Algorithm

The Powell's Dog Leg is combined with the initial estimate methods to solve the CDPR-based forward kinematics of the pelvic actuation system in the following sections.

### 3.3 Standard Forward Kinematics Algorithms

The desired pose  $\mathbf{x}^*$  of the pelvis is determined through the forward kinematics based on the SKM for the CDPR-based pelvic actuation system, actuating  $n = 3$  degrees of freedom via  $m = 4$  cables, by iteratively altering the initial estimate  $\mathbf{x}_0$  through the Levenberg-Marquardt or the Powell's Dog Leg algorithm. Therefore to utilize the algorithms the cable length error  $f_{SKM} : \mathbb{R}^3 \rightarrow \mathbb{R}^4$  based on the SKM in equation (2.12) is applied to  $\mathbf{f}$  in equation (2.15) to yield the objective function  $F : \mathbb{R}^4 \rightarrow \mathbb{R}$  for the optimization problem of the CDPR-based forward kinematics in equation (2.13). Hence, the standard cable vector  $\mathbf{l}_{SKM,i}$  in equation (2.2) only depends on the position  $\mathbf{r} = [r_x; r_y]^T$  and the transverse rotation  $\phi_z$  performed by a  $2 \times 2$  rotational matrix

$$\mathbf{R}_{2 \times 2} = \begin{bmatrix} \cos(\phi_z) & -\sin(\phi_z) \\ \sin(\phi_z) & \cos(\phi_z) \end{bmatrix}. \quad (3.24)$$

Applying equation (2.3) therefore yields the cable length

$$\begin{aligned} l_{SKM,i} &= \left\| \begin{bmatrix} l_{SKM,ix} \\ l_{SKM,iy} \end{bmatrix} \right\|_2 = \left\| \begin{bmatrix} a_{ix} - r_x - \cos(\phi_z)b_{ix} + \sin(\phi_z)b_{iy} \\ a_{iy} - r_y - \sin(\phi_z)b_{ix} - \cos(\phi_z)b_{iy} \end{bmatrix} \right\|_2 \\ &= \sqrt{l_{SKM,ix}^2 + l_{SKM,iy}^2} \end{aligned} \quad (3.25)$$

for the CDPR-based pelvic actuation system. The cable length error  $f_{SKM}$  is then obtained through

$$f_{SKM}(\mathbf{x}) = \begin{bmatrix} f_{SKM,1} \\ f_{SKM,2} \\ f_{SKM,3} \\ f_{SKM,4} \end{bmatrix} = \begin{bmatrix} l_{SKM,1} - l_{act,1} \\ l_{SKM,2} - l_{act,2} \\ l_{SKM,3} - l_{act,3} \\ l_{SKM,4} - l_{act,4} \end{bmatrix}. \quad (3.26)$$

Applying the cable length error in equation (3.26) to equation (2.15) transforms the Jacobian matrix in equation (2.16) under the consideration of  $n = 3$  degrees of freedom and  $m = 4$  cables to the  $4 \times 3$  Jacobian matrix

$$\mathbf{J}(\mathbf{x}) = \begin{bmatrix} \frac{\partial f_1}{\partial r_x} & \frac{\partial f_1}{\partial r_y} & \frac{\partial f_1}{\partial \phi_z} \\ \frac{\partial f_2}{\partial r_x} & \frac{\partial f_2}{\partial r_y} & \frac{\partial f_2}{\partial \phi_z} \\ \frac{\partial f_3}{\partial r_x} & \frac{\partial f_3}{\partial r_y} & \frac{\partial f_3}{\partial \phi_z} \\ \frac{\partial f_4}{\partial r_x} & \frac{\partial f_4}{\partial r_y} & \frac{\partial f_4}{\partial \phi_z} \end{bmatrix}. \quad (3.27)$$

### 3 Proposed Solution

---

This Jacobian matrix contains the first partial derivatives of  $\mathbf{f} = [f_1, f_2, f_3, f_4]^T$  in equation (2.15) derived by the components of the pelvic pose  $\mathbf{x} = [r_x, r_y, \phi_z]^T$  in equation (3.1) obtained through

$$\frac{\partial f_i}{\partial r_x} = -\frac{l_{SKM,ix}}{l_{SKM,i}} \quad \frac{\partial f_i}{\partial r_y} = -\frac{l_{SKM,iy}}{l_{SKM,i}} \quad \frac{\partial f_i}{\partial \phi_z} = \frac{l_{SKM,ix} \frac{\partial l_{SKM,ix}}{\partial \phi_z} + l_{SKM,iy} \frac{\partial l_{SKM,iy}}{\partial \phi_z}}{l_{SKM,i}} \quad (3.28)$$

with  $\frac{\partial l_{SKM,ix}}{\partial \phi_z}$  and  $\frac{\partial l_{SKM,iy}}{\partial \phi_z}$  being the partial derivations of the  $x$ - and  $y$ -components of equation (3.25) by  $\phi_z$  determined through

$$\frac{\partial l_{SKM,ix}}{\partial \phi} = \sin(\phi_z)b_{ix} + \cos(\phi_z)b_{iy} \quad \frac{\partial l_{SKM,iy}}{\partial \phi} = -\cos(\phi_z)b_{ix} + \sin(\phi_z)b_{iy}. \quad (3.29)$$

Having received the Jacobian matrix  $\mathbf{J}$  in equation (3.27) and having applied the cable length error  $\mathbf{f}_{SKM}$  in equation (3.26) to  $\mathbf{f}$  in equation (2.15), either the Levenberg-Marquardt algorithm, as described in table (3.1), or the Powell's Dog Leg as described in table (3.4) can be used to determine the pose  $\mathbf{x}^*$  of the pelvis with an initial estimate  $\mathbf{x}_0$  either evaluated by the Center Method in equation (3.2) or the Box Method in equation (3.7) or the Circle Method in equation (3.20) creating six combination of standard forward kinematics algorithm. These six combinations are tested in chapter (4).

In subsection (2.3.1) it was pointed out that the standard forward kinematics algorithms are prospectively real-time feasible but might not be applicable to the pelvic actuation system because of influences on the system's accuracy.

## 3.4 Consideration of Influences affecting the System's Accuracy

The possible influences on the pelvic actuation system's accuracy were summarized in table (2.1) and are now revisited and analysed.

Considering the cable properties, elasticity can have a non-negligible impact on the CDPR-based pelvic actuation system, modelled by the SKM, since the control modes of the assist-as-needed paradigm cannot function properly if the cables are elongated. Implementing a robot model, that takes cable elasticity into account could challenge this issue but would further complicate the model which should be avoided because of the real-time constraints as referred to [24]. To overcome the problem of cable elasticity, the pelvic acutation system is instead designed with cables made of dyneema fiber. Such cables shall have an elongation smaller than 1% under extreme conditions according to [9]. Also, the cable forces during a gait rehabilitation training

are assumed to be rather small, so that elongation should be negligible. However, to proof that the cable's elasticity is insignificant it is tested in subsection (3.4.1). Another cable property influence that can occur is creep but the system shall be calibrated during each rehabilitation training session in a defined position. Furthermore creep emerges if a material is exhibited to a permanent load but the CDPR-based system is only used during terminated periods of time. Thus, creep is a factor that is neglected. Deflection due to gravitational effects on the cable should also be negligible due to the cable's low dead weight according to [9] but is shortly analysed in subsection (3.4.2). Cable torsion is considered in [5] and geometrical deformation leading to cable ovalization in [24] but both are not part of this thesis. Cable wear is excluded but the cable's condition should be checked during each rehabilitation training session. Hysteresis is also unnecessary to take into account because the occurring load as well as the pretension of the cables are rather small. Temperature influences could happen if the cables are heated due to fast coiling and uncoiling. This heating might alter the cable properties but the pelvic movements are small and comparatively slow leading to small cable velocities so that heating cannot occur. Cable bending stiffness is also insignificant because the bending of the cables are not close to their minimum physical bending radius.

Considering drive train influences, manufacturing inaccuracies of the drive train components always have an impact but this impact is limited to a minimum because the cable winches were manufactured by CNC machines and the drives' manufacturing is also conforming to industrial standards. Additionally the drive train is designed with as few components as possible. Gears and pulleys for example do not belong to the drive train. Therefore inaccuracies due to friction are also limited and gear backlashes are not existent. The stiffness of the drive train should have no influence on the accuracy because the setup of the system is particularly rigid. Hysteresis in cable positioning exists but is already considered in [5] and therefore not taken into account. Coiling errors cannot occur because they are excluded through the design of the cable winches in [5]. The effects of a non-linear cable length to drive ratio are not part of this thesis. Errors in cable length due to an insufficient motor resolution are negligible. Since the drive train does not have any gears the motor torque can be directly used to alter the cable lengths through the winches. Each synchronous motor MSM031C-0300-NN-M5-MH1 possesses a multturn absolute optical encoder with a 20 bit resolution and each winch has a radius  $r_d = 2\text{ cm}$ . Therefore the motor is able to actuate the minimal cable length

$$l_{min} = 2\text{ cm} \frac{2\pi}{2^{20}} = 0.12\text{ }\mu\text{m}, \quad (3.30)$$

which is that small that the motor resolution should not cause any issues on position accuracy of the pelvic actuation system. The data sheet of the motor is given in [2].

### 3 Proposed Solution

---

Considering platform and frame influences, the setup of the frame can cause inaccuracies but the entire design of the pelvic actuation system in [5] is as stiff and robust as possible. Errors might occur due to the fact that the human pelvis is not rigid but rather soft but these errors are not considered in this thesis. Geometrical issues might arise if the pelvis is in a singular position. These singularities occur if two cables are on one line. Considering figure (2.2), a singularity appears if the pelvis moves too close to the sides of the rectangle configuration but such singularities should not occur because the assist-as-needed paradigm seeks to hold the human in a shell around the centre of the CDPR.

An important influence are the cable exit points on the winches' drum. The SKM does not consider the radius  $r_d$  of the drum. In fact the SKM considers the actuators  $A_i$  even as point shaped. So the forward kinematics works with cable length that differ from the inverse kinematics of the SKM in equation (2.5) possibly causing significant positioning errors. To deal with that influence an Extended Kinematic Model (EKM) also considering the radius  $r_d$  of the drum is introduced in chapter (3) and the impact of cable lengths differing from the inverse kinematics in equation (2.5) on a SKM-based forward kinematics algorithm examined.

Another influence on the pelvic actuation system's accuracy concerns the pelvic movements. A general pelvic movement with six degrees of freedom involves translations in all three directions, the pelvic drop  $\phi_x$ , the anterior tilt  $\phi_y$ , and the transverse rotation  $\phi_z$ . This could possibly cause positioning inaccuracies since the CDPR-based pelvic system only actuates the planar pelvic pose  $\mathbf{x} = [r_x, r_y, \phi_z]^T$  neglecting the pelvic drop  $\phi_x$ , the anterior tilt  $\phi_y$ , and the translation  $r_z$ . To determine the extent of this inaccuracy, a standard forward kinematic algorithm exerted to cable lengths  $\mathbf{l}_{act}$  determined through the inverse kinematic solution  $\mathbf{q}_{SKM}$  of the SKM with six degrees of freedom is implemented and tested in chapter (4). For this simulation the dimension of the standard cable vector  $\mathbf{l}_{SKM,i}$  in equation (2.2) is three-dimensional consisting of  $x$ -,  $y$ -, and  $z$ -components and the  $3 \times 3$  rotation matrix  $\mathbf{R}$  in equation (2.1) is applied to consider the spatial orientation of the pelvis.

The following two subsections analyse the cable elasticity and the impact of cable deflection due to gravitational effects.

#### 3.4.1 Cable Elasticity

As emphasized above, the cable elasticity can cause serious errors to position accuracy. Therefore the used dyneema cables are submitted to tests in order to achieve a rough insight into their elastic behaviour. The testing setup is designed to measure the length of the dyneema cable exerted to one specific load and comparing this cable length to the length of the cable exerted to a different load. The loads and the corresponding cable lengths are listed as results in table (3.5).

Test Row	1		2	
Loads [kg]	0	21.9	1	21
Measured Cable Length [cm]	27.1	27.1	20.6	20.6

**Table 3.5:** Experimental Results Cable Elasticity

Considering the experimental results in table (3.5), the cable load in test row 1 amounts 0kg and 21.9kg whereas in test row 2 the cable load amounts 1kg and 21kg. Applying Newton's law  $F_G = mg$ , these loads correspond to the forces in equation (3.31):

$$\begin{aligned} \text{test row 1} \quad F_{G,0} &= 0\text{kg} \cdot 9.81 \frac{\text{m}}{\text{s}^2} = 0\text{N}, \quad F_{G,21.9} = 21.9\text{kg} \cdot 9.81 \frac{\text{m}}{\text{s}^2} = 214.8\text{N} \\ \text{test row 2} \quad F_{G,1} &= 1\text{kg} \cdot 9.81 \frac{\text{m}}{\text{s}^2} = 9.81\text{N}; \quad F_{G,20} = 20\text{kg} \cdot 9.81 \frac{\text{m}}{\text{s}^2} = 196.2\text{N} \end{aligned} \quad (3.31)$$

Applying the calculated forces in equation (3.31) to the actuation system, they can be considered as cable forces. If elongation occurs the cable length between the two different forces in each test row has to change. However looking at the measured cable lengths in table (3.5), a changing cable length in the range of millimetres cannot be detected even under high forces such as  $F_{G,21.9} = 214.8\text{N}$  or  $F_{G,20} = 196.2\text{N}$ . These forces are also much higher than the targeted maximum cable force of 65N for the pelvic actuation system. Therefore cable elasticity has a negligible effect on the CDPR and cannot influence the actuation system's accuracy. It should also be noted that in gait rehabilitation such high forces as determined in equation (3.31) are unlikely to appear. Usually the cable forces are much smaller. In the next subsection the possible influence of deflecting cables due to gravitational effects is analytically analysed.

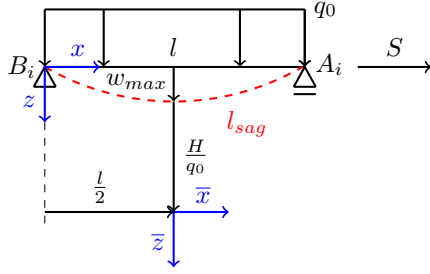
### 3.4.2 Deflection due to Gravitational Effects

The impact of gravitation is not to underestimate. The forward kinematics algorithms operate with the cable lengths  $l_{act,i}$  measured by the encoder. Due to the cable's dead weight, cable sagging can occur. This sagging is not taken into account in neither the standard forward kinematics nor the extended forward kinematics algorithm possibly influencing the systems accuracy. To check the impact of the cable sagging the maximum sag  $w_{max}$  is determined followed by the calculation of the length of a sagging cable  $l_{sag}$  via the catenary according to [7].

Depicted in figure (3.3), a cable of the CDPR-based pelvic actuation system under the influence of its dead weight can be modelled as a string pretensioned through the force  $S$  with a fixed and a floating bearing representing the actuator  $A_i$  and the cable

### 3 Proposed Solution

---



$A_i$	actuator	$l$	unsagging cable length
$B_i$	cable attachment	$l_{sag}$	sagging cable length
$H$	horizontal pull	$q_0$	distributed load
$S$	pretension	$w_{max}$	maximum sag

**Figure 3.3:** Cable Sagging

attachment point  $B_i$  respectively. The string is exerted to a constant distributed load  $q_0$  representing the dead weight. The cable length  $l$  corresponds to the distance between  $B_i$  and  $A_i$  and can be obtained by the inverse kinematic solution of the SKM if the dead weight and the resulting sagging is neglected. Otherwise the cable length corresponds to the dashed catenary which maximum sag  $w_{max}$  occurs at  $x = \frac{l}{2}$ . The cable's deflection  $w(x)$  due to the distributed load  $q_0$  is given through the equilibrium

$$\frac{d^2w}{x^2}(x) = -\frac{q_0}{S}. \quad (3.32)$$

Integrating equation (3.32) twice with the boundary conditions  $w(x=0) = 0$  and  $w(x=l) = 0$  yields the cable deflection

$$w(x) = \frac{q_0 l^2}{2S} \left( \frac{x}{l} - \left( \frac{x}{l} \right)^2 \right). \quad (3.33)$$

Applying equation (3.33) with  $x = \frac{l}{2}$  yields the cable's maximum sagging

$$w_{max} = \frac{q_0 l^2}{8S}. \quad (3.34)$$

The length of the sagging cable  $l_{sag}$  is determined through the catenary. Therefore figure (3.3) is now considered in the coordinate frame  $(\bar{x}, \bar{z})$ . The catenary

$$\bar{z}(\bar{x}) = \frac{H}{q_0} \cosh \left( \frac{q_0}{H} \bar{x} \right) \quad (3.35)$$

### 3.4 Consideration of Influences affecting the System's Accuracy

---

is adjusted to the given case through the boundary condition

$$\bar{z} \left( \frac{l}{2} \right) = \frac{H}{q_0} + w_{max} \quad (3.36)$$

with  $H$  being the unknown horizontal pull of the cable. Inserting equation (3.35) in the boundary condition (3.36) and defining  $u := \frac{q_0 l}{2H}$  obtains the relationship

$$\cosh(u) = 2 \frac{w_{max}}{l} u + 1. \quad (3.37)$$

In order to find the horizontal pull  $H$ , the associated  $u_{krit}$  needs to be determined by solving equation (3.37). This can only be conducted either graphically or numerically. Having determined  $u_{krit}$ , the horizontal pull is received through

$$H = \frac{q_0 l}{2u_{krit}}. \quad (3.38)$$

Taking the symmetry of the configuration in figure (3.3) into account the length of the sagging cable  $l_{sag}$  is then obtained by

$$l_{sag} = 2 \left[ \frac{H}{q_0} \sinh \left( \frac{q_0}{H} (\bar{x}) \right) \right]_{\bar{x}=0}^{\bar{x}=\frac{l}{2}}. \quad (3.39)$$

To apply the equations above to the pelvic actuation system the inverse kinematic solution of the SKM for the exemplary pose  $\mathbf{x} = [-0.4 \text{ m}; -0.4 \text{ m}; -20^\circ]$  is calculated through equation (2.5) resulting in

$$\mathbf{q}_{SKM} = \begin{bmatrix} 21.491984 \text{ cm} \\ 82.308984 \text{ cm} \\ 88.472212 \text{ cm} \\ 134.200268 \text{ cm} \end{bmatrix}. \quad (3.40)$$

The standard cable length  $l_{SKM,4} = 134.200268 \text{ cm}$  is an especially long cable and its sagging is to be investigated. The dyneema cable's weight per metre is  $\gamma_d = 0.0013 \frac{\text{kg}}{\text{m}}$  according to [9]. Therefore the distributed load due to the cable's dead weight is

$$q_0 = \gamma_d g = 0.01275 \frac{\text{N}}{\text{m}}. \quad (3.41)$$

Assuming the cable's pretension  $S = 5 \text{ N}$ , equation (3.34) yields with the cable length  $l = l_{SKM,4} = 134.200268 \text{ cm}$  the maximum sagging

### 3 Proposed Solution

---

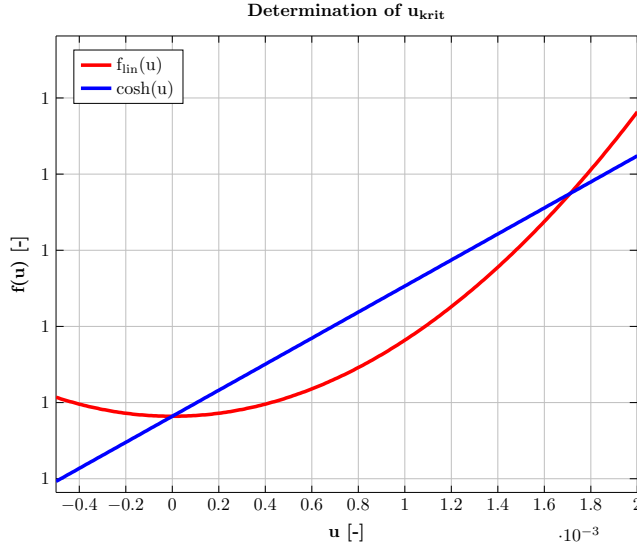


**Figure 3.4:** Determining  $u_{krit}$

$$w_{max} = 0.5719 \text{ mm.} \quad (3.42)$$

To determine the horizontal pull  $H$ , the parameter  $u_{krit}$  is received by solving equation (3.37) graphically, as depicted in figure (3.4) with  $f_{lin}(u) = 2 \frac{w_{max}}{l} u + 1$ , yielding

$$u_{krit} \approx 0.00173. \quad (3.43)$$

With the graphically determined value  $u_{krit}$  in equation (3.43) the horizontal pull

$$H = 4.946 \text{ N} \quad (3.44)$$

is obtained by applying equation (3.38). Inserting equation (3.44) and the cable length  $l = l_{SKM,4} = 134.200\,268 \text{ cm}$  into equation (3.39) obtains the sagging cable length

$$l_{sag} = 134.200\,335 \text{ cm.} \quad (3.45)$$

The difference  $\Delta l$  between the cable length  $l_{SKM,4} = 134.200\,268 \text{ cm}$  determined through the SKM and the cable length  $l_{sag}$  under the influence of the cable's dead weight is

$$\Delta l = l_{sag} - l_{SKM,4} = 67 \mu\text{m.} \quad (3.46)$$

This cable error  $\Delta l$  due to the influence of cable's dead weight ranges in the size of micrometres. The forward kinematics algorithms are parametrised to tolerate cable errors smaller than 0.1 mm. Therefore the influence of cable deflection due to gravitational forces with a pretension 5 N can be neglected.

Having analysed the influences on the CDPR-based pelvic actuation system, it is concluded that the only two influences possibly affecting the accuracy are the impact of the drum's radius  $r_d$  and general pelvic movements. To deal with the drum's radius  $r_d$ , the Extended Kinematic Model (EKM) is introduced in the following section.

### 3.5 Extended Kinematic Model

As discussed in subsection (2.3.2), neglecting the drum's radius  $r_d$  might cause serious errors to position accuracy if the forward kinematics of the pelvic actuation system is only based on the simple SKM elaborated in section (3.3). Therefore this section presents a new model that eliminates such accuracy errors by taking into account the drum's kinematics. This model is closely related to a model proposed in [21] which considers the kinematics of pulleys in CDPRs but the to be presented model focuses only on the effects due to the drum's kinematics.

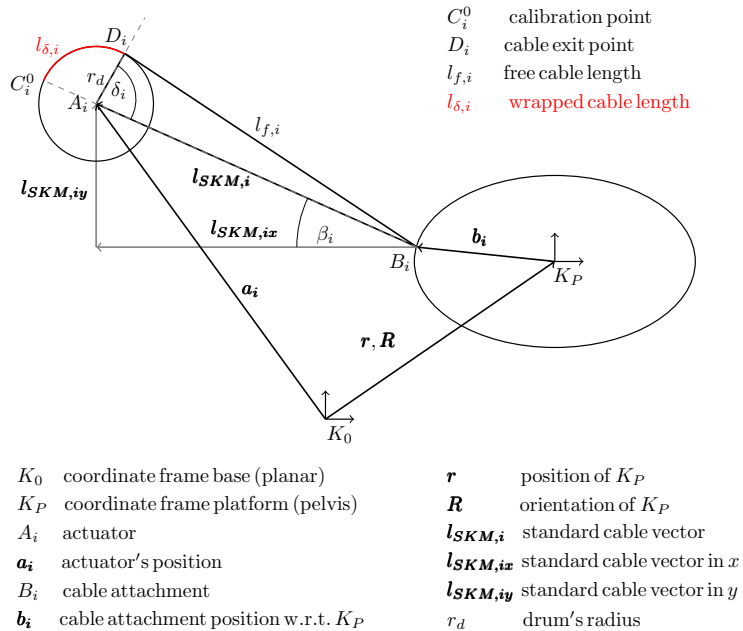


**Figure 3.5:** Extended Kinematic Model (planar)

Contrary to the SKM in subsection (2.2.1), this model is only derived for the planar case. Depicted in figure (3.5), the Extended Kinematic Model (EKM) adopts the no-

### 3 Proposed Solution

---

tations of the SKM in figure (2.3). In fact the EKM incorporates the planar SKM, as proven in the appendix in section (7.2), and adapts it to the new kinematics. The drum is illustrated as a circle with the drum's radius  $r_d$  around point  $A_i$  that belongs to the position  $\mathbf{a}_i$  of the actuator. The cable length  $l_{\delta,i}$  is wrapped around the drum and is always considered between the fixed calibration point  $C_i^0$  and the varying point  $D_i$  where the cable exits the drum. The free cable length  $l_{f,i}$  describes the cable length between  $D_i$  and the cable attachment point  $B_i$ . Since the triangle  $\triangle A_i B_i D_i$  is rectangular the free cable length  $l_{f,i}$  is determined applying Pythagoras theorem with the standard cable length  $l_{SKM,i}$  from equation (2.3) and the drum's radius  $r_d$  resulting in

$$l_{f,i} = \sqrt{l_{SKM,i}^2 - r_d^2}. \quad (3.47)$$

The cable length  $l_{\delta,i}$  is determined using the angle  $\delta_i$  which is obtained through

$$\delta_i = \arccos\left(\frac{r_d}{l_{SKM,i}}\right) \quad (3.48)$$

applying the drum's radius  $r_d$  and the standard cable length  $l_{SKM,i}$  in equation (3.25). With the drum's radius  $r_d$  and the angle  $\delta_i$  in equation (3.48) the cable length  $l_{\delta,i}$  is yielded by

$$l_{\delta,i} = (\pi - \delta_i)r_d. \quad (3.49)$$

Simply adding equations (3.47) and (3.49) does not result in the entire cable length  $l_{EKM,i}$  of the EKM, because applying equation (3.49) in a different pose obtains a cable length  $l_{\delta,i}$  which does not start at the calibration point  $C_i^0$  but at a new point  $C_i^{new}$ . Therefore a correcting factor  $l_{corr,i}$  needs to be incorporated taking into account this deviation of the cable length  $l_{\delta,i}$ .

The correcting factor  $l_{corr,i}$  is determined through a comparison between a calibration pose, which is in the case of the pelvic actuation system the pose  $\mathbf{x} = [0\text{m}, 0\text{m}, 0^\circ]^T$ , when all cable lengths are equally long, and a new pose. Depicted in figure (3.6), the dashed blue lines belong to the calibration pose whereas the black lines represent the new pose. The cable length  $l_{\delta,i}$  is always calibrated at point  $C_i^0$  generated by the intersection of the drum's edge and the line generated if the standard cable length  $l_{SKM,i}^0$  would be lengthened to the edge of the drum. In a new pose the line of the lengthened standard cable length  $l_{SKM,i}$  intersects with the drum's edge in  $C_i^{new}$  obviously differing from  $C_i^0$  as shown in figure (3.6). This cable length between  $C_i^0$  and  $C_i^{new}$  is the correcting cable length  $l_{corr,i}$ . In order to find that length the calibration angle

$$\beta_i = \arctan\left(\frac{l_{SKM,iy}^0}{l_{SKM,ix}^0}\right) \quad (3.50)$$

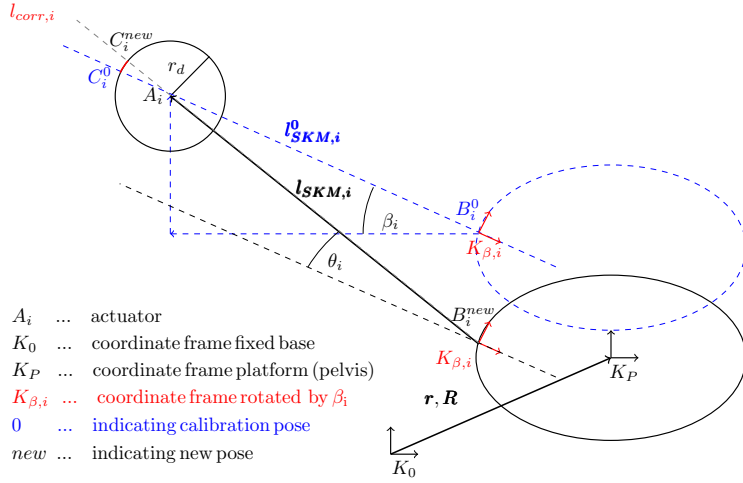


Figure 3.6: Correcting Factor

is determined for the calibration pose  $\mathbf{x} = [0\text{m}, 0\text{m}, 0^\circ]^T$  through the  $x$ - and  $y$ -components of  $l_{SKM,i}^0$ . Applying coordinate frame  $K_{\beta,i}$  which is fixed to the platform's attachment point  $B_i$  and rotated by the calibration angle  $\beta_i$ , yields through the angle  $\theta_i$  the standard cable vector  $l_{SKM,i}$  in the coordinate frame  $K_{\beta,i}$ . Thus, the standard cable vector  $l_{SKM,i}$  with reference to  $K_0$  can be transformed to the standard cable vector  $l_{SKM,i,\beta}$  with reference to coordinate frame  $K_\beta$  by applying a  $2 \times 2$  rotation matrix dependent on the calibration angle  $\beta_i$  in equation (3.50) resulting in

$$l_{SKM,i,\beta} = \begin{bmatrix} l_{SKM,i,\beta,x} \\ l_{SKM,i,\beta,y} \end{bmatrix} = \begin{bmatrix} \cos(-\beta_i) & -\sin(-\beta_i) \\ \sin(-\beta_i) & \cos(-\beta_i) \end{bmatrix} l_{SKM,i}. \quad (3.51)$$

Applying equation (3.51), the angle  $\theta_i$  is obtained by

$$\theta_i = \text{atan} \left( \frac{l_{SKM,i,\beta,y}}{l_{SKM,i,\beta,x}} \right) \quad (3.52)$$

to receive with the angle  $\theta_i$  the correcting cable length  $l_{corr,i}$  determined by

$$l_{corr,i} = -\chi_i r_d \theta_i \quad (3.53)$$

with  $\chi_i$  being the positive ( $\chi_i = 1$ ) or the negative ( $\chi_i = -1$ ) rotation direction of the actuator. Hence the cable length  $l_{EKM,i}$  of the EKM is yielded with the free cable length  $l_{f,i}$  in equation (3.47), the wrapped cable length  $l_{\delta,i}$  in equation (3.49), and the correcting factor  $l_{corr,i}$  in equation (3.53) as

$$l_{EKM,i} = l_{f,i} + l_{\delta,i} + l_{corr,i}. \quad (3.54)$$

### 3 Proposed Solution

---

Using equation (3.54) the inverse kinematics of the EKM is obtained through

$$\mathbf{q}_{EKM} = \begin{bmatrix} l_{EKM,i} \\ \vdots \\ l_{EKM,m} \end{bmatrix} \quad (3.55)$$

Applying equation (3.55) to the pelvic actuation system with  $m = 4$  cables the inverse kinematic solution of the EKM yields

$$\mathbf{q}_{EKM} = \begin{bmatrix} l_{EKM,1} \\ l_{EKM,2} \\ l_{EKM,3} \\ l_{EKM,4} \end{bmatrix}. \quad (3.56)$$

To utilize the EKM for the CDPR-based forward kinematics of the pelvic actuation system, the cable length error  $\mathbf{f}_{EKM} : \mathbb{R}^3 \rightarrow \mathbb{R}^4$  between the cable length  $\mathbf{l}_{act}$  measured by the encoder and the inverse kinematics solution of the EKM  $\mathbf{q}_{EKM}$  in equation (3.56) is received similar to the SKM in equation (2.12) through

$$\mathbf{f}_{EKM} = \mathbf{q}_{EKM} - \mathbf{l}_{act} \quad (3.57)$$

By applying this cable length error  $\mathbf{f}_{EKM}$  in equation (3.57) with the error vector

$$\mathbf{f} = \mathbf{f}_{EKM}(\mathbf{x}). \quad (3.58)$$

to the objective function  $F : \mathbb{R}^4 \rightarrow \mathbb{R}$  in equation (2.14) results in the optimization problem of the CDPR-based forward kinematics in equation (2.13) only this time based on the EKM instead of the SKM. This optimization problem is solved by the extended forward kinematics algorithms described in the following section (3.6).

## 3.6 Extended Forward Kinematics Algorithms

Equally to the standard forward kinematics algorithms in section (3.3) the forward kinematics based on the EKM requires an initial estimate  $\mathbf{x}_0$  which is iteratively altered until the pelvic pose  $\mathbf{x}^*$  is determined. For the determination of the initial estimate are also either the Center Method in equation (3.20), or the Box Method in equation (3.7), or the Circle Method in equation (3.20) utilized equivalent to the standard forward kinematics algorithm in section (3.3). The proposed iterative methods are also the Levenberg-Marquardt, described in table (3.1), or the Powell's Dog Leg algorithm, described in table (3.4) but contrary to the standard forward kinematics algorithms the

EKM cable length error  $\mathbf{f}_{EKM}$  is applied via equation (3.58) to the objective function  $F$  in equation (2.14). The cable length error  $\mathbf{f}_{EKM} : \mathbb{R}^3 \rightarrow \mathbb{R}^4$  for the CDPR-based pelvic actuation system is obtained with equation (3.57) through

$$\mathbf{f}_{EKM} = \begin{bmatrix} f_{EKM,1} \\ f_{EKM,2} \\ f_{EKM,3} \\ f_{EKM,4} \end{bmatrix} = \begin{bmatrix} l_{f,1} + l_{\delta,1} + l_{corr,1} - l_{act,1} \\ l_{f,2} + l_{\delta,2} + l_{corr,2} - l_{act,2} \\ l_{f,3} + l_{\delta,3} + l_{corr,3} - l_{act,3} \\ l_{f,4} + l_{\delta,4} + l_{corr,4} - l_{act,4} \end{bmatrix}. \quad (3.59)$$

This EKM cable length error  $\mathbf{f}_{EKM}$  in equation (3.59) is applied through the error vector  $\mathbf{f} = [f_1, f_2, f_3, f_4]^T$  in equation (3.58) to the Jacobian matrix in equation (2.16) which yields the  $4 \times 3$  Jacobian matrix in equation (3.27), but this time based on the EKM with

$$\begin{aligned} \frac{\partial f_i}{\partial r_x} &= \frac{\partial l_{f,i}}{\partial r_x} + \frac{\partial l_{\delta,i}}{\partial r_x} + \frac{\partial l_{corr,i}}{\partial r_x} \\ \frac{\partial f_i}{\partial r_y} &= \frac{\partial l_{f,i}}{\partial r_y} + \frac{\partial l_{\delta,i}}{\partial r_y} + \frac{\partial l_{corr,i}}{\partial r_y} \\ \frac{\partial f_i}{\partial \phi_z} &= \frac{\partial l_{f,i}}{\partial \phi_z} + \frac{\partial l_{\delta,i}}{\partial \phi_z} + \frac{\partial l_{corr,i}}{\partial \phi_z} \end{aligned} \quad (3.60)$$

as the first partial derivatives of the error vector  $\mathbf{f}$  in equation (3.58). It is reviewed that  $\frac{\partial l_{SKM,ix}}{\partial \phi_z}$  and  $\frac{\partial l_{SKM,iy}}{\partial \phi_z}$  are determined through equation (3.29) and

$$\begin{aligned} \frac{\partial l_{SKM,i,\beta,x}}{\partial r_x} &= -\cos(-\beta_i) \\ \frac{\partial l_{SKM,i,\beta,y}}{\partial r_x} &= -\sin(-\beta_i) \\ \frac{\partial l_{SKM,i,\beta,x}}{\partial r_y} &= \sin(-\beta_i) \\ \frac{\partial l_{SKM,i,\beta,y}}{\partial r_y} &= -\cos(-\beta_i) \\ \frac{\partial l_{SKM,i,\beta,x}}{\partial \phi_z} &= \cos(-\beta_i) \frac{\partial l_{SKM,ix}}{\partial \phi_z} - \sin(-\beta_i) \frac{\partial l_{SKM,iy}}{\partial \phi_z} \\ \frac{\partial l_{SKM,i,\beta,y}}{\partial \phi_z} &= \sin(-\beta_i) \frac{\partial l_{SKM,ix}}{\partial \phi_z} + \cos(-\beta_i) \frac{\partial l_{SKM,iy}}{\partial \phi_z} \end{aligned} \quad (3.61)$$

are introduced. Applying equations (3.29) and (3.61), the first partial derivatives in equations (3.60) are obtained by

### 3 Proposed Solution

---

$$\begin{aligned}
\frac{\partial l_{f,i}}{\partial r_x} &= -\frac{l_{SKM,ix}}{l_{f,i}} \\
\frac{\partial l_{f,i}}{\partial r_y} &= -\frac{l_{SKM,iy}}{l_{f,i}} \\
\frac{\partial l_{f,i}}{\partial \phi_z} &= \frac{(l_{SKM,ix}) \frac{\partial l_{SKM,ix}}{\partial \phi_z} + (l_{SKM,iy}) \frac{\partial l_{SKM,iy}}{\partial \phi_z}}{l_{f,i}} \\
\frac{\partial l_{\delta,i}}{\partial r_x} &= \frac{r_d^2 l_{SKM,ix}}{\sqrt{\left(1 - \left(\frac{r_d}{l_{SKM,i}}\right)^2\right) \left(l_{SKM,ix}^2 + l_{SKM,iy}^2\right)^3}} \\
\frac{\partial l_{\delta,i}}{\partial r_y} &= \frac{r_d^2 l_{SKM,iy}}{\sqrt{\left(1 - \left(\frac{r_d}{l_{SKM,i}}\right)^2\right) \left(l_{SKM,ix}^2 + l_{SKM,iy}^2\right)^3}} \\
\frac{\partial l_{\delta,i}}{\partial \phi_z} &= -\frac{r_d^2 \left(l_{SKM,ix} \frac{\partial l_{SKM,ix}}{\partial \phi_z} + l_{SKM,iy} \frac{\partial l_{SKM,iy}}{\partial \phi_z}\right)}{\sqrt{\left(1 - \left(\frac{r_d}{l_{SKM,i}}\right)^2\right) \left(l_{SKM,ix}^2 + l_{SKM,iy}^2\right)^3}} \quad . \\
\frac{\partial l_{corr,i}}{\partial r_x} &= -\chi_i r_d \frac{l_{SKM,i,\beta,x} \frac{\partial l_{SKM,i,\beta,y}}{\partial r_x} - l_{SKM,i,\beta,y} \frac{\partial l_{SKM,i,\beta,x}}{\partial r_x}}{\left(\left(1 + \left(\frac{l_{SKM,i,\beta,y}}{l_{SKM,i,\beta,x}}\right)\right) l_{SKM,i,\beta,x}\right)^2} \\
\frac{\partial l_{corr,i}}{\partial r_y} &= -\chi_i r_d \frac{l_{SKM,i,\beta,x} \frac{\partial l_{SKM,i,\beta,y}}{\partial r_y} - l_{SKM,i,\beta,y} \frac{\partial l_{SKM,i,\beta,x}}{\partial r_y}}{\left(\left(1 + \left(\frac{l_{SKM,i,\beta,y}}{l_{SKM,i,\beta,x}}\right)\right) l_{SKM,i,\beta,x}\right)^2} \\
\frac{\partial l_{corr,i}}{\partial r_{\phi_z}} &= -\chi_i r_d \frac{l_{SKM,i,\beta,x} \frac{\partial l_{st,i,\beta,y}}{\partial \phi_z} - l_{SKM,i,\beta,y} \frac{\partial l_{SKM,i,\beta,x}}{\partial \phi_z}}{\left(\left(1 + \left(\frac{l_{SKM,i,\beta,y}}{l_{SKM,i,\beta,x}}\right)\right) l_{SKM,i,\beta,x}\right)^2}
\end{aligned} \tag{3.62}$$

Having determined the EKM cable length error in (3.59) for  $\mathbf{f}$  in equation (3.58) as well as the  $4 \times 3$  Jacobian matrix of the EKM in equation (3.27) with its components in equation (3.60) the Levenberg-Marquardt algorithm is executed as explained in table (3.1) and the Powell's Dog Leg algorithm, as explained in table (3.4). Thus, combining the three initial estimate methods with the Levenberg-Marquardt and the Powell's Dog Leg generates six different extended forward kinematics algorithms. These are tested in chapter (4) and compared to the results of the standard forward kinematics algorithms especially under the consideration of real-time constraints because too detailed kinematic models might not be real-time feasible, as pointed out in subsection (2.3.1).

# 4 Experimental Results

This chapter presents the results of the exerted experiments. Therefore the used robot prototype for the simulations is introduced in section (4.1). Then the setup of the simulations is discussed in section (4.2). The experimental results of the simulations exerted with the 12 forward kinematics algorithms are presented in section (4.3), (4.4), and (4.5). The impact of general pelvic movements is tested in section (4.6).

## 4.1 Robot Prototype for Simulations

The CDPR-based pelvic actuation system is a planar CDPR actuating  $n = 3$  degrees of freedom via  $m = 4$  cables, as depicted in configuration 2 of figure (2.2). The robot prototype's parameter introduced in [5] are adopted. The coordinate frame of the base  $K_0$  is located at  $[0\text{m}, 0\text{m}]^T$  in the center of the rectangular configuration 2 in figure (2.2). The parameters of the prototype are given in table (4.1).

Parameter	Formula Symbol	Value	Unit
position of actuator 1	$a_1$	$[-0.6, -0.4]^T$	[m]
position of actuator 2	$a_2$	$[0.6, -0.4]^T$	[m]
position of actuator 3	$a_3$	$[-0.6, 0.4]^T$	[m]
position of actuator 4	$a_4$	$[0.6, 0.4]^T$	[m]
position of attachment point 1	$b_1$	$[-\frac{\sqrt{2}}{10}, \frac{\sqrt{2}}{10}]^T$	[m]
position of attachment point 2	$b_2$	$[\frac{\sqrt{2}}{10}, \frac{\sqrt{2}}{10}]^T$	[m]
position of attachment point 3	$b_3$	$[-\frac{\sqrt{2}}{10}, -\frac{\sqrt{2}}{10}]^T$	[m]
position of attachment point 4	$b_4$	$[\frac{\sqrt{2}}{10}, -\frac{\sqrt{2}}{10}]^T$	[m]
radius of each drum	$r_d$	0.02	[m]
rotation direction actuator 1	$\chi_1$	-1	[—]
rotation direction actuator 2	$\chi_2$	1	[—]
rotation direction actuator 3	$\chi_3$	1	[—]
rotation direction actuator 4	$\chi_4$	-1	[—]

**Table 4.1:** Robot Prototype

It is defined that the walking direction shown in figure (2.2) is along the  $x$ -axis of  $K_0$ . The  $y$ -axis of  $K_0$  points towards the side defined through the actuators  $A_3$  and  $A_4$ . Having introduced the robot prototype, the setup of the simulations is explained in the following section (4.2).

## 4.2 Setup of the Simulations

The code of the CDPR-based forward kinematics of the pelvic actuation system is written using MATLAB R2013a. Equally all simulations are performed by a MATLAB R2013a system on a Windows 10 computer running with an Intel®Core™i5 processor. Each standard forward kinematics and extended forward kinematics algorithm is tested on an analysis field which has the form of a square with its centre located at  $K_0$  and sides having 0.6 m in length. In this square the position accuracy, the orientation accuracy, the iteration's efficiency, and the duration are determined for each forward kinematics algorithm by considering 225 different poses calculated through the chosen forward kinematics algorithm. The position accuracy is measured through the error in position  $\Delta r$  between the position  $r^{calc}$  determined by the forward kinematics algorithm and the actual position  $r^*$  of the pelvic pose  $x^*$ . The error in position  $\Delta r$  is obtained by

$$\Delta r = \sqrt{(r_x^{calc} - r_x^*)^2 + (r_y^{calc} - r_y^*)^2}. \quad (4.1)$$

A measure for the orientation accuracy is received by the error in orientation, in this planar case given through  $\Delta\phi_z$ , determined using the actual orientation  $\phi_z^*$  and the orientation  $\phi_z^{calc}$  calculated by the forward kinematics algorithm yielding

$$\Delta\phi_z = |\phi_z^{calc} - \phi_z^*|. \quad (4.2)$$

The iterations efficiency is described by the number of executed iterations  $\Delta k$  in the applied optimization method, either Levenberg-Marquardt or Powell's Dog Leg, taken to calculate the pelvic pose  $x^*$ . Similar the duration characterizes the time  $\Delta t$  each forward kinematics algorithm needs to find the pelvic pose  $x^*$  starting with the chosen initial estimate method and stopping after the last iteration of the chosen optimization algorithm.

The error in position  $\Delta r$ , the error in orientation  $\Delta\phi_z$ , the number of executed iterations  $\Delta k$ , and the time  $\Delta t$  is determined for each of the 225 poses. Following, the average of the error in position  $\bar{\Delta r}$  using the position errors  $\Delta r$  determined through equation (4.1), the average of the error in orientation  $\bar{\Delta\phi_z}$  using the orientation errors  $\Delta\phi_z$  in equation (4.2), as well as the average number of executed iterations  $\bar{\Delta k}$  and the average time  $\bar{\Delta t}$  are calculated for each forward kinematics algorithm. The results are presented in section (4.3) and section (4.4).

Considering the error in cable length  $f_{SKM}$  for the standard forward kinematics algorithm in equation (3.26) and the error in cable length  $f_{EKM}$  for the extended forward kinematics algorithm in equation (3.59), it is recognized that the actual cable length  $l_{act,i}$ , measured by the encoder and belonging to the to be determined pelvic pose  $x^*$ , is needed. In all following tests, the actual cable length vector  $l_{act}$ , containing

the measured cable lengths of the four cables, is either given through the inverse kinematic solution  $\mathbf{q}_{SKM}$  of the SKM in equation (2.5) or through the inverse kinematic solution  $\mathbf{q}_{EKM}$  of the EKM in equation (3.56) because all experiments are only simulations conducted on the computer.

As pointed out in subsection (2.3.1), the parametrisation of iterative optimization methods such as the Levenberg-Marquardt and the Powell's Dog Leg, remains a challenge. Therefore each combination of the standard and the extended forward kinematics algorithms were extensively tested to find the most suitable parametrisation to ensure decent results. The parameters are calibrated, so that only small deviations to the position and the orientation in a range of 0.1 mm and 0.01° respectively are permitted. The parametrisation for each algorithm is presented in the following sections (4.3) and (4.4).

## 4.3 Testing the Standard Forward Kinematics

Parameter/ Input	SKM LM Center Method	SKM LM Box Method	SKM LM Circle Method	SKM DL Center Method	SKM DL Box Method	SKM DL Circle Method
$\mathbf{x}_0$	$\mathbf{x}_0^{center}$	$\mathbf{x}_0^{box}$	$\mathbf{x}_0^{circle}$	$\mathbf{x}_0^{center}$	$\mathbf{x}_0^{box}$	$\mathbf{x}_0^{circle}$
$k_{max}$ [-]	100	100	100	100	100	100
$\tau$ [-]	$10^{-3}$	$10^{-3}$	$10^{-3}$	—	—	—
$\Delta$ [m]	—	—	—	0.7	0.8	0.5
$\varepsilon_1$ [m]	$10^{-6}$	$10^{-5}$	$10^{-5}$	$10^{-5}$	$10^{-5}$	$10^{-5}$
$\varepsilon_2$ [-]	$10^{-6}$	$10^{-5}$	$10^{-5}$	$10^{-5}$	$10^{-5}$	$10^{-5}$
$\varepsilon_3$ [m]	—	—	—	$10^{-5}$	$10^{-5}$	$10^{-5}$

**Table 4.2:** Parametrisation and Inputs Standard Forward Kinematics Algorithms

There are six combinations of the standard forward kinematics algorithms to be tested in this section:

- Center Method and Levenberg-Marquardt algorithm (SKM LM Center Method)
- Box Method and Levenberg-Marquardt algorithm (SKM LM Box-Method)
- Circle Method and Levenberg-Marquardt algorithm (SKM LM Circle Method)
- Center Method and Powell's Dog Leg algorithm (SKM DL Center Method)
- Box Method and Powell's Dog Leg algorithm (SKM DL Box Method)

- Circle Method and Powell's Dog Leg algorithm (SKM DL Circle Method)

All user defined parameters either of the Levenberg-Marquardt or the Powell's Dog Leg were introduced in table (3.1) and table (3.4) respectively. Their values and the inputs for each standard forward kinematics algorithm are listed in table (4.2). The initial estimate  $\mathbf{x}_0$  is either determined through equations (3.2), or (3.8), or (3.20) depending on the applied initial estimate method.

The standard forward kinematics algorithm are tested by applying table (3.1) and table (3.4) respectively with the defined inputs and parameters in table (4.2), the cable length error  $f_{SKM}$  in equation (3.26) applied to the error vector  $\mathbf{f}$  via equation (2.15), the Jacobian matrix  $\mathbf{J}$  in equation (3.27), and its components in equation (3.28). In all tests it is assumed that a transverse rotation of  $\phi_z = 20^\circ$  is existent because the pelvis normally exerts a rotation during gait as pointed out in section (2.1). The rotation's value is conservatively chosen because the combined pelvic forward and backward transverse rotation does not exceed  $\phi_z = 10^\circ$  during normal gait. Thus,  $\phi_z = 20^\circ$  is a safety set to ensure that the forward kinematics algorithms do not work worse than in this extreme pose. The average orientation accuracy is also determined in comparison to a rotation of  $\phi_z = 20^\circ$ . The experimental results yield the average error in position  $\Delta\bar{r}$ , the average error in orientation  $\Delta\bar{\phi}_z$ , the average number of executed iterations  $\Delta\bar{k}$ , and the average time  $\Delta\bar{t}$  arranged in table (4.3).

Algorithm	$\Delta\bar{r}$ [μm]	$\Delta\bar{\phi}_z$ [°]	$\Delta\bar{k}$ [-]	$\Delta\bar{t}$ [ms]
SKM LM Center Method	0.05	0.00001	3.3	0.97
SKM LM Box Method	0.39	0.00027	2.8	0.93
SKM LM Circle Method	1.05	0.00050	2.7	0.86
SKM DL Center Method	0.96	0.00031	2.9	0.90
SKM DL Box Method	0.54	0.00040	2.7	0.88
SKM DL Circle Method	1.91	0.00062	2.4	0.80

**Table 4.3:** Experimental Results Standard Forward Kinematics Algorithms

## 4.4 Testing the Extended Forward Kinematics

After having tested the standard forward kinematics algorithms , the same testing procedure is repeated with the extended forward kinematics algorithms. Similar to the standard forward kinematics algorithms, following six combinations of the extended forward kinematics algorithms are investigated:

- Center Method and Levenberg-Marquardt algorithm (EKM LM Center Method)
- Box Method and Levenberg-Marquardt algorithm (EKM LM Box Method)

- Circle Method and Levenberg-Marquardt algorithm (EKM LM Circle Method)
- Center Method and Powell's Dog Leg algorithm (EKM DL Center Method)
- Box Method and Powell's Dog Leg algorithm (EKM DL Box Method)
- Circle Method and Powell's Dog Leg algorithm (EKM DL Circle Method)

The definition of the parameters and inputs for the two iterative optimization algorithms, Levenberg-Marquardt and Powell's Dog Leg, conducted according to table (3.1) and table (3.4) respectively, are given in table (4.4). Equally to the standard forward kinematics algorithms, the initial estimate  $\mathbf{x}_0$  is defined via the Center, Box, or Circle Method utilizing equations (3.2), (3.8), and (3.20) respectively.

Parameter/ Input	EKM LM Center Method	EKM LM Box Method	EKM LM Circle Method	EKM DL Center Method	EKM DL Box Method	EKM DL Circle Method
$\mathbf{x}_0$	$\mathbf{x}_0^{center}$	$\mathbf{x}_0^{box}$	$\mathbf{x}_0^{circle}$	$\mathbf{x}_0^{center}$	$\mathbf{x}_0^{box}$	$\mathbf{x}_0^{circle}$
$k_{max}$ [-]	100	100	100	100	100	100
$\tau$ [-]	$10^{-3}$	$10^{-3}$	$10^{-3}$	—	—	—
$\Delta_0$ [m]	—	—	—	0.7	0.8	0.6
$\varepsilon_1$ [m]	$10^{-5}$	$10^{-5}$	$10^{-5}$	$10^{-5}$	$10^{-5}$	$10^{-5}$
$\varepsilon_2$ [-]	$10^{-5}$	$10^{-5}$	$10^{-5}$	$10^{-5}$	$10^{-5}$	$10^{-5}$
$\varepsilon_3$ [m]	—	—	—	$10^{-5}$	$10^{-5}$	$10^{-5}$

**Table 4.4:** Parametrisation and Inputs Extended Forward Kinematics Algorithms

Both the Levenberg-Marquardt and the Powell's Dog Leg are operated with their defined inputs and parameters in table (4.4), the cable length error  $f_{EKM}$  in equation (3.59) applied to the error vector  $\mathbf{f}$  through equation (3.58) and the Jacobian matrix  $\mathbf{J}$  in equation (3.27) with its components in equation (3.60). Due to the same reasons as in section (4.3), the tests are undertaken with a rotation of  $\phi_z = 20^\circ$ . The error in orientation  $\Delta\phi_z$  is also tested in comparison to a rotation of  $\phi_z = 20^\circ$ . The testing operations are conducted according to the algorithms description in table (3.1) and table (3.4) respectively gaining the experimental results in table (4.5).

As pointed out in subsection (2.3.1) algorithms based on complicated kinematic models as the extended forward kinematics algorithms risk to violate real-time constraints. Therefore the standard forward kinematic algorithm with the shortest average duration  $\bar{\Delta t}$  is tested in the following section dealing with cable lengths calculated by the EKM to examine if a simple algorithm is still able to determine the pelvic pose  $\mathbf{x}^*$  accurately.

Algorithm	$\Delta\bar{r}$ [μm]	$\Delta\bar{\phi}_z$ [°]	$\Delta\bar{k}$ [-]	$\Delta\bar{t}$ [ms]
EKM LM Center Method	1.39	0.00018	3.7	2.12
EKM LM Box Method	1.45	0.00020	3.3	2.01
EKM LM Circle Method	1.40	0.00019	3.1	1.94
EKM DL Center Method	2.13	0.00027	3.5	2.05
EKM DL Box Method	1.96	0.00026	3.2	1.93
EKM DL Circle Method	1.88	0.00023	3.0	1.86

**Table 4.5:** Experimental Results Extended Forward Kinematics Algorithms

## 4.5 Testing the Standard Forward Kinematics based on the Extended Kinematic Model

Calculating the actual cable length vector  $\mathbf{l}_{act}$  through the inverse kinematic solution  $\mathbf{q}_{EKM}$  of the EKM in equation (3.56) offers the possibility to simulate the forward kinematics algorithm closer to reality because it takes the drums of the winches into account. Considering the possibility that the extended forward kinematics algorithms might not be real-time feasible, it is advantageous to seek a preferably simple algorithm also providing accurate results even though the cable lengths differ from those for which it was designed. Therefore the SKM Dog Leg Circle Method is chosen. The parametrisation of the SKM Dog Leg Circle Method in table (4.2) is adopted. The testing is conducted equally as described in section (4.3) but the simulation's setup in section (4.2) is adjusted. The actual cable length vector  $\mathbf{l}_{act}$  is now provided by the inverse kinematic solution  $\mathbf{q}_{EKM}$  of the EKM in equation (3.56). The experimental results of testing the SKM Dog Leg Circle Method with cable lengths calculated by the EKM are summarized in table (4.6).

Algorithm	$\Delta\bar{r}$ [mm]	$\Delta\bar{\phi}_z$ [°]	$\Delta\bar{k}$ [-]	$\Delta\bar{t}$ in [ms]
SKM DL Circle Method	12.14	0.79	5.37	1.34

**Table 4.6:** Experimental Results SKM DL Circle Method based on EKM

Considering the high average error in position  $\Delta\bar{r}$  in table (4.6), it has to be noted that this result is biased because the errors in position for poses comparatively far away from the position  $\mathbf{r} = [0\text{cm}; 0\text{cm}]^T$  are much higher. Poses close to the position  $\mathbf{r} = [0\text{cm}; 0\text{cm}]^T$  have much smaller errors in position (e.g.  $\Delta\mathbf{r} = 3.09\text{ mm}$  for  $\mathbf{r} = [-4.3\text{ cm}; -4.3\text{ cm}]^T$ ).

The accuracy of the standard forward kinematics algorithms becomes even more important if the general pelvic movement during gait is considered. Pointed out in subsection (2.3.2) the CDPR-based pelvic actuation system working as a planar robot has actually to deal with general pelvic movements that are spatial not planar. This

possible impact on the accuracy of the standard forward kinematics algorithms is investigated in the next section.

## 4.6 Testing the Impact of General Pelvic Movements

The algorithms in the previous sections of chapter (4) only considered the transverse rotation  $\phi_z$  of the pelvis during gait. However, a general pelvic movement also contains a pelvic drop  $\phi_x$  and an anterior tilt  $\phi_y$  as well as a translation  $r_z$ . To investigate the impact of general pelvic movements to the accuracy of the developed standard forward kinematics algorithms, the algorithm SKM DL Circle Method tested in sections (4.3) and (4.5) is exerted to general pelvic movements. Therefore the actual cable length vector  $\mathbf{l}_{act}$  is determined through the inverse kinematic solution  $\mathbf{q}_{SKM}$  in equation (2.4) as proposed in section (3.4). For determining the inverse kinematic solution  $\mathbf{q}_{SKM}$  the  $z$ -coordinate for  $\mathbf{a}_i$  and  $\mathbf{b}_i$  has to be added through  $a_{iz} = 0\text{m}$  and  $b_{iz} = 0\text{m}$  to the actuator's position  $\mathbf{a}_i$  and the cable attachment position  $\mathbf{b}_i$  in table (4.1). The remaining setup of the simulations for the forward kinematics is according to section (4.2) and the procedure to section (4.3). To gain a profound knowledge of the impact on position accuracy, iterations efficiency, and duration, the pelvic drop  $\phi_x$  and the anterior tilt  $\phi_y$  are tested separately in the extreme orientation  $\phi_x = 10^\circ$  and  $\phi_y = 10^\circ$  respectively without rotation ( $\phi_z = 0^\circ$ ) and  $z$ -translation ( $r_z = 0\text{cm}$ ). These angles are usually not reached during normal gait as pointed out in section (2.1) and are hence considered as a conservative approach. In addition the  $z$ -translation is tested without any rotations. The assumed translation  $r_z = 6\text{cm}$  is also conservatively chosen because a usual translation is normally around  $r_z = 3\text{cm}$  or even lower according to [14]. Following a general pelvic movement in an extreme pose involving a pelvic drop  $\phi_x = 10^\circ$ , an anterior tilt  $\phi_y = 10^\circ$ , a transverse rotation  $\phi_z = 20^\circ$  and  $z$ -translation  $r_z = 6\text{cm}$  is tested as well as a general pelvic movement in a usual pose involving a pelvic drop  $\phi_x = 4^\circ$ , an anterior tilt  $\phi_y = 4^\circ$ , a transverse rotation  $\phi_z = 5^\circ$  and  $z$ -translation  $r_z = 3\text{cm}$ . The average error in position  $\Delta\bar{r}$ , the average error in orientation  $\Delta\bar{\phi}_z$ , the average number of executed iterations  $\Delta k$ , and the average time  $\Delta\bar{t}$  of the experimental results, obtained in the analysis field of 225 poses, are summarized in table (4.7).

Having gained the experimental results of the standard and extended forward kinematics algorithm in sections (4.3) and (4.4) as well as of the standard forward kinematics algorithm exerted to cable lengths determined through the EKM in section (4.5) and of the impact of a general pelvic movement, these results are analysed and interpreted in the following chapter.

#### 4 Experimental Results

---

Orientation/ $z$ -Translation	$\Delta\bar{r}$ [mm]	$\Delta\bar{\phi}_z$ [ $^\circ$ ]	$\Delta\bar{k}$ [-]	$\Delta\bar{t}$ [ms]
$\phi_x = 10^\circ$ $\phi_y = 0^\circ$ $\phi_z = 0^\circ$ $r_z = 0\text{cm}$	0.59	0.03	2.8	0.77
$\phi_x = 0^\circ$ $\phi_y = 10^\circ$ $\phi_z = 0^\circ$ $r_z = 0\text{cm}$	0.89	0.04	3.2	0.80
$\phi_x = 0^\circ$ $\phi_y = 0^\circ$ $\phi_z = 0^\circ$ $r_z = 0.6\text{cm}$	0.89	0.04	3.2	0.80
$\phi_x = 4^\circ$ $\phi_y = 4^\circ$ $\phi_z = 5^\circ$ $r_z = 0.3\text{cm}$	0.88	0.05	2.7	0.73
$\phi_x = 10^\circ$ $\phi_y = 10^\circ$ $\phi_z = 20^\circ$ $r_z = 0.6\text{cm}$	4.57	0.29	3.89	0.99

**Table 4.7:** Impact of General Pelvic Movements

# 5 Analysis

This chapter analyses the experimental results of chapter (4). The standard forward kinematics algorithms as well as the extended forward kinematics algorithms are evaluated in section (5.1) and (5.2) respectively by an approach according to Pahl/Beitz [4]. Following the results of the standard forward kinematics algorithm based on the EKM are interpreted in section (5.3). Thereafter the impact of general pelvic movements on the planar operating CDPR-based pelvic actuation system is interpreted in section (5.4). Finally the chosen forward kinematics algorithms are discussed under the aspect of real-time feasibility in section (5.5).

## 5.1 Evaluation of the Standard Forward Kinematics Algorithms with Pahl/Beitz

The experimental results of the standard forward kinematics algorithm, displayed in table (4.3), are evaluated to determine the most accurate and possibly real-time feasible algorithm. Thus, the evaluation criteria position accuracy, orientation accuracy, iteration's efficiency, and duration and their associated evaluation properties are weighted. This weighting is especially important. The real-time constraints depend majorly on the criteria iteration's efficiency and duration whereas the accuracy of the determined poses depends on the position and orientation accuracy of the algorithm. Choosing the weighting of the evaluation criteria, accuracy is stronger weighted than real-time feasibility because the forward kinematics shall yield the pelvic pose as accurate as possible. The applied criteria weighting is shown in table (5.1) together with the criteria and their associated properties such as the average error in position  $\Delta\bar{r}$ , the average error in orientation  $\Delta\bar{\phi}_z$ , the average number of executed iterations  $\Delta\bar{k}$ , and the average time  $\Delta\bar{t}$ .

After introducing the weighting of the evaluation criteria, a rating scala is configured to grade the average error in position  $\Delta\bar{r}$ , the average error in rotation  $\Delta\bar{\phi}_z$ , the average number of executed iterations  $\Delta\bar{k}$ , and the average time  $\Delta\bar{t}$ . Several rating scalas exist. This thesis is applying the VDI 2225 scala according to [28] providing an explicit but not too detailed rating system. Each grade corresponds to a certain value of the associated property. The chosen values are given in table (5.2).

Concerning the error in position, the parameter were calibrated in order to permit

## 5 Analysis

---

Criterion	Associated Property	Weighting $w_{pa}$
Position accuracy	$\Delta\bar{r}$	0.3
Orientation accuracy	$\Delta\bar{\phi}_z$	0.3
Iterations efficiency	$\Delta\bar{k}$	0.2
Duration	$\Delta\bar{t}$	0.2
$\Sigma$		1

**Table 5.1:** Weighting of Evaluation Criteria

only a maximum error  $\Delta\bar{r} < 1 \text{ mm}$ . Therefore all values that exceed this error are considered as insufficient. Since the standard forward kinematics algorithms base on a rather idealized model, the smaller the average error in position  $\Delta\bar{r}$  becomes the more advantageous if additional inaccuracies due to the idealizations of the SKM occur. If the algorithm has an average error in position  $\Delta\bar{r} < 50 \mu\text{m}$ , it is considered as excellent because it is close to the motor resolution determined in equation (3.30).

Grade	Meaning	$\Delta\bar{r} [\mu\text{m}]$	$\Delta\bar{\phi}_z [^\circ]$	$\Delta\bar{k} [-]$	$\Delta\bar{t} [\text{ms}]$
0	insufficient	$\geq 1000 \mu\text{m}$	$\geq 0.1^\circ$	$> 4$	$> 1$
1	acceptable	$< 1000 \mu\text{m}$	$< 0.1^\circ$	$\leq 4$	$\leq 1$
2	sufficient	$< 500 \mu\text{m}$	$< 0.01^\circ$	$\leq 3$	$\leq 0.9$
3	good	$< 100 \mu\text{m}$	$< 0.005^\circ$	$\leq 2$	$\leq 0.85$
4	excellent	$< 50 \mu\text{m}$	$< 0.001^\circ$	$= 1$	$\leq 0.8$

**Table 5.2:** Rating Scale VDI 2225

Similar is the determination of the corresponding values concerning the average error in orientation  $\Delta\bar{\phi}_z$ . A forward transverse rotation of the pelvis during normal gait does usually not exceed more than  $\phi_z = 5^\circ$ . Therefore an acceptable algorithm has to determine the average error in orientation better than  $0.1^\circ$  especially considering that more inaccuracies to orientation can appear due to the idealization of the SKM. Algorithms achieving an error beneath  $0.001^\circ$  are excellent. These challenging requirements for  $\Delta\bar{r}$  and  $\Delta\bar{\phi}_z$  are especially advantageous if errors to the accuracy occur because the occurring known and unknown errors possibly have less influence due to the challenging accuracy requirements.

The average executed number of iterations  $\Delta\bar{k}$  is closely linked to real-time constraints if the algorithm is run on a programmable logic controller (PLC) but also if the algorithm is run on a computer because algorithms with too many iterations also require more time and could therefore violate real-time constraints. A PLC guarantees real-time feasibility because of its single cycle process with a single core but only 2048 simple operations can be conducted. Each operation requires the same amount of

time and its real-time processing cannot be accelerated. Therefore it is crucial that the number of operations of the forward kinematics algorithm does not exceed these 2048 operations if the CDPR-based forward kinematics shall be implemented on a PLC. It is also even more favourable if the algorithm requires less than 2048 operations because other algorithms for the rehabilitation also need to be implemented. Since the algorithms contain an iterative procedure, the iterations are a measure if the maximum number of operations is maintained. The standard forward kinematics algorithms need approximately 500 operations for each iteration. Therefore it is insufficient if  $\bar{k} > 4$ . Excellent means the algorithm requires only 1 iteration, but this is only possible if the initial estimate is extremely close to the actual pose.

If the algorithms are not run on a PLC but on a computer, it is trivial that the average duration  $\bar{\Delta t}$  decides if an algorithm fulfils real-time constraints. Through a multi cycle process with different cycle times and through parallel processing of the operations each algorithm's operation can be processed efficiently but a real-time package is necessary. Mentioned in subsection (2.3.1) information at rate up to 1 kHz are real-time feasible for industrial applications. However, it is even better if the forward kinematics algorithm runs faster since other algorithms for the rehabilitation also require a certain time. Therefore algorithms being faster than 0.8 ms are considered as excellent.

Considering table (4.3) it has to be pointed out that all standard forward kinematics algorithms exceed the expectations of accuracy by far and will therefore receive the best grades. Hence the iteration's efficiency and the duration will majorly contribute to the determination of the most suitable algorithm. The grading of the standard forward kinematics algorithms is shown in table (5.3). Hereby is  $e_{pa}$  as generalized term for the associated properties introduced with the indices  $p$  and  $a$  indicating the associated property  $p \in \{1, 2, 3, 4\}$  and the algorithm  $a \in \{1, 2, 3, 4, 5, 6\}$  respectively.

Analysing the grading of the standard forward kinematics algorithms, each algorithm fulfils the minimum requirement. All algorithms receive the best grades with regards to position and orientation accuracy. The evaluation criteria iteration's efficiency and duration actually distinguish the algorithms. The iteration's efficiency is for all algorithms except the SKM LM Center Method sufficient. Therefore the algorithms could possibly be implemented on a PLC. Looking at the duration it seems that the real-time constraint of 1 ms is at least acceptably fulfilled. It is noted that the SKM DL Circle Method achieves the highest grade. To choose the most suitable algorithms for the forward kinematics problem, the weighted grades need to be determined. Applying the chosen weighting in table (5.1) to the graded associated properties  $e_{pa}$  of each algorithm in table (5.3) receives the weighted values  $wg_{pa}$  of the graded associated properties through

$$wg_{pa} = w_{pa} \cdot e_{pa}. \quad (5.1)$$

## 5 Analysis

---

Algorithm ( $a$ )	$e_{1a} = \Delta\bar{r}$ [ $\mu\text{m}$ ]	$e_{2a} = \Delta\bar{\phi}_z$ [ $^\circ$ ]	$e_{3a} = \Delta\bar{k}$ [-]	$e_{4a} = \Delta\bar{t}$ [ms]
SKM LM Center Method ( $a = 1$ )	4	4	1	1
SKM LM Box Method ( $a = 2$ )	4	4	2	1
SKM LM Circle Method ( $a = 3$ )	4	4	2	2
SKM DL Center Method ( $a = 4$ )	4	4	2	2
SKM DL Box Method ( $a = 5$ )	4	4	2	2
SKM DL Circle Method ( $a = 6$ )	4	4	2	4

**Table 5.3:** Grading of the Standard Forward Kinematics Algorithms

The absolute evaluation of an entire algorithm  $Gwg_a$  is then obtained by summing up the corresponding weighted values  $wg_{pa}$  determined by equation (5.1) yielding

$$Gwg_a = \sum_{p=1}^4 wg_{pa}. \quad (5.2)$$

The algorithm with the highest absolute evaluation  $Gwg_a$  compared to the best grade (excellent = 4) is considered as the most suitable algorithm of the considered combinations. Calculating the relative evaluation

$$Wg_a = Gwg_a / 4 \quad (5.3)$$

provides information about how close each algorithm is to an ideal algorithm. The evaluation  $Gwg_a$  of each standard forward kinematics algorithm and its ratio  $Wg_a$  are obtained by applying equations (5.1), (5.2), and (5.3) and displayed in table (5.4).

Algorithm ( $a$ )	$Gwg_a$	$Wg_a$
SKM LM Center Method ( $a = 1$ )	2.8	0.7
SKM LM Box Method ( $a = 2$ )	3	0.75
SKM LM Circle Method ( $a = 3$ )	3.2	0.8
SKM DL Center Method ( $a = 4$ )	3.2	0.8
SKM DL Box Method ( $a = 5$ )	3.2	0.8
SKM DL Circle Method ( $a = 6$ )	3.6	0.9

**Table 5.4:** Determining the Most Suitable Algorithm

## 5.1 Evaluation of the Standard Forward Kinematics Algorithms with Pahl/Beitz

Considering the results of the evaluation according to Pahl/Beitz, all algorithms based on the Powell's Dog Leg are generally better as their counterparts based on the Levenberg-Marquardt. In addition it is advantageous to attempt to apply an initial estimate method that is highly accurate. The Box and Circle method lead to a higher evaluation with the Circle Method being the best. According to table (5.4) the SKM DL Circle Method is therefore the best algorithm based on the SKM to challenge the forward kinematics problem under real-time constraints. However, since the associated properties  $e_{pa}$  are only averages, it is important to examine if there are outliers in the region where the CDPR-based pelvic actuation system is designed to operate. Thus, a detailed analysis of the workspace is conducted by examining the contour plot figure (5.1).

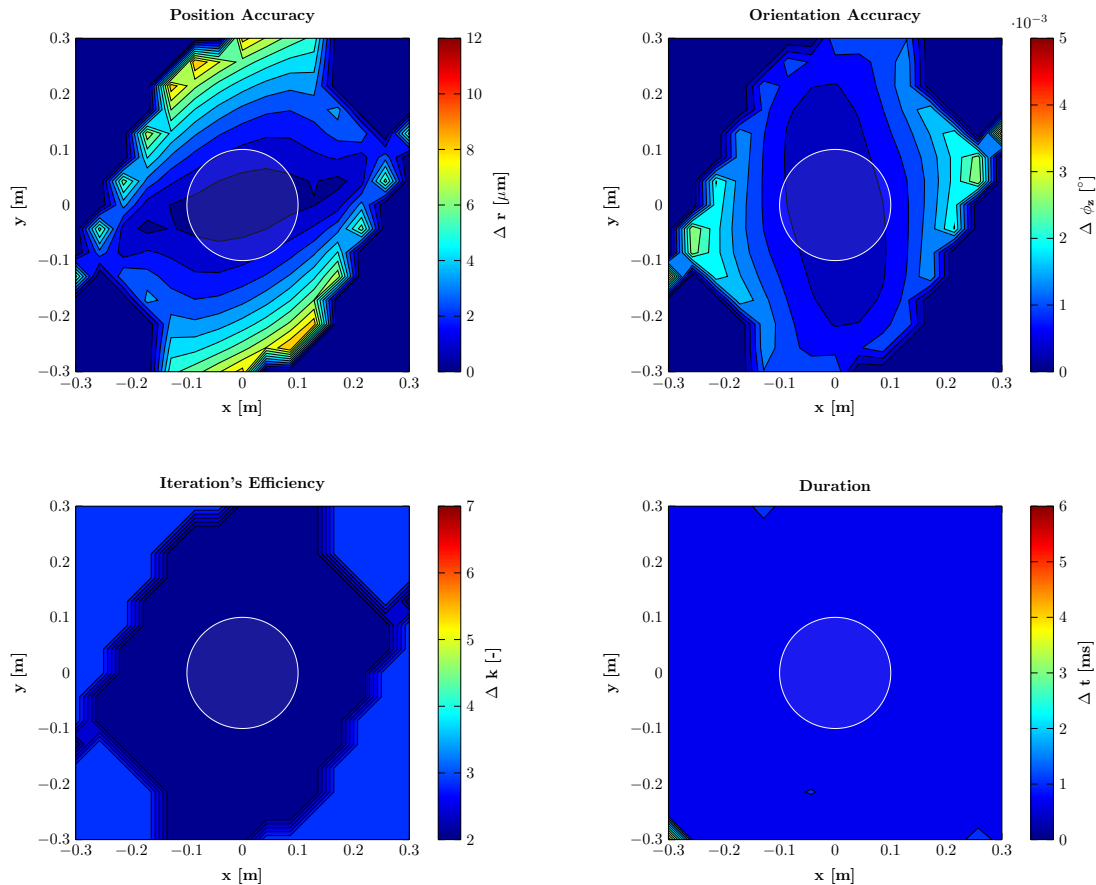


**Figure 5.1:** Contour Plots SKM DL Circle Method in Transverse Plane

Each contour plot analyses either the position accuracy, or the orientation accuracy, or the iteration's efficiency, or the duration by depicting the value of the associated properties on the analysis field. The pelvis is not expected to leave the white circle with the radius of 0.1 m. Therefore it is crucial that all requirements in this region are satisfying.

Considering figure (5.1), proves that no outliers in each contour plot for each criterion exist in this region . The highest values of  $\Delta r$  and  $\Delta\phi_z$  do never exceed the range of more than  $2\mu\text{m}$  and  $0.001^\circ$  respectively, confirming the high grades in table (5.3) indicating the excellent position and orientation accuracy of the algorithm. Focussing on the iteration's efficiency the executed number of iterations  $\Delta k$  never exceeds 2 in the white circular region, possibly suggesting the applicability of the SKM DL Circle Method on a PLC. Also the duration stays well below the real-time constraint 1 ms. Therefore the SKM DL Circle Method is the most suitable of the developed standard forward kinematics algorithms. The contour plots of the other standard forward kinematics algorithms are given in the appendix in section (7.3). Having determined the most suitable standard forward kinematics algorithm, the same solution process is applied to the extended forward kinematics algorithms in the next section.

## 5.2 Evaluation of the Extended Forward Kinematics Algorithms with Pahl/Beitz

The approach according to Pahl/Beitz in section (5.1) is adopted for the extended forward kinematics algorithms. Since the EKM is more accurate due to less modelling assumptions the position and orientation accuracy criteria could be adjusted but since the error in position  $\Delta\bar{r}$  and the error in orientation  $\Delta\bar{\phi}_z$  are very close to zero, the criteria remain unchanged. This provides the possibility to compare the standard forward kinematics algorithm and the extended forward kinematics algorithms in the following. Hence, the evaluation criteria, their associated properties and their weighting in table (5.1), and the rating scale in table (5.2) are applied to the experimental results in table (4.5) yielding the grading in table (5.5).

Analysing the grades in table (5.5), the position and orientation accuracy is excellent but contrary to the standard forward kinematics algorithms, the iteration's efficiency is only acceptable except for the sufficient EKM DL Circle Method. The real-time constraint of 1 ms cannot be met by any extended forward kinematics algorithm. The EKM DL Circle Method possesses the best duration but it is still not considerable as real-time feasible according to industrial standards. To choose the best of the extended forward kinematics algorithms equations (5.1), (5.2), and (5.3) are applied to table (5.3) as previously conducted in section (5.1). The resulting evaluation of each algorithm is summarized in table (5.6).

Analysing the results in table (5.6), indicates that only the EKM DL Circle Method distinguishes itself because of its better iteration's efficiency. The other algorithms exhibit an equal performance. According to the criteria no algorithm is able to fulfil real-time constraints. Nevertheless the criteria are related to averages. It might be possible to have real-time feasible results inside the circular region around  $K_0$  with a

## 5.2 Evaluation of the Extended Forward Kinematics Algorithms with Pahl/Beitz

---

Algorithm ( $a$ )	$e_{1a} = \Delta\bar{r}$ [μm]	$e_{2a} = \Delta\bar{\phi}_z$ [°]	$e_{3a} = \Delta\bar{k}$ [-]	$e_{4a} = \Delta\bar{t}$ [ms]
EKM LM Center Method ( $a = 1$ )	4	4	1	0
EKM LM Box Method ( $a = 2$ )	4	4	1	0
EKM LM Circle Method ( $a = 3$ )	4	4	1	0
EKM DL Center Method ( $a = 4$ )	4	4	1	0
EKM DL Box Method ( $a = 5$ )	4	4	1	0
EKM DL Circle Method ( $a = 6$ )	4	4	2	0

**Table 5.5:** Grading of the Extended Forward Kinematics Algorithms

Algorithm ( $a$ )	$Gwg_a$	$Wg_a$
EKM LM Center Method ( $a = 1$ )	2.6	0.65
EKM LM Box Method ( $a = 2$ )	2.6	0.65
EKM LM Circle Method ( $a = 3$ )	2.6	0.65
EKM DL Center Method ( $a = 4$ )	2.6	0.65
EKM DL Box Method ( $a = 5$ )	2.6	0.65
EKM DL Circle Method ( $a = 6$ )	2.8	0.7

**Table 5.6:** Determining the Most Suitable Algorithm

diameter of 0.2 m. If the results are real-time feasible in that region, then the EKM DL Circle Method can be used for the pelvic actuation system. Thus, the contour plots of the EKM DL Circle Method in figure (5.2) are studied as carried out in the previous section.

Considering the contour plots of the position and orientation accuracy prove that pose errors are unlikely to occur. The iteration's efficiency in the circular region only requires majorly 2 and rarely 3 executed iterations but the code of the algorithm has to many operations (approximately 1500 for each iteration) to run it on a real-time guaranteeing PLC. The needed time is also shorter than the average time  $\Delta\bar{t}$  but still exceeds the 1 ms by approximately 0.5 ms. Thus, the extended forward kinematics algorithm cannot achieve the industrial real-time constraint. Running the CDPR-based forward kinematics of the pelvic actuation system at a slower information rate could achieve real-time feasibility. This is discussed in section (5.5). The contour plots of the other extended forward kinematics algorithms are given in the appendix in section

## 5 Analysis

---

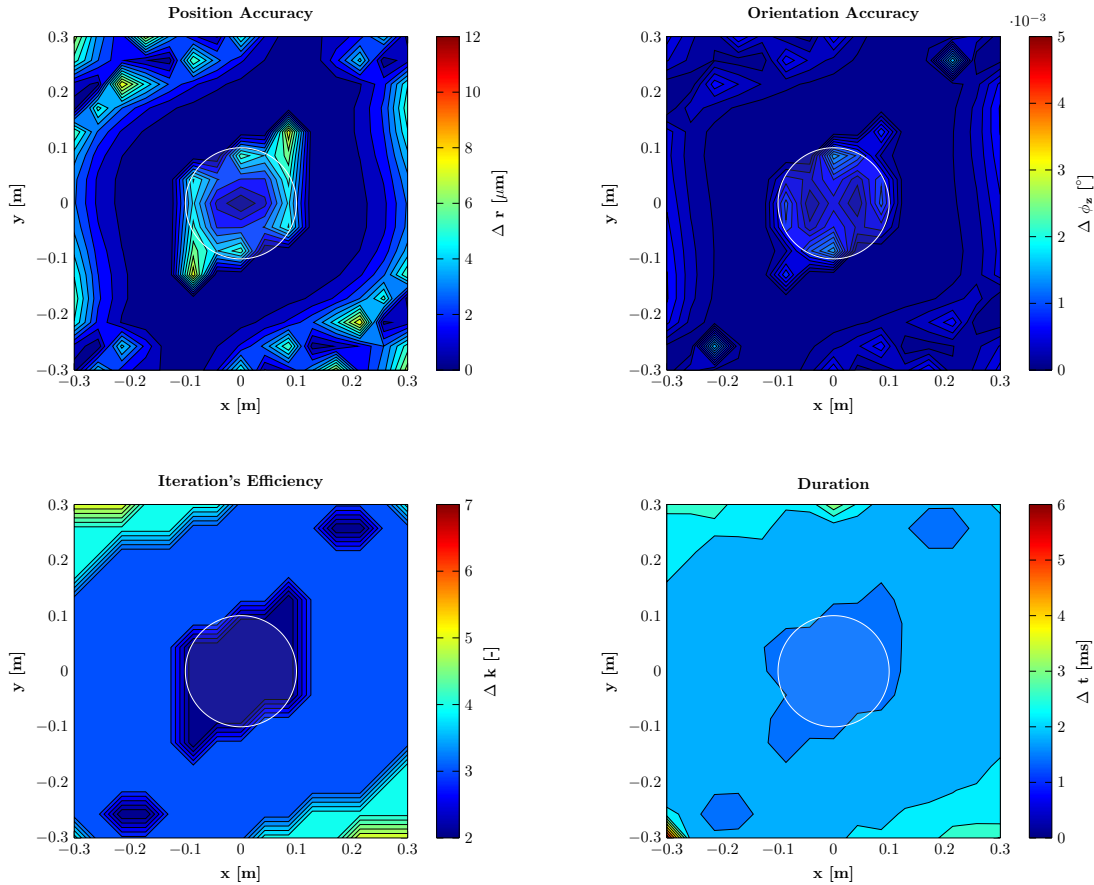


**Figure 5.2:** Contour Plots EKM DL Circle Method in Transverse Plane

(7.4). Having recognized, that only the standard forward kinematics algorithm meets the real-time constraints and that the extended forward kinematics algorithm cannot achieve real-time feasibility due to its too complex model, the standard forward kinematics algorithms SKM DL Circle Method is examined if it runs with cable lengths  $l_{act,i}$  that are not determined through the simple SKM but the EKM. Therefore the experimental results of section (4.5) are analysed in the following section.

### 5.3 Standard Forward Kinematic Algorithms based on Extended Kinematic Model

The first glance at the experimental results of testing the SKM DL Circle Method with cable lengths calculated by the EKM in table (4.6) to generate a more realistic test environment, shows that the average errors in position  $\bar{\Delta r}$  and orientation  $\bar{\Delta \phi_z}$  as well as the average number of executed iterations  $\bar{\Delta k}$  and the average time  $\bar{\Delta t}$  are much higher than the ones received through a standard forward kinematics algorithm based

### 5.3 Standard Forward Kinematic Algorithms based on Extended Kinematic Model

on cable lengths calculated by the SKM. Considering the results the algorithms seems to be inapplicable to the forward kinematics problem, since it is neither accurate nor real-time feasible. Therefore a closer look at the circular region in which the pelvis is expected to move is necessary. The contour plots are given in figure (5.3).

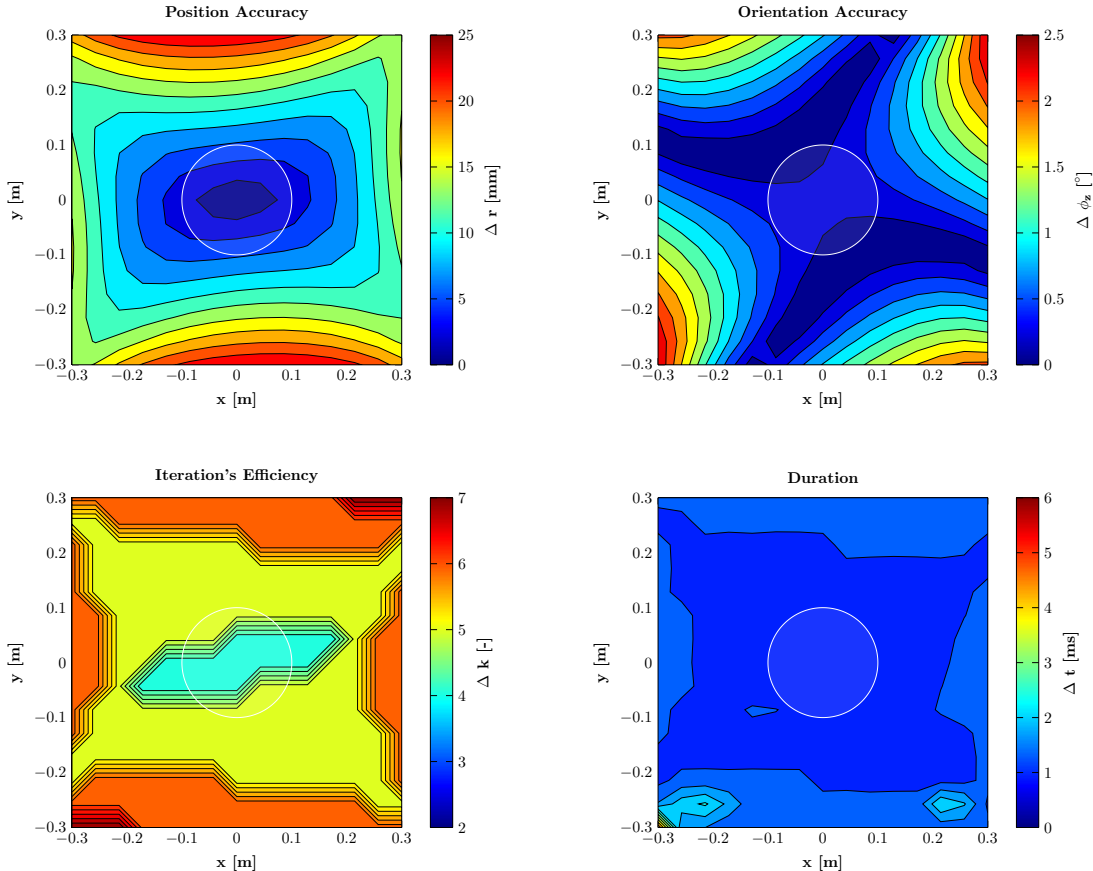


**Figure 5.3:** Contour Plots SKM DL Circle Method based on EKM in Transverse Plane

Analysing the position accuracy in the circular region the maximum error in position ranges at  $\Delta r = 5$  mm. This exceeds of course the aim to stay beneath 1 mm but putting into perspective that a classic manual gait rehabilitation cannot even actuate in the millimetre range, makes this inaccuracy acceptable. Examining the orientation accuracy the error in orientation reaches ranges of  $\Delta\phi_z = 0.3^\circ$  which roughly compares to a 15% error in orientation. Considering that this error becomes much smaller, because the tested pose is an extreme, also makes the orientation accuracy tolerable. The executed iterations in the circular region are majorly in the range of  $\Delta k = 4$  but sometimes even reach  $\Delta k = 5$ . Considering the number of operations conducted by the code it might be impossible to run it on a PLC. However a shorter code such as the SKM DL Center Method could be implementable on a PLC. Considering the duration the algo-

rithm cannot perform at a rate of 1 ms in the circular region. A possible adjustment of the information could deal with this matter and is equally to the real-time feasibility of the EKM DL circle method discussed in section (5.5). The contour plots of the other standard forward kinematics algorithms based on cable lengths determined through the EKM are given in the appendix in section (7.5). Besides inaccuracies due to model assumptions an analysis of the general pelvic movements is necessary. Hence, the experimental results of table (4.7) are interpreted in section (5.4).

## 5.4 Impact of General Pelvic Movements

General pelvic movements are an impact that must be analysed. The pelvis moves spatial whereas the pelvic actuation systems acts planar. Studying the experimental results of the extreme pelvic pose in table (4.7) clarifies that pelvic movements have an impact on the position and the orientation accuracy. The other results concerning the pelvic drop, the anterior tilt, the  $z$ -translation, and a usual pelvic movement in table (4.7) are not analysed because the extreme pose also incorporates their information but their contour plots are given in the appendix in section (7.6). The average error in position  $\Delta\bar{r}$  ranges in the size of millimetres instead of micrometres as in table (4.3). Also, the average error in orientation  $\Delta\bar{\phi}_z$  increases by a factor of  $10^3$  but stays under  $1^\circ$ . The iterations efficiency also increases to  $\Delta\bar{k} = 3.9$  and the duration  $\Delta\bar{t}$  is slightly below 1  $\mu$ s. To interpret the results in detail the evaluation criteria are interpreted in the circular region in which the pelvis is expected to move. The contour plots are depicted in figure (5.4).

Analysing the contour plot of the position accuracy, the error in position  $\Delta r$  reaches 5 mm in the circular region and therefore exceeds the tolerable error of  $\Delta r = 1$  mm in the contour plot. Considering the orientation accuracy, the error in orientation reaches values of  $\Delta\phi_z = 0.29^\circ$ . These results prove that general pelvic movement could cause significant errors to the system's accuracy but it should also be noted that these errors belong to an extreme pose which is not achieved during a usual gait pattern. Considering the results of a usual pose during gait in table (4.7), shows that the average error in position  $\Delta\bar{r} = 0.88$  mm stays below the tolerable error of  $\Delta r = 1$  mm. Also the average error in orientation  $\Delta\bar{\phi}_z = 0.05^\circ$  is acceptable because the error is below  $0.1^\circ$ . The CDPR-based forward kinematics of the pelvic actuation system should therefore yield accurate results and the errors in position and orientation can be neglected due to the conservative testing procedure of the CDPR-based forward kinematics. Similar is the analysis of the real-time feasibility. Considering the average of executed iterations  $\Delta\bar{k} = 3.89$  in table (4.7) suggests that the algorithm can be implemented on a PLC. This is further confirmed by considering the usual pelvic movement where the average number of executed iterations  $\Delta\bar{k} = 2.7$  is even lower. The duration  $\Delta\bar{t} = 0.99$  ms for the extreme pelvic pose might cause issues because it is only slightly below 1 ms but putting into perspective that a usual pelvic pose is definitely real-time feasible with an

## 5.4 Impact of General Pelvic Movements

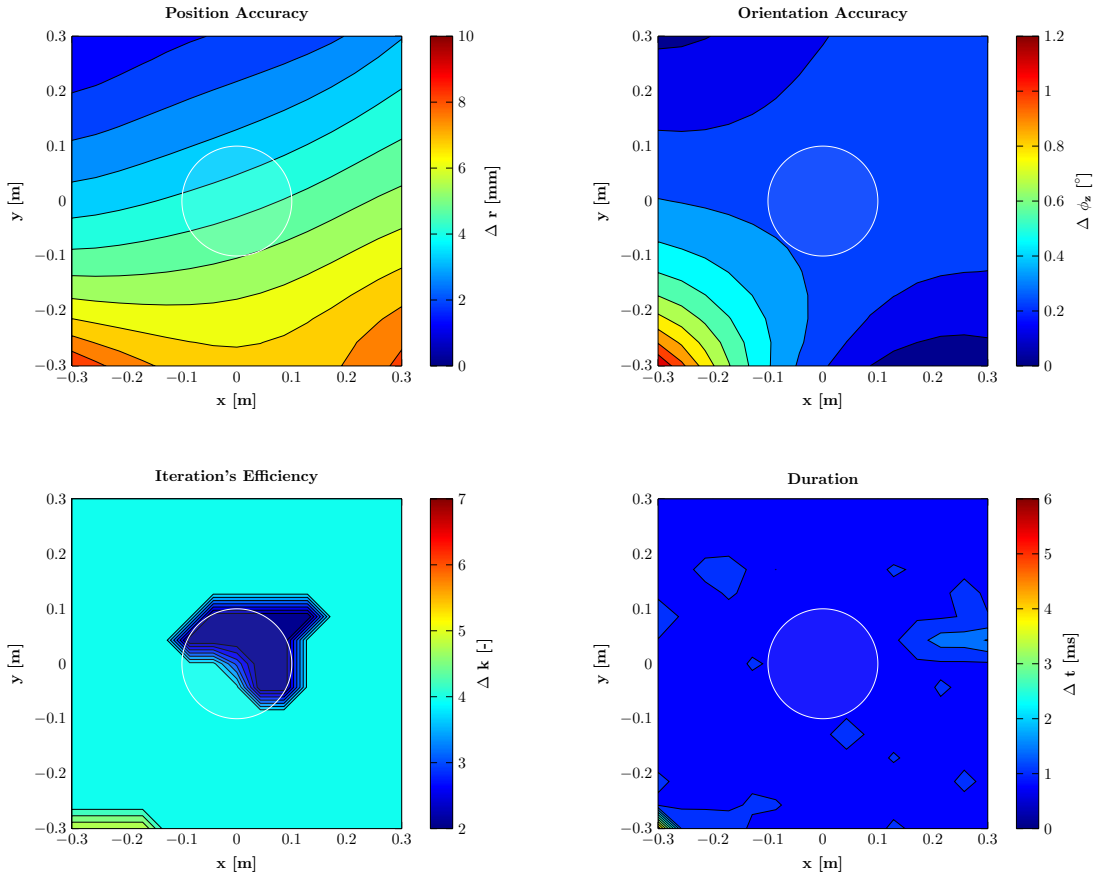


**Figure 5.4:** Contourplots SKM DL Circle Method Pelvic Movements Transverse Plane

average duration of  $\bar{\Delta t} = 0.73$  ms also hints that the SKM DL Circle Method should be a real-time feasible algorithm. This is confirmed by analysing the circular region in the contour plot of the extreme pelvic movements in figure (5.4). The SKM DL Circle Method requires  $k = 2$  or  $k = 4$  iterations. This means that the SKM DL Circle Method can be implemented on a PLC but that could involve that there are only few operations left for other algorithms concerning the rehabilitation. However, since these pelvic movements are an extreme case and considering that only  $k = 3$  iterations in the contour plot of usual pelvic movements in figure (7.20) in the appendix are needed for the entire circular region, confirms that the SKM DL Circle Method should be implementable on a PLC. Considering the duration in the contour plot of the extreme pelvic movements in figure (5.4), the duration  $\Delta t$  stays below 1 ms in the entire circular region and considering that the SKM DL Circle Method is even significantly faster if usual pelvic movements occur proves that the SKM DL Circle Method can challenge general pelvic movements under real-time constraints.

Having dealt with the impact of general pelvic movements, the results of the standard

forward kinematics algorithms in section (5.1), the extended forward kinematics algorithms in section (5.2), the standard forward kinematics algorithms based on the EKM in section (5.3), the impact of general pelvic movement in section (5.4), and the factors affecting accuracy are finally discussed all together in the next section.

## 5.5 A Suitable Real-Time Feasible Algorithm

A suitable algorithm for the CDPR-based forward kinematics of the pelvic actuation system has to be accurate and has to fulfil real-time constraints. In subsection (2.3.1) this constraint is introduced as an information rate up to 1 kHz which corresponds to an algorithm's duration of 1 ms. It is noted that this information rate is considered for industrial applications.

To challenge the problem of real-time feasibility, iterative optimization algorithms combined with initial estimate methods were analysed in the previous sections. The analysed experimental results for the standard forward kinematics algorithms in section (5.1) and the extended forward kinematics algorithm in (5.2) both confirm the hypothesis that the better the initial estimate is, the faster the algorithms performs. Comparing the methods that apply the same iterative optimization method, proves that algorithms seeking to determine the initial estimate, such as the Box and Circle Method, generally perform faster than methods that provide a constantly fixed estimate as the Center Method does. It is also profitable for the duration to attempt to apply a very close estimate because the analysed experimental results in section (5.1) and (5.2) show that equal iterative algorithms perform faster if the Circle Method rather than the Box Method is applied.

In section (3.4.2) it is recommended in [11] to apply the Powell's Dog Leg rather than the Levenberg-Marquardt as iterative optimization due to its faster performance for a non-CDPR related issue. This hypothesis is also confirmed for the forward kinematics of CDPRs by considering the experimental results of the standard and the extended forward kinematics algorithms in section (4.3) and section (4.4) because combinations applying the Powell's Dog Leg have generally a shorter duration than combinations applying the Levenberg-Marquardt. In addition the Powell's Dog Leg requires less iterations than its counterpart.

Bringing together the two hypothesis concerning the initial estimate and the iterative optimization algorithm, means that the fastest standard as well as extended forward kinematics algorithm consists of the Circle Method and the Powell's Dog Leg. This is also proved by determining the best algorithm through the solution finding procedure of Pahl/Beitz in section (5.1) and section (5.2).

A major reason to prefer a rather simple solution of the forward kinematics to

more detailed solutions bases on the possibility that a complex kinematic model threatens real-time constraints. However, detailed modelling also increases the system's accuracy. Considering the analysed standard and extended forward kinematics algorithms in section (5.1) and (5.2) it is recognized that both algorithms determine the CDPR's pose very accurately but only the standard forward kinematics algorithms fulfil the real-time constraint. All extended forward kinematics algorithms exceed the maximum permissible duration of 1 ms. Running the standard forward kinematics algorithms on cable lengths provided by the EKM also generates issues as explained in section (5.3). The SKM DL Circle Method as well as the other ones in the appendix are quite sensitive to cable lengths differing from the SKM. The accuracy of the algorithms worsens producing errors in position up to  $\Delta r = 5$  mm in the region where the pelvic actuation system is expected to operate. Also the number of executed iterations increases possibly in a way that the number of operations needed to run the algorithm on a PLC is also exceeded. Additionally the algorithms cannot achieve the real-time constraint of 1 ms.

This leads to a discussion of the proposed real-time constraint as well as the desired system's accuracy. The constraint of 1 ms is reasonable for industrial applications and usually applied in manufacturing to achieve high accuracy and tolerance specifications of the produced part. The idea of rehabilitation robotics bases on the hypothesis that a robot intensifies a rehabilitation therapy due to its precise controllability, repeatability, and accuracy, which cannot be achieved by a human. Therefore a rehabilitation robot allowing errors in the range of a couple of millimetres as well as performing at an information rate up to 100 Hz will still outperform a rehabilitation therapy conducted by a human. Hence it is convenient to adjust the real-time constraint to a rate up to 100 Hz, which corresponds to a duration of 10 ms. Also the accuracy is sufficient if the errors in position and orientation range in the size up to 5 mm and  $0.3^\circ$  respectively.

Introducing these new constraints, all extended forward kinematics become real-time feasible on a computer and the standard forward kinematics algorithms still fulfil the accuracy requirements. A different approach is to implement the algorithms on a PLC but it is noted that only the standard forward kinematics algorithms are possibly applicable on a PLC due to the maximum number of 2048 operations. The extended forward kinematics algorithms need too many operations to be implemented on a PLC. Applying a SKM combination that includes the Powell's Dog Leg is especially advantageous since the Powell's Dog Leg algorithm requires less iterations than the Levenberg-Marquardt.

The experimental results concerning the duration could also be enhanced by changing the simulation setup. All simulation were conducted by a Windows 10 which does not necessarily provide a very accurate real-time simulation. Upgrading the Windows via a RTX64, offered in [8], enables the computer to perform in a real-time environment. This could yield better experimental results. Applying a faster processor could also

## 5 Analysis

---

improve the results. Considering the code of the algorithms, it should be mentioned that the complexity of the code causes varying results. The algorithm generally performs faster when simple operations instead of powerful functions are applied. In addition the algorithm could possibly be accelerated if the code is improved through a better memory and processing organisation.

Concluding the issue of real-time feasibility, several options exist to choose a suitable algorithm. The easiest way is to implement a standard forward kinematics algorithm on a PLC. Depending on the number of conducted operations it is preferable to implement a combination applying the Powell's Dog Leg algorithm because of the fewer number of iterations compared to the Levenberg Marquardt. Running the forward kinematics on a computer the real-time constraint can be adjusted to 100Hz, so that the standard forward kinematics algorithms as well as the extended forward kinematics algorithm perform at real time.

The accuracy of the pose determined through the forward kinematics algorithm depends on the one hand on the kinematic model on the other hand on other influences. Cable elasticity can be excluded as well as the impact of deflection due to gravitational forces as explained in subsection (3.4.1) and (3.4.2). General pelvic movements being spatial cause inaccuracies since the actuation system operates planar but they are comparatively small, if usual pelvic movements are considered. In addition the analysed general pelvic movements in extreme poses are rather unlikely to occur. Therefore general pelvic movements can also be neglected as explained in section (5.4) All other errors connected to the design of the actuation system are excluded since the actuation system was designed as robust and stiff as possible.

Nevertheless the errors exist and if all errors occur and are summed up it might be possible that major accuracy errors occur. That can be partially prevented by applying black-box accuracy compensation, as proposed in [26]. The black box accuracy deals with systematic errors such as the error in position  $\Delta r$  or the orientation  $\Delta\phi_z$ . Measuring these errors the system can be adjusted to the desired pelvic pose  $\mathbf{x}^*$ .

# 6 Conclusion & Outlook

This thesis examined the determination of a suitable CDPR-based forward kinematics for a new pelvic actuation system for gait rehabilitation of stroke patients proposed in [5]. To determine the pelvic pose, the CDPR-based forward kinematics had to be solved by numerical methods because the system is kinematically over-constrained. Several approaches such as interval arithmetic, neural networks, genetic algorithms or iterative optimization were discussed to challenge the forward kinematics. The chosen suitable forward kinematics algorithms consists of an iterative optimization algorithm combined with an algebraic initial estimate method.

Considering the iterative optimization, the Levenberg-Marquardt, generally applied for CDPRs, was tested and compared to the Powell's Dog Leg which was firstly tested for a CDPR application. The experimental results proved, that the Powell's Dog Leg outperforms the Levenberg-Marquardt. To deal with the initial estimate, the Center Method, Box Method, and Circle Method were implemented and tested. The new Circle Method inspired by the Box Method yields the best approximate to the position of the pelvis followed by the Box Method.

To apply the pelvic actuation system to rehabilitation the forward kinematics algorithms have to be real-time feasible. All algorithms fulfil the real-time constraint of an information rate up to 100Hz if they are run on a computer. The standard forward kinematics algorithms could also be possibly implemented on a PLC guaranteeing real-time feasibility.

Besides the real-time constraints other impacts on the pelvic actuation system were discussed. The applicability of standard forward kinematics algorithms to cable lengths differing from the Standard Kinematic Model was investigated. It was confirmed, that standard forward kinematics algorithms yield sufficiently accurate results and are therefore applicable to the pelvic actuation system. Also the impact of general spatial pelvic movements on the planar working pelvic actuation system were tested with standard forward kinematics algorithm. The standard forward kinematics algorithms were also proven to be sufficient to deal with these pelvic movements. Therefore the impact of spatial pelvic movements can be considered as negligibly small. A major impact on the system's accuracy is the radius of the winches' drums. To challenge the influence of the drum's radius an Extended Kinematic Model, closely related to the model in [21], was developed and applied to the forward kinematics. The results of the forward kinematics algorithms based on the Extended Kinematic

## *6 Conclusion & Outlook*

---

Model are real-time feasible according to an information rate up to 100Hz but do not fulfil the real-time constraints of an information rate up to 1kHz which is valid for industrial applications but it was also discussed that for rehabilitation purposes an information rate up to 100Hz should be acceptable. Nevertheless inaccuracies occur and if they are summed up, they could possibly cause greater accuracy errors. A solution to challenge that problem might be the black box accuracy compensation in [26].

It is also noted that a testing of the algorithms applied to the pelvic actuation system during a gait rehabilitation training session have not yet been conducted. Therefore the influence of factors affecting accuracy cannot be finally answered. Also the tests concerning the real-time feasibility were only conducted on a computer. The CDPR-based pelvic actuation system has to be tested to obtain a final answer if the algorithms fulfil real-time constraints and are applicable to rehabilitation.

In addition the performance of the forward kinematics algorithms could be further improved if a real-time package is installed on the computer and a faster processor is applied.

Considering CDPRs in general, the problem specific Circle Method could provide a decent method to approximate the position of a CDPR with six degrees of freedom and should therefore be expanded from the planar to the spatial case. Still unanswered remains the determination of an estimate to the CDPR's orientation.

# 7 Appendix

## 7.1 Comparison of the Box- and the Circle-Method

The newly developed Circle Method bases on the same idea as the Box Method discussed in subsection (2.3.1) but should achieve an even more accurate estimate of the platform's position due to the smaller intersection region. This hypothesis is examined in the following test. The simulation setup described in section (4.2) and the robot prototype in table (4.1) is adopted. The actual cable length vector  $\mathbf{l}_{act}$  is determined through the inverse kinematic solution  $\mathbf{q}_{SKM}$  of the SKM in equation( 2.5). The methods are compared on the analysis field in section (4.2) which has the form of a square with its center located at  $K_0$  and sides having 0.6 m in length. Again, there are 225 tested poses. The position difference between the ideal position  $\mathbf{r}^*$  and the position calculated through the Circle Method  $\mathbf{r}^{circle}$  in equation (3.19) is yielded by

$$\Delta r^{circle} = \sqrt{(r_x^{circle} - r_x^*)^2 + (r_y^{circle} - r_y^*)^2}, \quad (7.1)$$

whereas the position difference between the ideal position  $\mathbf{r}^*$  and the position calculated through the Box Method  $\mathbf{r}^{box}$  in equation (3.7) is obtained by

$$\Delta r^{box} = \sqrt{(r_x^{box} - r_x^*)^2 + (r_y^{box} - r_y^*)^2}. \quad (7.2)$$

The difference in position  $\Delta r^{circle}$  in equation (7.1) and  $\Delta r^{box}$  is tested for the 225 poses one time without a transverse rotation ( $\phi_z = 0^\circ$ ) and the other time with a transverse rotation  $\phi_z = 20^\circ$ . For these results the averages of the position determined through the circle method  $\bar{\Delta r}_{\phi_z}^{circle}$  and the averages of the position determined through the box method  $\bar{\Delta r}_{\phi_z}^{box}$  with the index  $\phi_z$  indicating the value of the transverse rotation  $\phi_z$  are calculated. The experimental results are given in table (7.1).

$\bar{\Delta r}_{0^\circ}^{box}$ [cm]	$\bar{\Delta r}_{20^\circ}^{box}$ [cm]	$\bar{\Delta r}_{0^\circ}^{circle}$ [cm]	$\bar{\Delta r}_{20^\circ}^{circle}$ [cm]
5.21	9.24	3.67	6.11

**Table 7.1:** Experimental Results Comparison Box and Circle Method

Considering the results in table (7.1) proves the hypothesis that the Circle Method determines an even closer estimate to the position  $\mathbf{r}$  of the platform than the Box Method. If a transverse rotation  $\phi_z$  is involved the estimate is worse than without a transverse rotation because both methods neglect the orientation of the platform.

## 7.2 Comparison of the Standard Kinematic Model and the Extended Kinematic Model

In order to gain a deeper understanding of the EKM generated in section (3.5) this section compares the EKM with the SKM. It is supposed that the EKM incorporates the SKM only adding the detail of the drum's kinematics. Therefore the inverse kinematic solution  $\mathbf{q}_{EKM}$  of the EKM in equation (3.55) should converge to the planar inverse kinematic solution  $\mathbf{q}_{SKM}$  of the SKM in equation (2.4) if the radius of the drum  $r_d$  is reduced. This relationship is investigated by calculating the difference  $\Delta\mathbf{q}$  between the inverse kinematic solution in equation (2.5) and the inverse kinematic solution in equation (3.56) whose parameters are consistent with the robot prototype in table (4.1) except the drum's radius which is repetitively reduced starting at  $r_d = 0.02\text{m}$ . To illustrate the results the euclidean norm of the vector  $\Delta\mathbf{q}$  is determined for each reduced drum radius  $r_d$ . The results are depicted in figure (7.1).

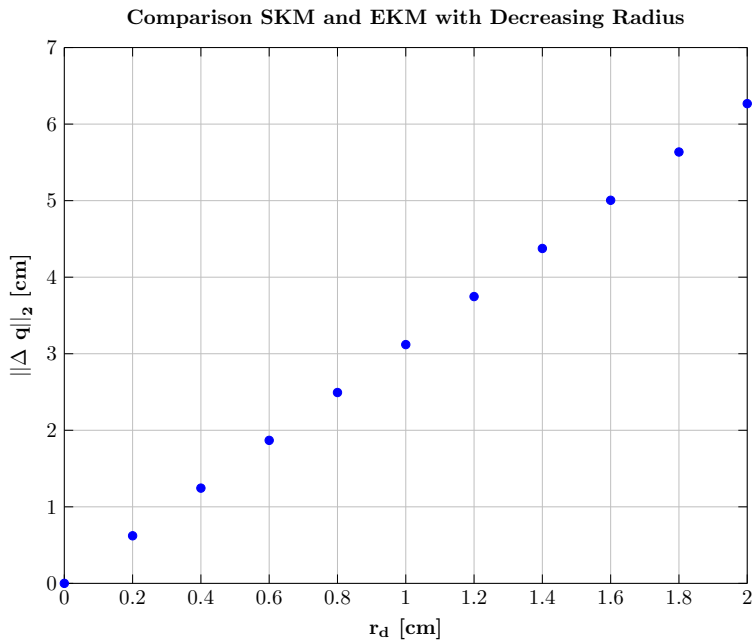


**Figure 7.1:** Comparison of SKM and EKM Relating to the Radius  $r_d$

Considering the graph in figure (7.1), proves the hypothesis, that the EKM incorporates the SKM. If the drum's radius  $r_d$  is gradually reduced, the difference between the inverse kinematics solution of the EKM and SKM decreases. In the special case of  $r_d = 0\text{cm}$  the EKM is therefore equivalent to the SKM.

## 7.3 Contour Plots of the Standard Forward Kinematics Algorithm

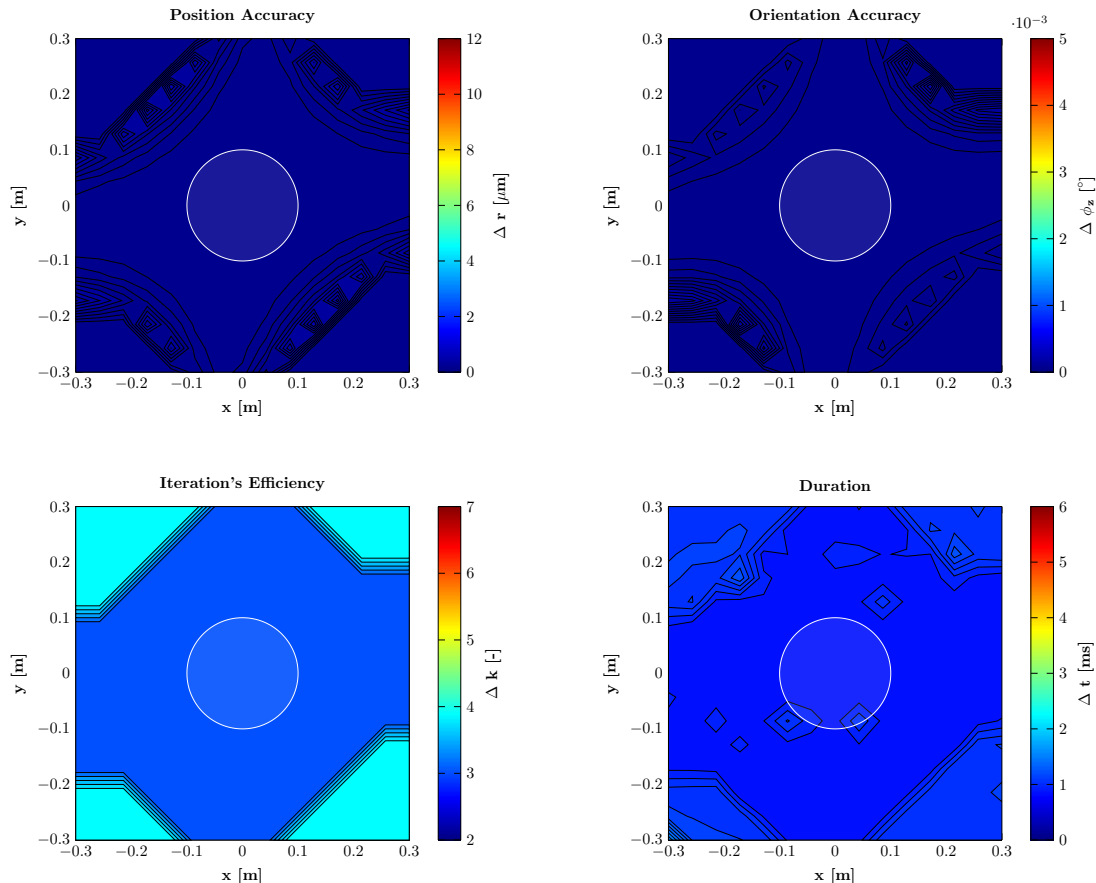


**Figure 7.2:** Contour Plots SKM LM Center Method in Transverse Plane

## 7 Appendix

---

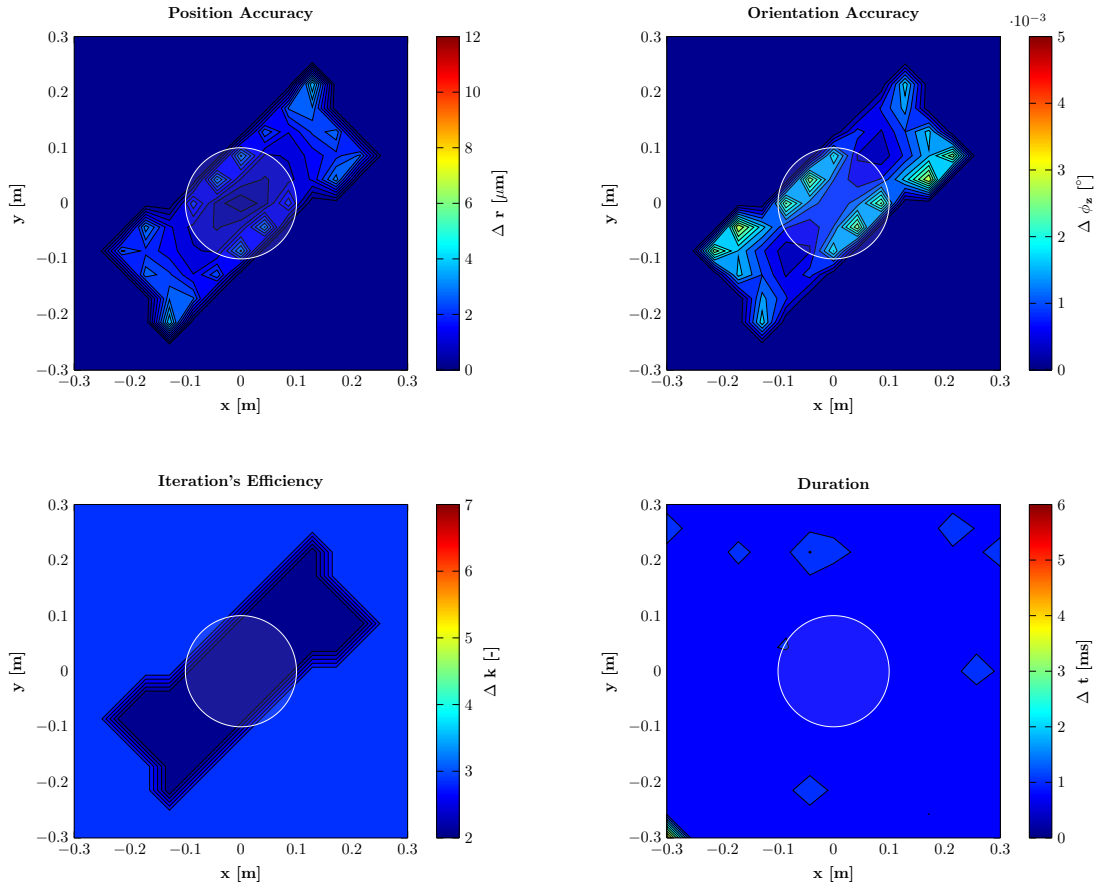


**Figure 7.3:** Contour Plots SKM LM Box Method in Transverse Plane

### 7.3 Contour Plots of the Standard Forward Kinematics Algorithm

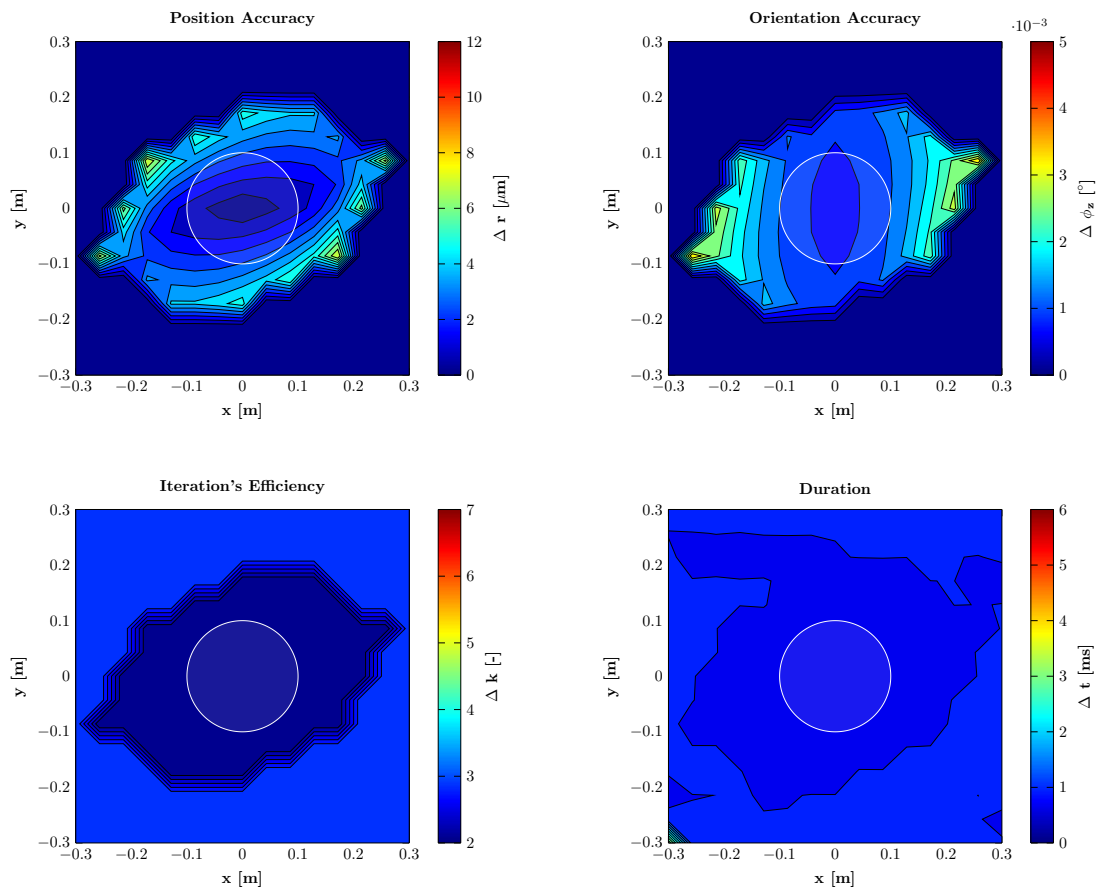


**Figure 7.4:** Contour Plots SKM LM Circle Method in Transverse Plane

## 7 Appendix

---

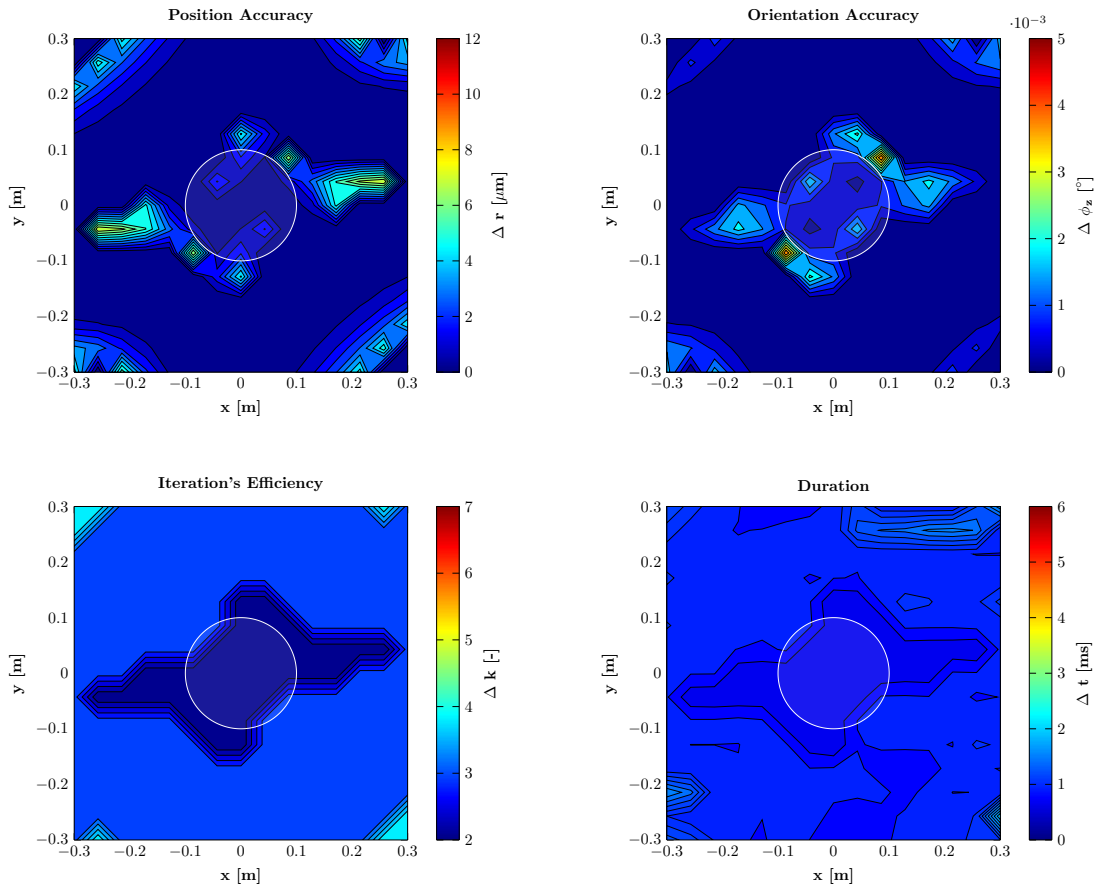


**Figure 7.5:** Contour Plots SKM DL Center Method in Transverse Plane

### 7.3 Contour Plots of the Standard Forward Kinematics Algorithm

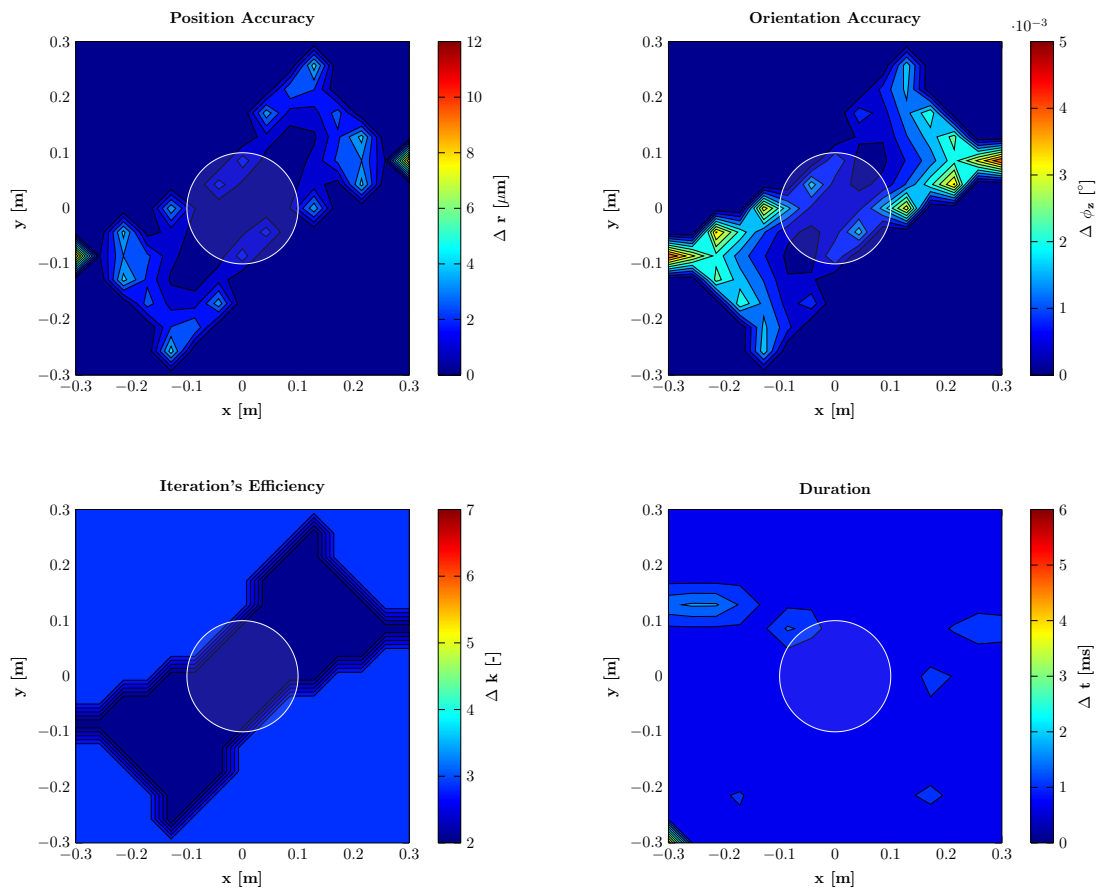


**Figure 7.6:** Contour Plots SKM DL Box Method in Transverse Plane

## 7.4 Contour Plots of the Extended Forward Kinematics Algorithm

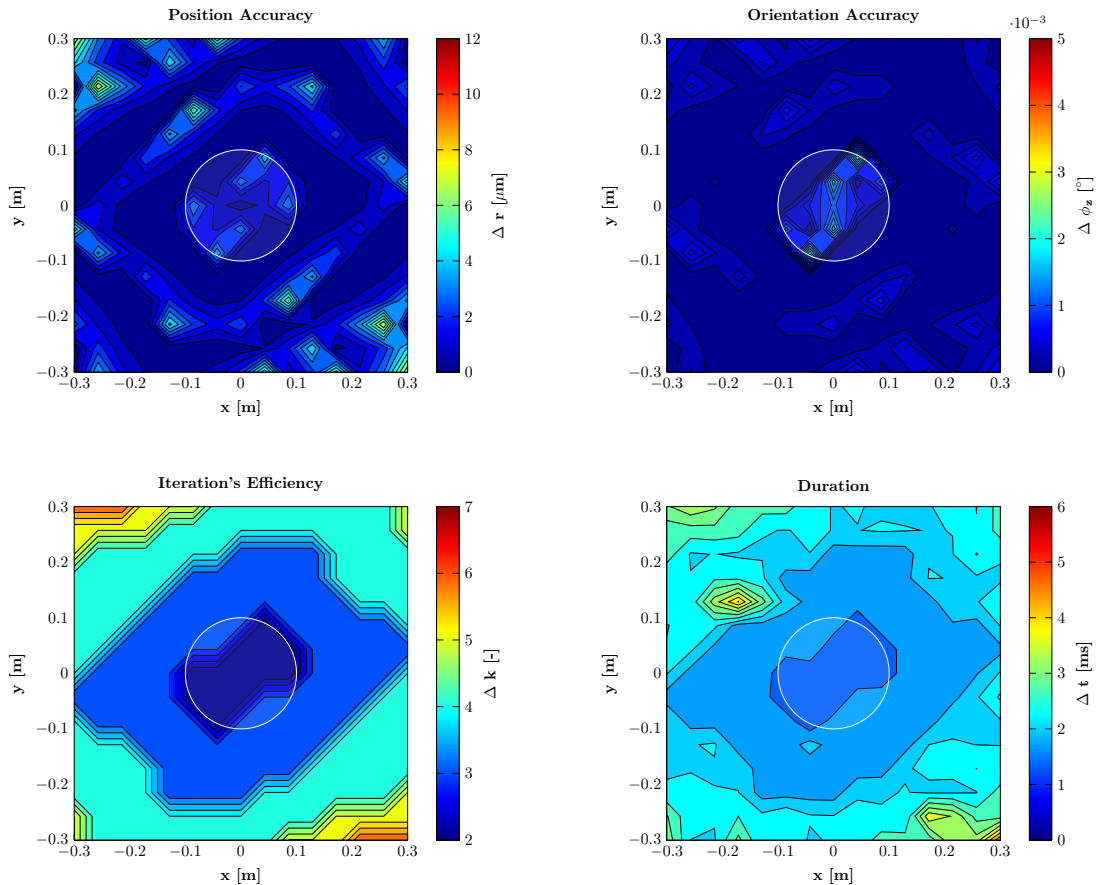


**Figure 7.7:** Contour Plots EKM LM Center Method in Transverse Plane

## 7.4 Contour Plots of the Extended Forward Kinematics Algorithm

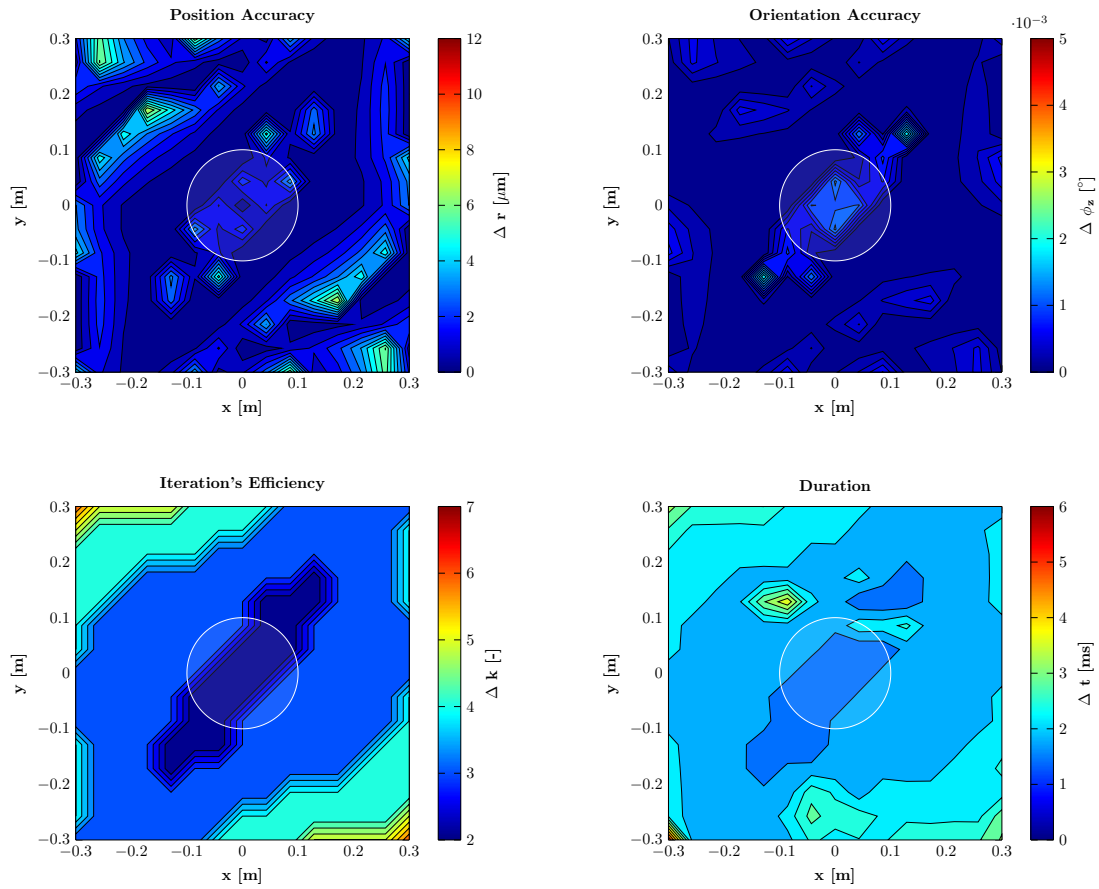


**Figure 7.8:** Contour Plots EKM LM Box Method in Transverse Plane

## 7 Appendix

---

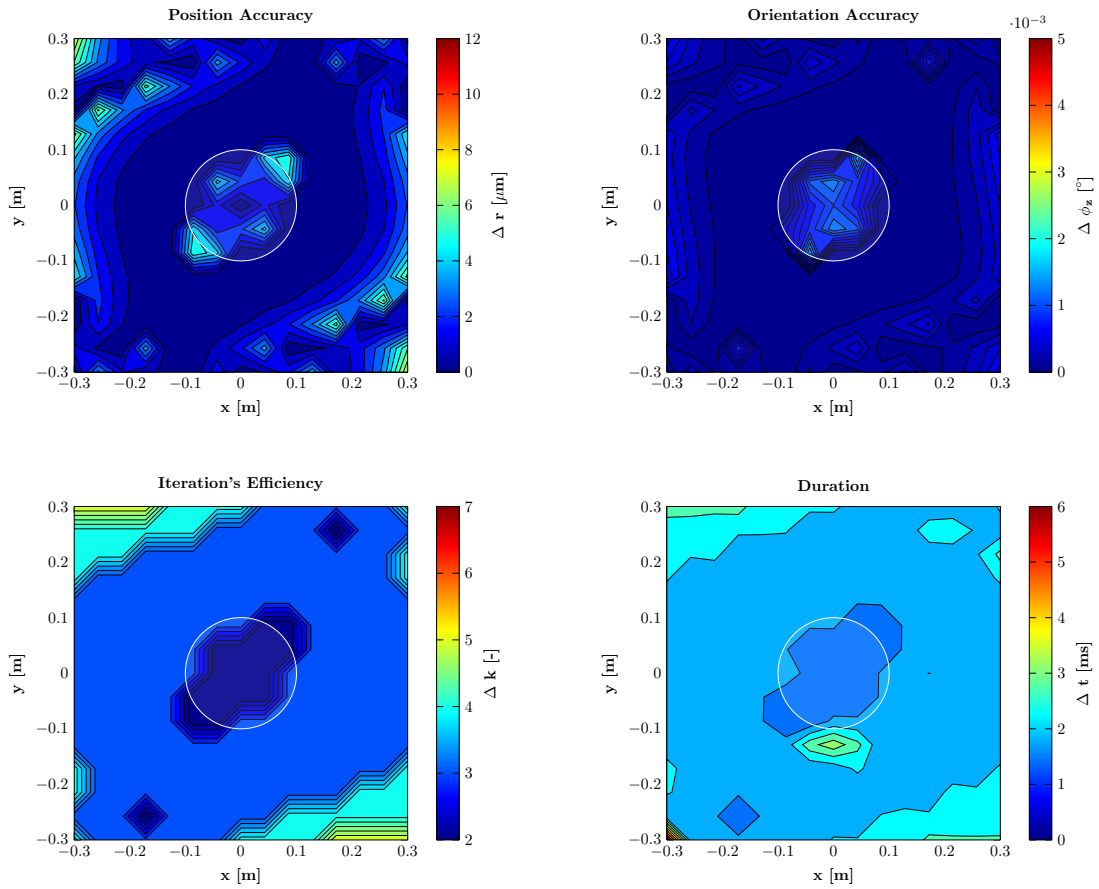


**Figure 7.9:** Contour Plots EKM LM Circle Method in Transverse Plane

## 7.4 Contour Plots of the Extended Forward Kinematics Algorithm

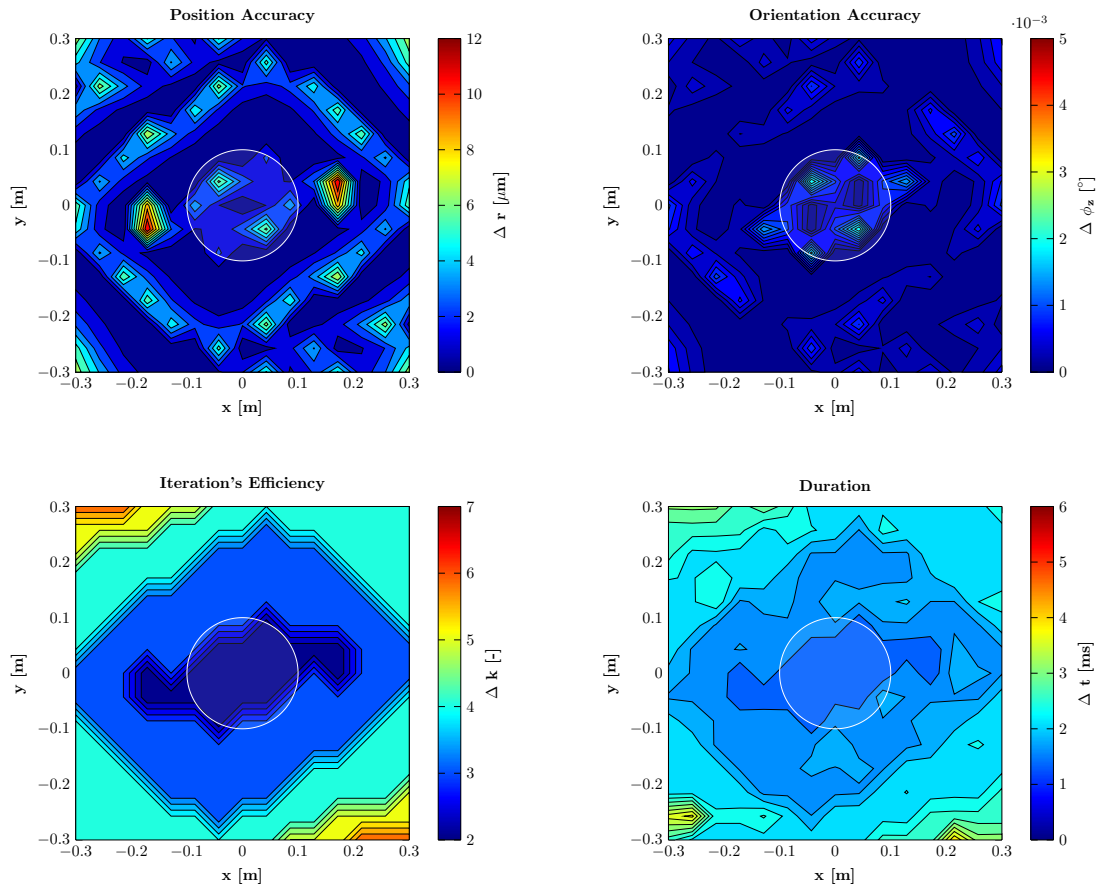


**Figure 7.10:** Contour Plots EKM DL Center Method in Transverse Plane

## 7 Appendix

---

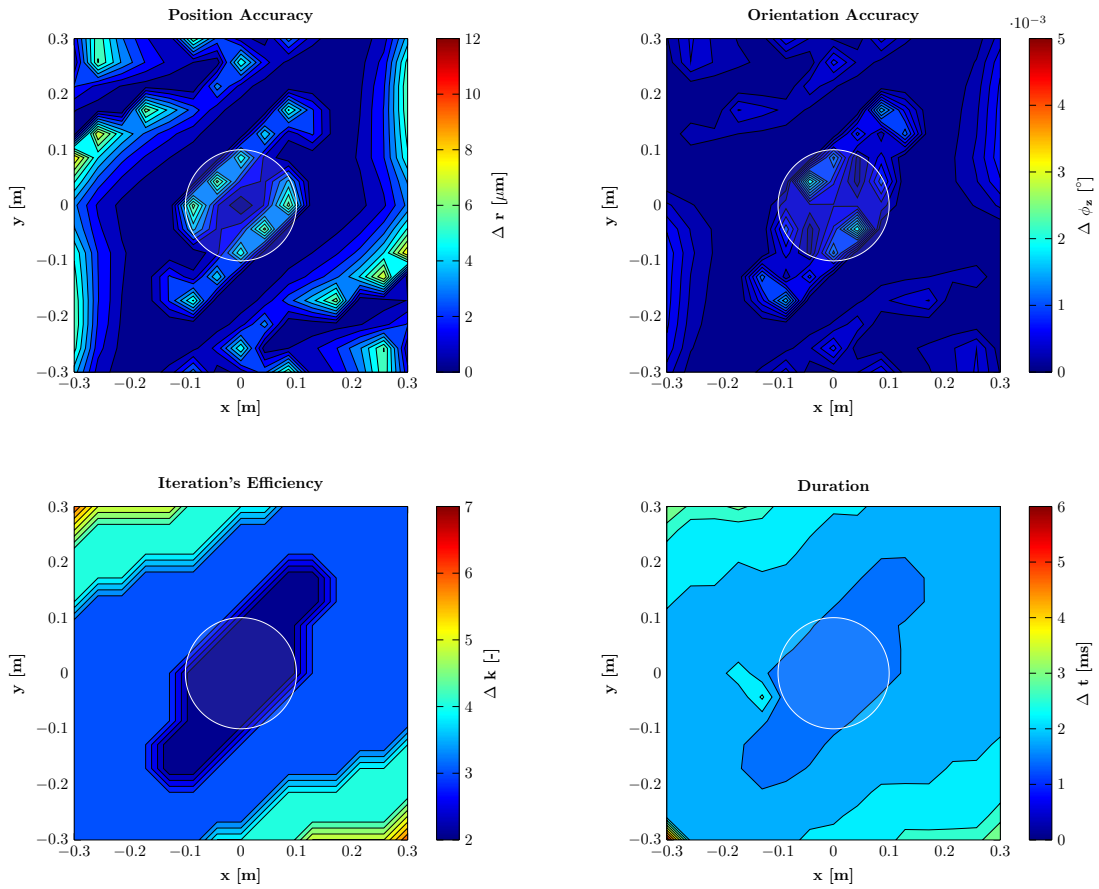


**Figure 7.11:** Contour Plots EKM DL Box Method in Transverse Plane

## 7.5 Contour Plots of the Standard Forward Kinematics Algorithm based on EKM

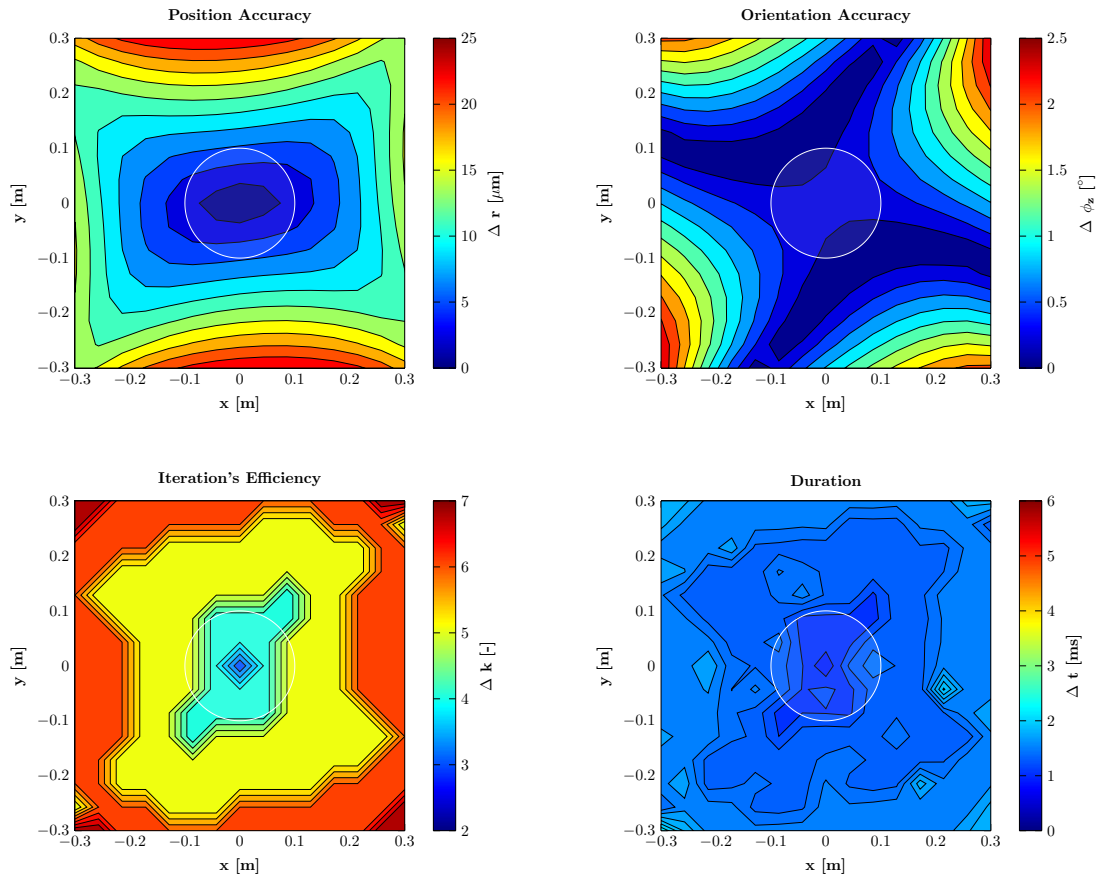


**Figure 7.12:** Contour Plots SKM LM Center Method based on EKM in Transverse Plane

## 7 Appendix

---

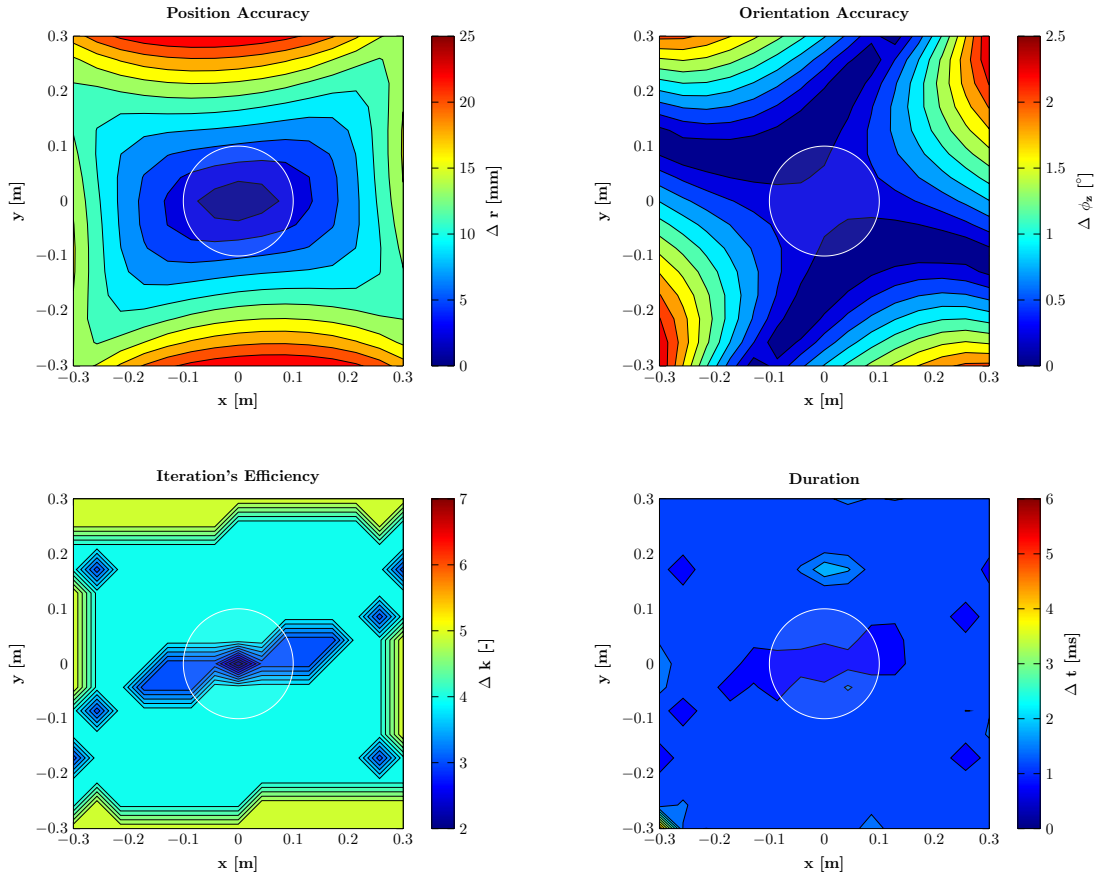


**Figure 7.13:** Contour Plots SKM LM Box Method based on EKM in Transverse Plane

## 7.5 Contour Plots of the Standard Forward Kinematics Algorithm based on EKM

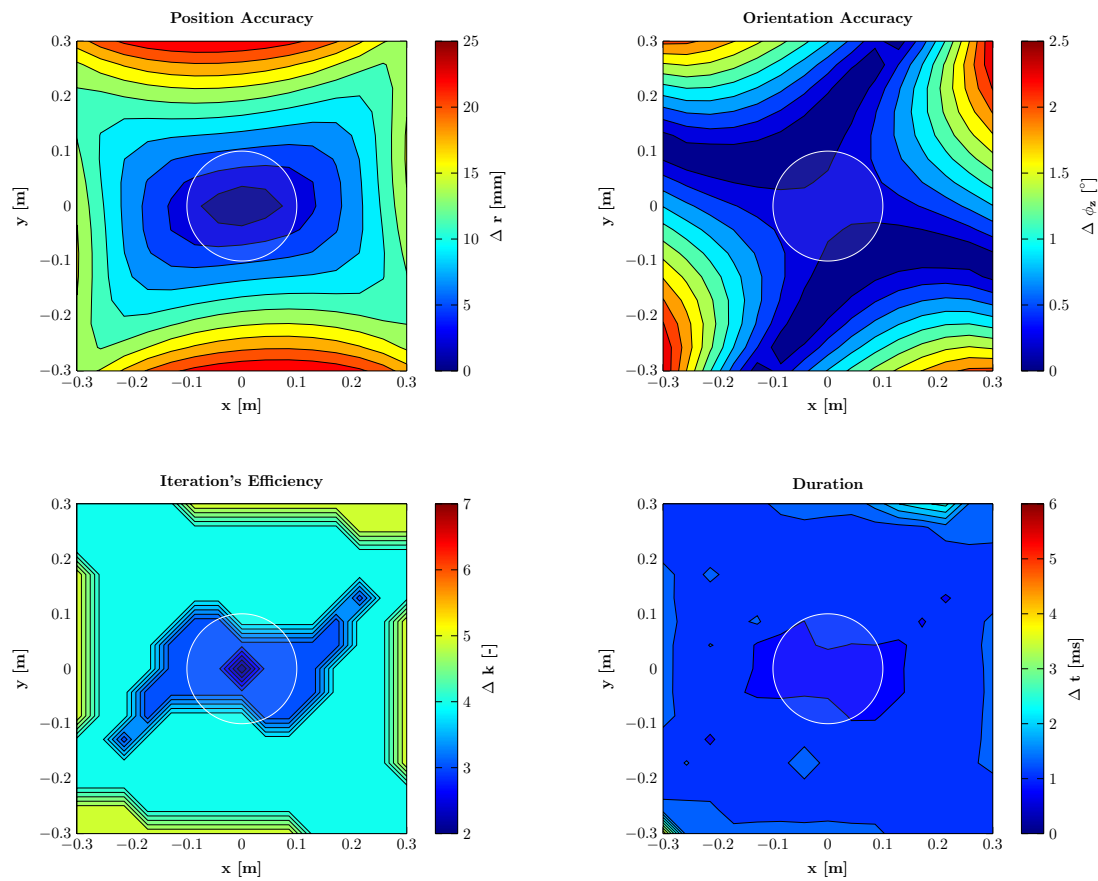


**Figure 7.14:** Contour Plots SKM LM Circle Method based on EKM in Transverse Plane

## 7 Appendix

---

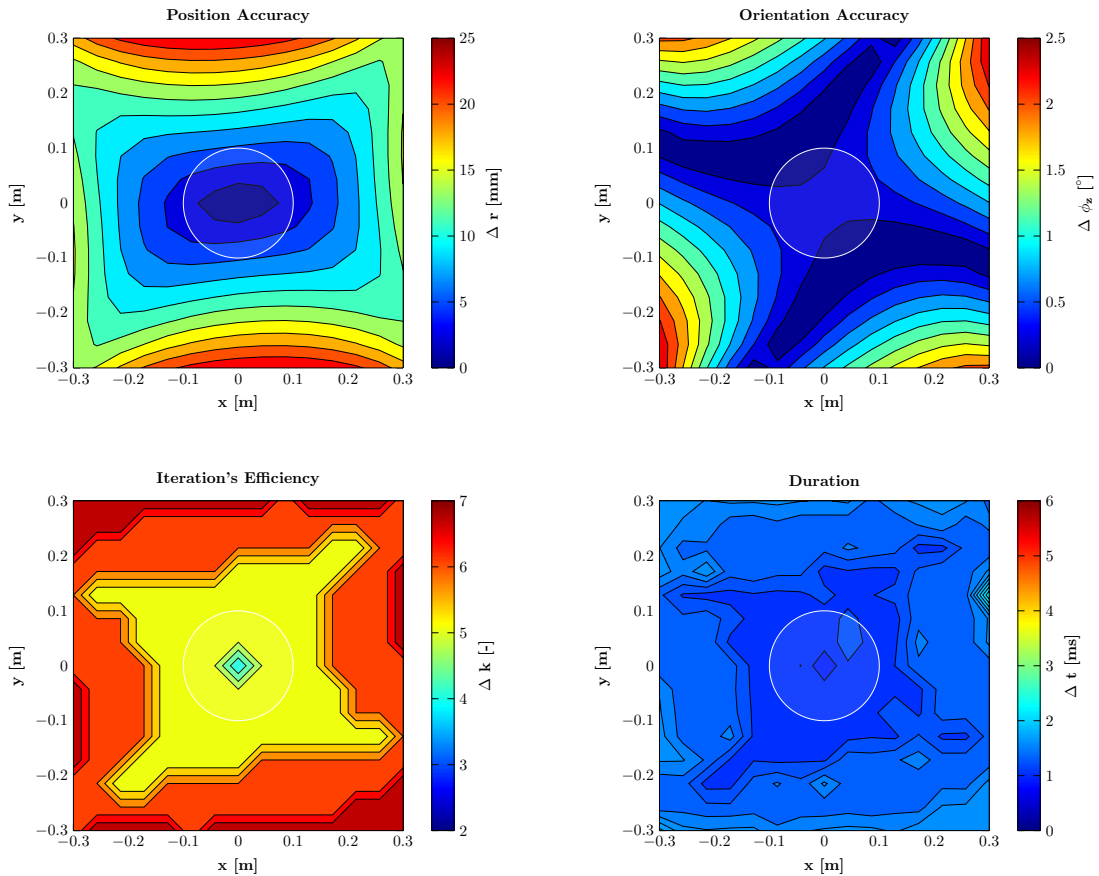


**Figure 7.15:** Contour Plots SKM DL Center Method based on EKM in Transverse Plane

## 7.5 Contour Plots of the Standard Forward Kinematics Algorithm based on EKM

---

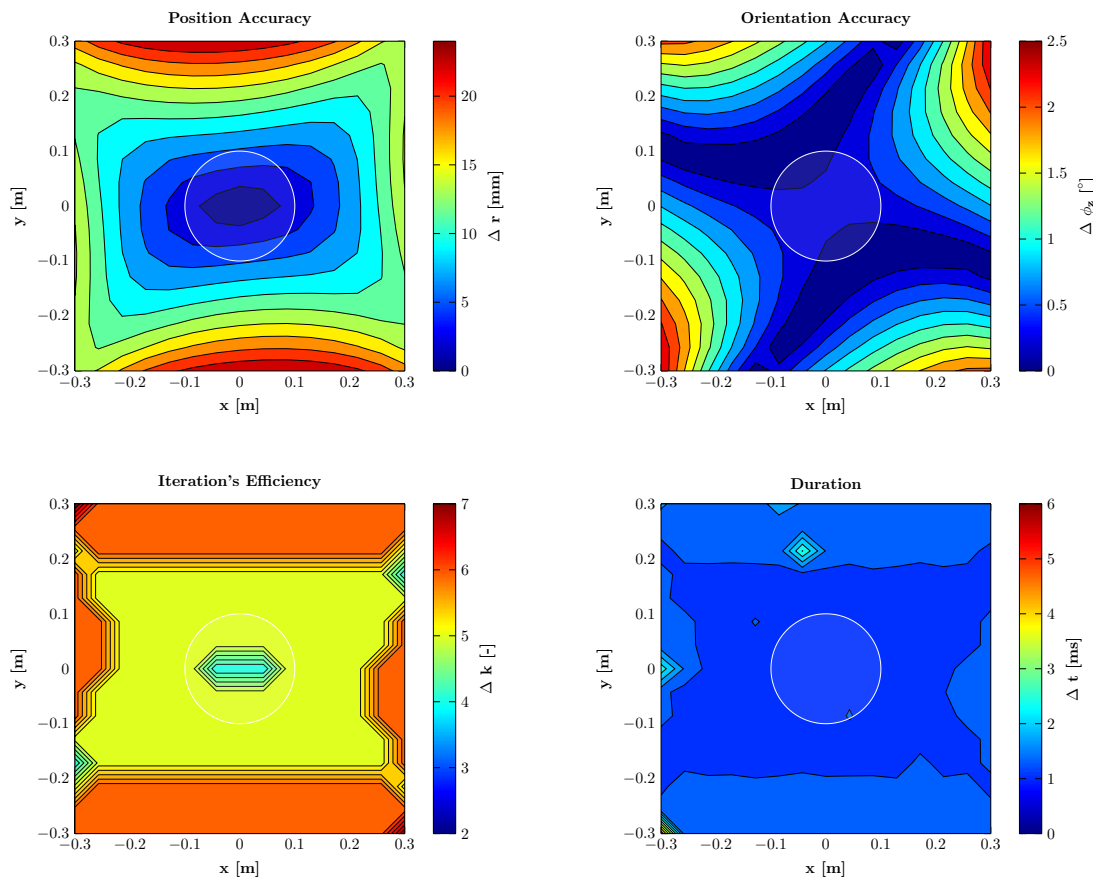


**Figure 7.16:** Contour Plots SKM DL Box Method based on EKM in Transverse Plane

## 7.6 Contour Plots of General Pelvic Movements

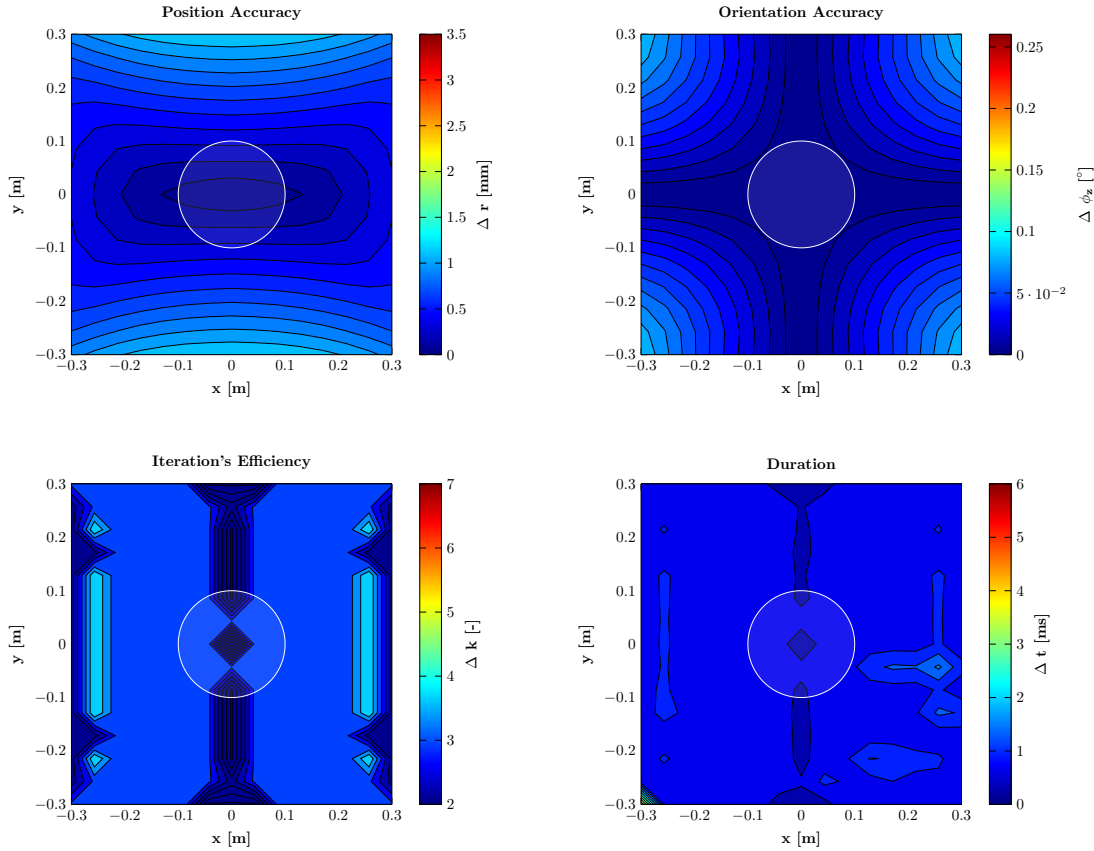


**Figure 7.17:** Contour Plots SKM DL Circle Method Pelvic Drop in Transverse Plane

## 7.6 Contour Plots of General Pelvic Movements

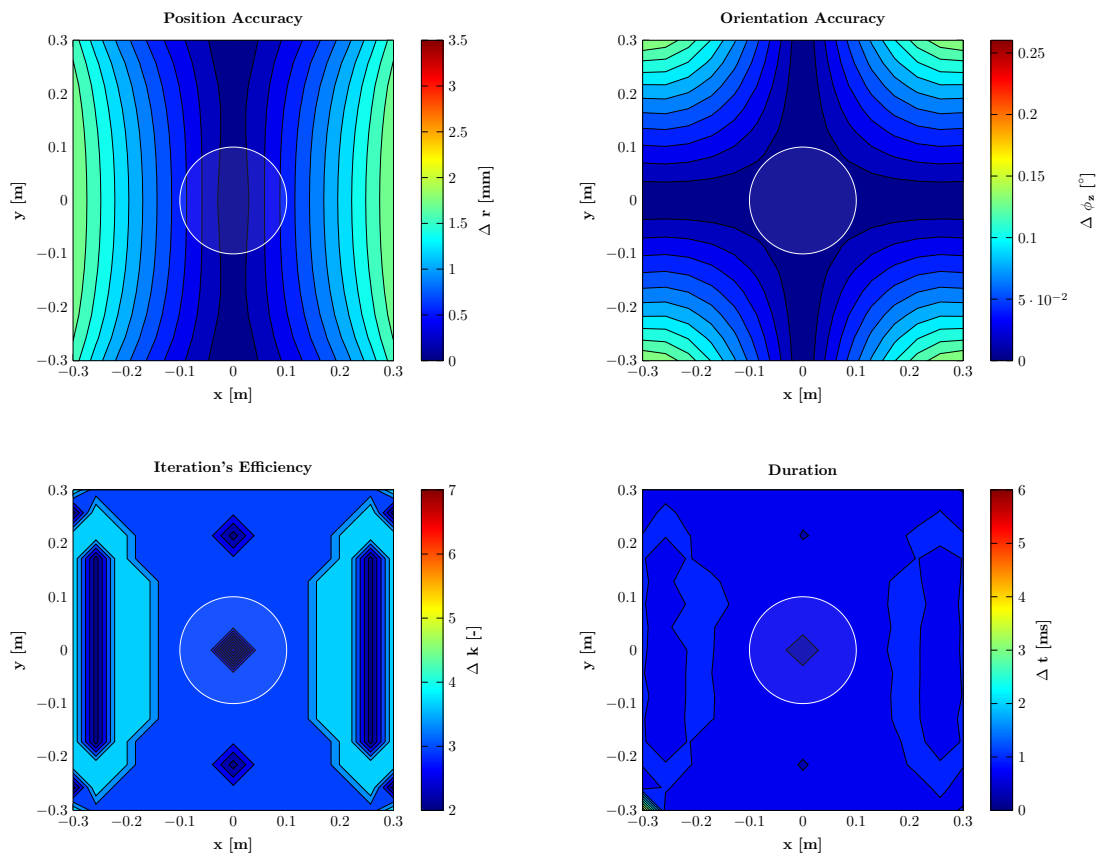


**Figure 7.18:** Contour Plots SKM DL Circle Method Anterior Tilt in Transverse Plane

## 7 Appendix

---

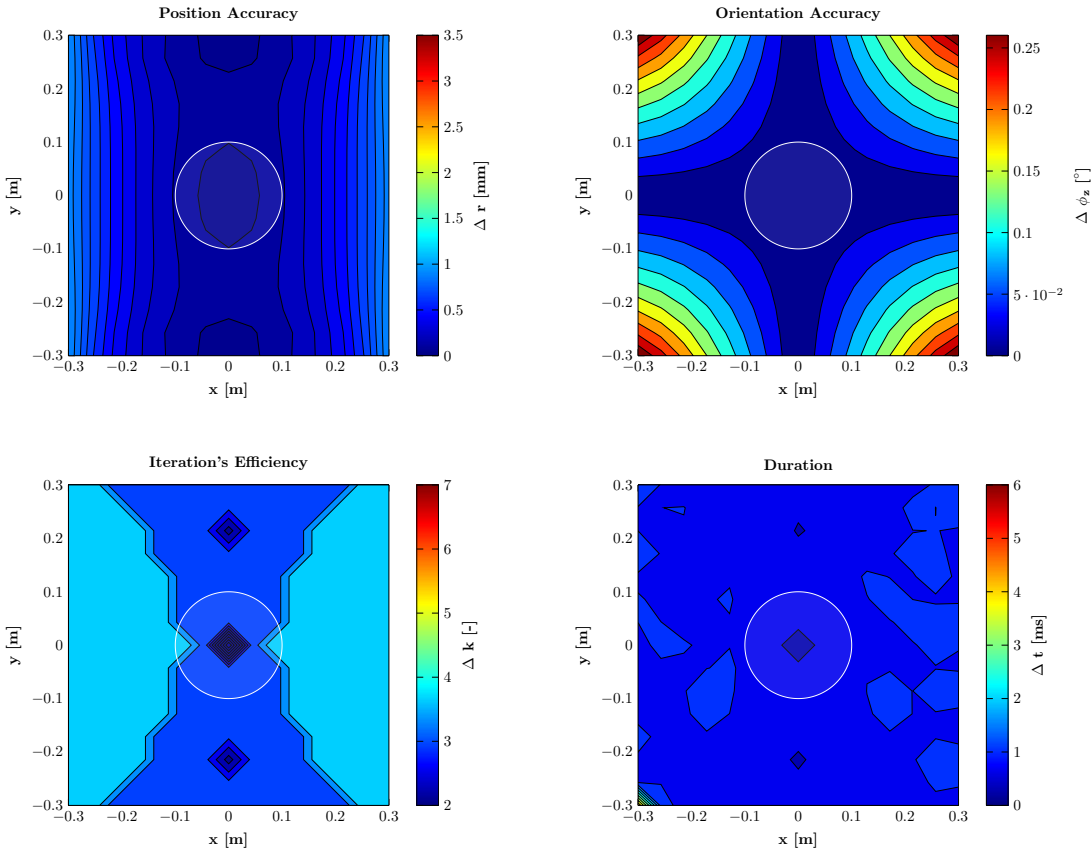


**Figure 7.19:** Contour Plots SKM DL Circle Method  $z$ -Translation in Transverse Plane

## 7.6 Contour Plots of General Pelvic Movements

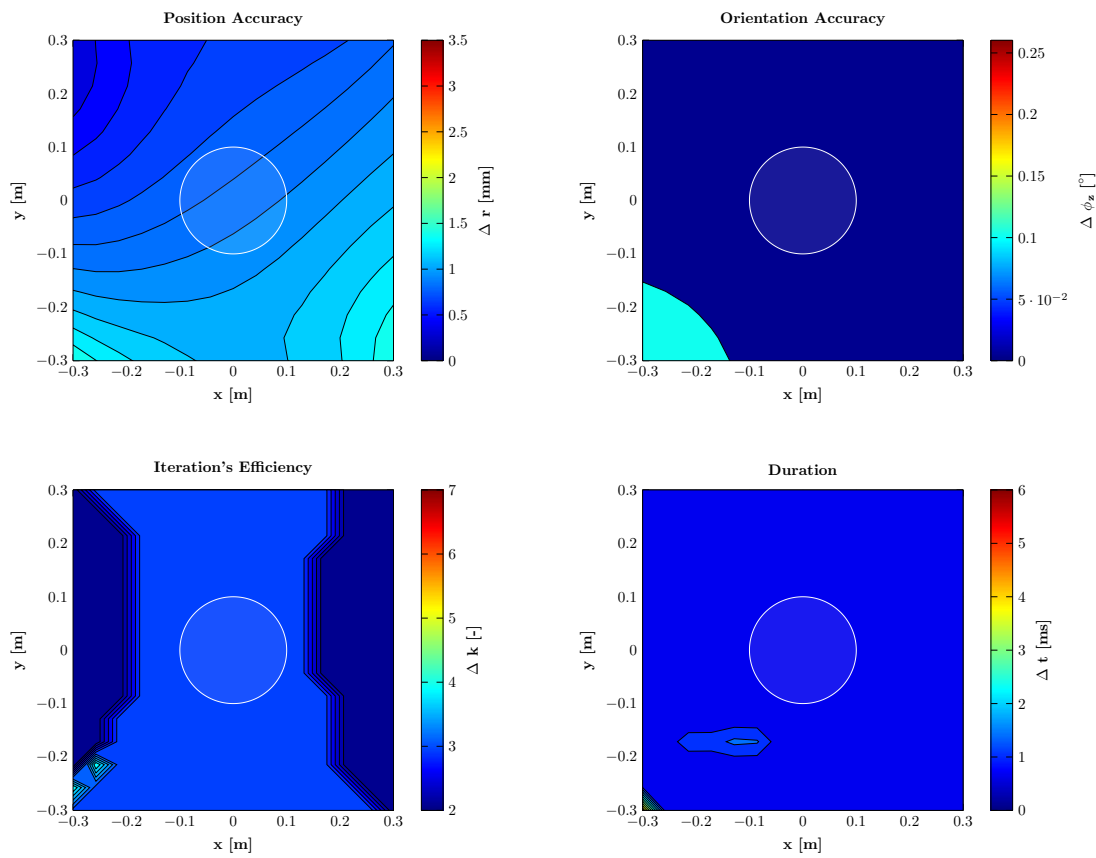


**Figure 7.20:** Contour Plots SKM DL Circle Method Usual Pelvic Movements in Transverse Plane

## *7 Appendix*

---

# Bibliography

- [1] J.-M. Belda-Lois, S. Mena-del Horno, I. Bermejo-Bosch, J. Moreno, J. Pons, D. Farina, M. Iosa, M. Molinari, F. Tamburella, A. Ramos, A. Caria, T. Solis-Escalante, C. Brunner, and M. Rea. Rehabilitation of gait after stroke: a review towards a top-down approach. *Journal of NeuroEngineering and Rehabilitation*, 8:66, December 2011. doi: 10.1186/1743-0003-8-66. URL <https://doi.org/10.1186/1743-0003-8-66>.
- [2] Bosch Rexroth AG. IndraDyn S Synchronous Motors MSM Data Sheet R911329338 Edition 04, September 2017. URL [https://md.boschrexroth.com/modules/BRMV2PDFDownload-internet.dll/R911329338\\_04.pdf?db=brmv2&lvid=1203810&mvid=13251&clid=20&sid=1041E660DD79E95E63FFC4C7D1E8CA9B.borex-tc&sch=M&id=13251,20,1203810](https://md.boschrexroth.com/modules/BRMV2PDFDownload-internet.dll/R911329338_04.pdf?db=brmv2&lvid=1203810&mvid=13251&clid=20&sid=1041E660DD79E95E63FFC4C7D1E8CA9B.borex-tc&sch=M&id=13251,20,1203810). visited 2018-03-07.
- [3] P. Dietmaier. The Stewart-Gough Platform of General Geometry can have 40 Real Postures. In *Advances in Robot Kinematics: Analysis and Control*, pages 7–16, 1998. doi: 10.1007/978-94-015-9064-8\_1. URL [https://doi.org/10.1007/978-94-015-9064-8\\_1](https://doi.org/10.1007/978-94-015-9064-8_1).
- [4] J. Feldhusen and K.-H. Grote. *Pahl/Beitz Konstruktionslehre - Methoden und Anwendung erfolgreicher Produktentwicklung*. Springer Vieweg, Berlin Heidelberg, 8 edition, 2013. ISBN 978-3-642-29569-0. doi: 10.1007/978-3-642-29569-0. URL <https://doi.org/10.1007/978-3-642-29569-0>.
- [5] J.-P. Goppold. Kinematikentwicklung und Konstruktion eines Seilantriebssystems für ein Laufbandbasiertes Gangrehabilitationsrobotersystem. Diploma thesis, Technische Universität Berlin, April 2017.
- [6] C. Gosselin, R. Poulin, and D. Laurendeau. A planar parallel 3-dof cable-driven haptic interface. *Journal of Systemics,Cybernetics and Informatics*, 7:66–71, June 2009.
- [7] D. Gross, W. Hauger, P. Wriggers, and W. Schnell. *Technische Mechanik 4 - Hydromechanik, Elemente der Höheren Mechanik, Numerische Methoden*, chapter 3 Statik spezieller Tragwerke, pages 173–189. Springer Vieweg.
- [8] IntervalZero Inc. RTX64 Downloads- IntervalZero’s RTX64 is a key component of the IntervalZero RTOS Platform, 2018. URL <https://www.www.>

## Bibliography

---

- intervalzero.com/rtx-downloads/rtx64-downloads/. visited 2018-02-28.
- [9] Kanirope- professional ropes & equipment. Dyneema Seil PRO, Dyneema Schnur von Kanirope. URL <https://www.kanirope.de/dyneema-seil-kanirope-pro-1-5mm-12-fach-geflochten>. visited 2018-03-04.
  - [10] W. Kraus. *Force Control of Cable-Driven Parallel Robots*. PhD thesis, Universität Stuttgart, September 2015.
  - [11] M. Lourakis and A. Argyros. Is Levenberg-Marquardt the Most Efficient Optimization Algorithm for Implementing Bundle Adjustment? In *10th IEEE International Conference on Computer Vision (ICCV'05)*, volume 2, pages 1526–1531, October 2005. doi: 10.1109/ICCV.2005.128. URL <https://doi.org/10.1109/ICCV.2005.128>.
  - [12] K. Madsen, H. Nielsen, and O. Tingleff. Methods for Non-Linear Least Squares Problems. Technical report, Technical University of Denmark, 2004. lecture notes.
  - [13] D. Marquardt. An Algorithm for Least-Squares Estimation of Nonlinear Parameters. *Journal of the Society for Industrial and Applied Mathematics*, 11(2):431–441, June 1963. doi: 10.1137/0111030. URL <https://doi.org/10.1137/0111030>.
  - [14] F. Massaad, T. M. Lejeune, and C. Detrembleur. The up and down bobbing of human walking: a compromise between muscle work and efficiency. *The Journal of Physiology*, 582(2):789–799, July 2007. doi: 10.1113/jphysiol.2007.127969. URL <https://doi.org/10.1113/jphysiol.2007.127969>.
  - [15] J.-P. Merlet. Kinematics of the wire-driven parallel robot MARIONET using linear actuators. In *2008 IEEE International Conference on Robotics and Automation*, pages 3857–3862, May 2008. doi: 10.1109/ROBOT.2008.4543803. URL <https://doi.org/10.1109/ROBOT.2008.4543803>.
  - [16] A. Omran, M. Bayoumi, A. Kassem, and G. El-Bayoumi. Optimal Forward Kinematics Modeling of Stewart Manipulator Using Genetic Algorithms. *Jordan Journal of Mechanical and Industrial Engineering*, 3(4):280–293, December 2009.
  - [17] J. Perry, J.; Burnfield. *Gait analysis: normal and pathological function*. SLACK Incorporated, Thorofare, New Jersey, 2 edition, 2010. ISBN 978-1-55642-766-4.
  - [18] E. Peters, R. Pritzkuleit, F. Beske, and A. Katalinic. Demografischer Wandel und Krankheitshäufigkeiten - Eine Projektion bis 2050. In *Bundesgesundheitsblatt*,

## Bibliography

---

- volume 53, pages 417–426, April 2010. doi: 10.1007/s00103-010-1050-y. URL <https://doi.org/10.1007/s00103-010-1050-y>.
- [19] A. Pott. Forward Kinematics and Workspace Determination of a Wire Robot for Industrial Applications. In *Advances in Robot Kinematics: Analysis and Design*, pages 451–458, January 2008. doi: 10.1007/978-1-4020-8600-7\_47. URL [https://doi.org/10.1007/978-1-4020-8600-7\\_47](https://doi.org/10.1007/978-1-4020-8600-7_47).
  - [20] A. Pott. An Algorithm for Real-Time Forward Kinematics of Cable-Driven Parallel Robots. In *Advances in Robot Kinematics. Motion in Man and Machine : 12th International Symposium on Advances in Robot Kinematics*, pages 529–538, June 2010. doi: 10.1007/978-90-481-9262-5\_57. URL [https://doi.org/10.1007/978-90-481-9262-5\\_57](https://doi.org/10.1007/978-90-481-9262-5_57).
  - [21] A. Pott. Influence of Pulley Kinematics on Cable-Driven Parallel Robots. In *Latest Advances in Robot Kinematics*, pages 197–204, January 2012. doi: 10.1007/978-94-007-4620-6\_25. URL [https://doi.org/10.1007/978-94-007-4620-6\\_25](https://doi.org/10.1007/978-94-007-4620-6_25).
  - [22] A. Pott. On the Limitations on the Lower and Upper Tensions for Cable-Driven Parallel Robots. In *Advances in Robot Kinematics*, pages 243–251, 2014. doi: 10.1007/978-3-319-06698-1\_26. URL [https://doi.org/10.1007/978-3-319-06698-1\\_26](https://doi.org/10.1007/978-3-319-06698-1_26).
  - [23] A. Pott, T. Bruckmann, and L. Mikelsons. Closed-form Force Distribution for Parallel Wire Robots. In *Computational Kinematics*, pages 25–34, 2009. doi: 10.1007/978-3-642-01947-0\_4. URL [https://doi.org/10.1007/978-3-642-01947-0\\_4](https://doi.org/10.1007/978-3-642-01947-0_4).
  - [24] V. Schmidt. *Modeling Techniques and Reliable Real-Time Implementation of Kinematics for Cable-Driven Parallel Robots using Polymer Fiber Cables*. PhD thesis, Universität Stuttgart, December 2016.
  - [25] V. Schmidt, B. Müller, and A. Pott. Solving the Forward Kinematics of Cable-Driven Parallel Robots with Neural Networks and Interval Arithmetic. In *Computational Kinematics - Proceedings of the 6th International Workshop on Computational Kinematics (CK2013)*, pages 103–110, May 2014. doi: 10.1007/978-94-007-7214-4\_12. URL [https://doi.org/10.1007/978-94-007-7214-4\\_12](https://doi.org/10.1007/978-94-007-7214-4_12).
  - [26] V. Schmidt, W. Kraus, C. Martin, X. Jin, and A. Pott. Black-Box Accuracy Compensation for a Cable-Driven Parallel Robot. In *2017 17th International Conference on Control, Automation and Systems (ICCAS 2017)*, pages 428–431, October 2017. doi: 10.23919/ICCAS.2017.8204477. URL <https://doi.org/10.23919/ICCAS.2017.8204477>.

## Bibliography

---

- [27] Stiftung Deutsche Schlaganfall-Hilfe. Einige Daten und Fakten zum Schlaganfall, August 2016. URL <https://www.schlaganfall-hilfe.de/stiftung>. visited 2018-01-29.
- [28] VDI-Richtlinien. Konstruktionsmethodik - Technisch-wirtschaftliches Konstruieren - Technisch-wirtschaftliche bewertung. Standard VDI 2225 Blatt 3, Verein Deutscher Ingenieure e.V., Berlin, November 1998.
- [29] J. F. Veneman, J. Menger, F. C. T. van Asseldonk, and H. van der Kooij. Fixating the pelvis in the horizontal plane affects gait characteristics. *Gait & Posture*, 28(1):157–163, July 2008. doi: 10.1016/j.gaitpost.2007.11.008. URL <https://doi.org/10.1016/j.gaitpost.2007.11.008>.
- [30] R. Verhoeven. *Analysis of the Workspace of Tendon-based Stewart Platforms*. PhD thesis, Universität Duisburg-Essen, July 2004.
- [31] T. Watanbe, E. Ohki, Y. Kobayashi, and M. G. Fujie. Leg-dependent Force Control for Body Weight Support by Gait Cycle Estimation from Pelvic Movement. In *IEEE International Conference on Robotics and Automation*, pages 2235–2240, May 2010. doi: 10.1109/ROBOT.2010.5509514. URL <https://doi.org/10.1109/ROBOT.2010.5509514>.